ISBN 978-82-471-2074-3 (printed ver.)
ISBN 978-82-471-2075-0 (electronic ver.)
ISSN 1503-8181

Angela De Leebeeck

Doctoral theses at NTNU, 2010:59

Angela De Leebeeck

A roll wave and slug tracking scheme for gas-liquid pipe flow

NTNU
Norwegian University of
Science and Technology
Thesis for the degree of
philosophiae doctor
Faculty of Engineering Science and Technology
Department of Energy and Process Engineering

Doctoral theses at NTNU, 2010:59

NTNU

Angela De Leebeeck

A roll wave and slug tracking scheme for gas-liquid pipe flow

Thesis for the degree of philosophiae doctor

Trondheim, January 2010

Norwegian University of
Science and Technology
Faculty of Engineering Science and Technology
Department of Energy and Process Engineering

NTNU
Norwegian University of
Science and Technology

NTNU
Norwegian University of Science and Technology

Thesis for the degree of philosophiae doctor

Faculty of Engineering Science and Technology
Department of Energy and Process Engineering

©Angela De Leebeeck

ISBN 978-82-471-2074-3 (printed ver.)
ISBN 978-82-471-2075-0 (electronic ver.)
ISSN 1503-8181

Doctoral Theses at NTNU, 2010:59

Printed by Tapir Uttrykk

Dedication

To Mom, Dad and Lisa.

Abstract

The main objective of this work is to explore ways of introducing large roll waves as computational objects into a one-dimensional slug tracking scheme for gas-liquid pipe flow. The tracking scheme uses a moving and adaptive grid, as opposed to capturing schemes which require a fine grid to resolve sharp fronts. Experiments on the dynamic behavior of individual waves were made and following that, an integral wave model that is simple, dynamic and allows continuous transition to slug flow and stratified flow was developed.

In the first part of this work, an existing steady state roll wave model and a commercial multiphase flow simulator were compared to existing experimental data on a gas-condensate system so that current methods of modelling large amplitude waves could be investigated. This comparison resulted in similarly accurate predictions from both simulation methods.

Secondly, due to similarities between large waves and slugs, and a lack of pressure data on waves in the literature, the pressure change across roll wave fronts in air-water pipe flow at atmospheric pressure was measured experimentally. Holdup and pressure time traces along with synchronized video recordings showed that large roll waves were associated with a pressure jump.

These pressure measurements and other similarities between roll waves and slugs formed a basis for modelling wave fronts as moving objects with a pressure variation across them in a tracking scheme. A model is proposed where the pressure variation corresponding to liquid acceleration at the wave front is equal to an orifice type loss in the gas phase. The wave model also includes a simplified relationship for wave speed, allowing for smooth transition to slug flow. The large roll wave model was implemented and tested in the slug tracking scheme and model dynamics such as a waves growing to slugs and slugs decaying to waves were also demonstrated.

The roll wave model and its incorporation in the tracking scheme as well as its demonstration in comparison to data made up the third and fourth parts of this work. In the third part, simulations gave a reasonable approximation of wave speeds and pressure drops from the experiments at atmospheric pressure. The simulations also compared well to other experiments on roll waves at high gas densities when waves were initiated at the experimental frequency.

In the final part of this work, simulations with the tracking scheme were compared to experiments where a water front enters an initially empty undulating pipeline. The pipeline was either flushed with water or the flow would stop if there was insufficient inlet pressure. The end states of the simulation compared favorably with experiments but differed in the time to reach the final state. Slug formation, decay, and bubble turning were also observed in the simulations as in the experiments.

Preface

This thesis is submitted in partial fulfillment of the requirements for the degree of Philosphiae Doctor (PhD) at the Norwegian University of Science and Technology (NTNU).

This doctoral work has been performed at the Department of Energy and Process Engineering in the Faculty of Engineering Science and Technology with Professor Ole Jørgen Nydal (NTNU) as supervisor.

The work was carried out between October 2006 and December 2009, as a part of the PhD program 'Multiphase Transport' and has been generously supported by Total E&P Norge.

Acknowledgements

First of all, I owe the deepest gratitude to my supervisor Ole Jørgen Nydal for the opportunity to work with him, my visit to Australia while he was on sabbatical, the great research environment, the helpful talks, and the friendly group dinners at his house.

I am grateful to Total E&P Norge for their financial support of my PhD work. I would like to thank my contacts within Total Jon Ingar Monsen, Alexandre Goldszal, and Pascale Morin. Thank you for your the kind support while my supervisor was on sabbatical in Australia, the yearly status meetings in November, and for organizing the mini conferences of PhD students in Stavanger.

I thank the following people for helping with my research work: Masters students Andreas Hoel Gaarder and Andreas N. Winnem for running the experiments discussed in this thesis, and Jørn Kjølaas for help getting started on the slug tracking scheme.

I also want to thank the department administration for their help, especially when I didn't speak any Norwegian.

I would like to thank my fellow PhD students for the coffee breaks and lunches with interesting discussions from the practical issues of being a PhD candidate to Norwegian translations, and the PhD student meetings for providing a friendly environment to practice and receive feedback on conference presentations. A special thanks as well to my colleagues in the Multiphase Flow Group.

Finally, Mom, Dad and Lisa thank you for your love and support along the way.

Contents

List of Figures

List of Tables

Chapter 1

Introduction

This introductory chapter provides some background on multiphase flow in pipes, specifically gas-liquid flows with large amplitude waves and slugs. The objectives of this thesis work are given followed by a short description of the research papers included.

1.1 Background

Multiphase flow occurs when more than one phase (gas, liquid or solid) is transported at the same time. The present work is concerned with gas-liquid two-phase flow in pipelines which can occur in the nuclear, oil and process industries, for example, natural gas and oil pipelines. As opposed to single phase flow, multiphase flow is more complex in that different flow regimes can occur depending on gas and liquid phase velocities, fluid properties, and pipe geometries. The phase fractions and pressure drop in the pipeline can vary substantially depending on which flow regime is present.

Horizontal gas-liquid pipe flow can be divided into approximately four different flow patterns occurring at different superficial gas and liquid velocity combinations, as shown in the flow regime map in figure 1.1. These regimes are described as follows:

Stratified flow: The less dense gas phase flows on top of the heavier liquid phase. The two phases are separated by a continuous interface which can be smooth at lower flow rates or wavy as flow rates increase.

Annular flow: The gas phase flows at the center of the pipe cross-section while the heavier liquid phase flows as a thin film along the pipe wall. The film is in the form of an annulus around the gas phase and will typically be thicker on the bottom pipe wall due to gravity.

Slug flow: Slug flow is an intermittent flow regime where alternating liquid slugs and large gas bubbles propagate through the pipe. The liquid slugs completely fill the pipe

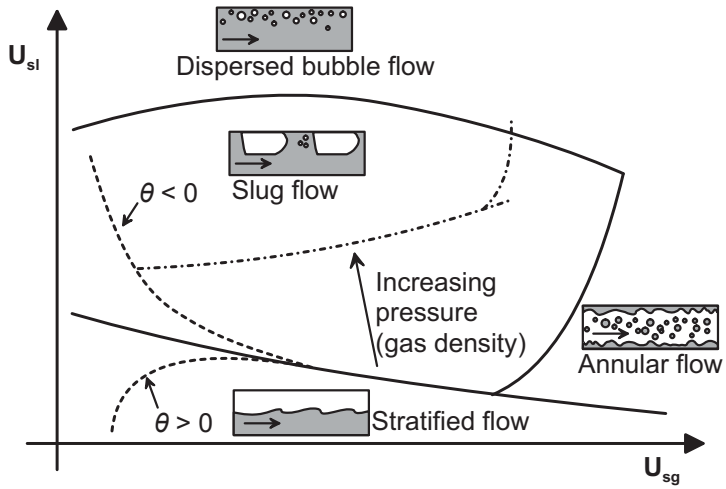

Figure 1.1: Flow regime map for gas-liquid pipe flow [19]. The effect of increasing or decreasing the angle of pipe inclination (θ) and of increasing the pressure or gas density is also shown. $\theta < 0$ indicates downward inclined pipes and vice versa.

cross-section and may contain small entrained gas bubbles. Slugs are formed either from unstable stratified flow or when liquid accumulates in a low point in the pipeline.

Dispersed bubble flow: Small gas bubbles are dispersed in a continuous liquid phase which fills the entire pipe cross-section.

Flow with large amplitude waves: Although not shown on the map (figure 1.1), flow with large amplitude roll waves can be thought of as an intermediate regime between stratified flow and slug flow, either before large waves completely block the pipe and form slugs or when slugs decay to waves.

Liquid slugs, as shown in figure 1.2, completely block the pipe cross-section and normally exceed 10 pipe diameters in length. They transport most of the liquid phase and propagate faster than the total mixture velocity. As slugs advance over the thin liquid film of the stratified region before them, liquid is absorbed and accelerated to the liquid phase velocity in the slug front. Liquid is then shed at the tail of the slug (bubble nose), and decelerated through the trailing bubble. Several experimental studies have looked at measuring slug properties such as their propagation velocity, pressure variation, length and frequency [24, 12, 10, 34, 33, 30]. Some of the slug flow experiments have resulted in mathematical correlations, for example bubble nose velocity [5], which have been used in later numerical models [7, 1, 18, 14, 27, 6, 22].

Flow with large amplitude roll waves occurs in gas condensate pipelines, in particular for high pressure systems corresponding to high gas densities. Although this regime has some similarities with slug flow, it is often treated as averaged stratified flow in existing flow

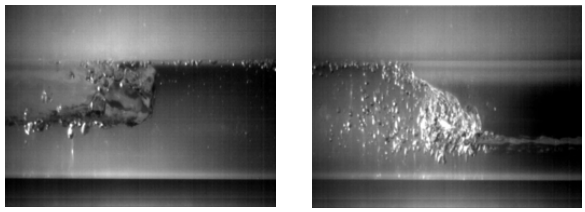

Figure 1.2: Photograph of a slug front (right) and its tail (left) in an air/water system.

Figure 1.3: Photograph of a large roll wave in an air/water system.

models. An experimental study has been made on roll waves before in a 0.1 m internal diameter (I.D.) pipe with high gas densities [17] measuring their characteristic quantities, for example velocity, amplitude, and the length between consecutive wave fronts. An example of a large roll wave is shown in figure 1.3.

Similarities between flows with large amplitude roll waves and slug flow include the sharp propagating front which overruns a liquid layer and a gradually decreasing liquid profile at the tail where liquid is decelerated. Roll waves also transport liquid and propagate at a velocity greater than the liquid phase velocity.

Typical differences between the two flow regimes are in the length scales and the magnitude of the front velocities. Waves are on the order of a few pipe diameters long as opposed to tens of diameters for slugs. Wave front velocities are much slower than slug velocities. The roll wave regime is also more irregular, with a larger spread in velocities and amplitudes. Waves can be seen to collapse and to merge with other waves, or grow to slugs. The wave regime can perhaps be thought of as a transitional regime towards slug flow. Many experimental studies have focused on the transition to wavy flow or to slug flow [31, 23, 3, 4, 11].

In undulating pipelines, severe slugging can occur where liquid accumulates at low points, blocking the flow of gas. The gas trapped behind the liquid slug is compressed until it reaches sufficient pressure to push out the long liquid slug in front of it. Liquid will then start accumulating in low points again and the sequence repeats itself. This severe slugging is an operational problem as the slugs can result in large fluctuations in pressure and flow rates.

Simulation of multiphase flows is important in the design and operation of sub-sea pipelines carrying mixtures of oil and gas. Design considerations include steady operation related to pressure drop, liquid content and temperatures, and dynamic flow conditions such as

operational transients and unstable flows. The basic flow models in these simulators are one dimensional, and as the closure relations cover averaged physical phenomena they are normally empirically determined. Experimental data at realistic flow conditions then becomes important for the modelling work.

One-dimensional flow simulators for dynamic flows are based on the numerical integration of a set of conservation equations on a spatial grid. The time evolution from some initial conditions is then determined yielding steady or unsteady solutions according to the physics of the model. Flows in pipelines have a large span in time and length scales, ranging from short waves and slugs to long severe slugs. In the capturing method, the idea is to capture small scale dynamics by refining the grid size. At the pipe diameter length scale, individual slug and wave dynamics can then be captured numerically on a small grid. This has been demonstrated for both slugs and waves using a two-fluid model, with a set of conservation equations for both phases [15, 8, 29, 13]. Slug or wave initiation can be captured, however, such models are sensitive to the numerical scheme, and the computational times can be prohibitive for simulation in long pipelines.

Alternatively, tracking schemes [18, 27, 14] which employ a grid moving with the fronts allow for computations often with orders of magnitude fewer grid points than with a capturing scheme. In a tracking scheme, stratified flow between slugs is modelled with a two-fluid model while slugs are modelled as moving objects and the boundaries between slugs and bubbles are tracked with a moving grid. Front physics such as bubble nose velocities or gas entrainment rates can also be implemented. Tracking schemes have also been tested for plug simulations where plugs were treated as rigid moving objects [18], as well as hybrid schemes where slug initiation is captured and the slugs are tracked [29]. The slug tracking scheme of [14] includes the liquid height profile (tail) behind waves and slugs, solving the two-fluid model in combination with modelling the wave front as a hydraulic jump.

The small scale dynamics of slug or wave flow is often of minor importance when simulating long pipelines with lengths up to tens and hundreds of kilometers. In these cases, slug flow is treated as a quasi-stationary flow, with averaged pressure drop and liquid fraction over a numerical grid containing several slug-bubble units. Stratified wavy flow is often modelled as averaged stratified flow using empirically determined interface friction relations [28, 2]. For the roll wave regime, with breaking waves and significant liquid transport in the waves, improvements may be possible by using averaging approaches similar to slug flow.

Approximating slug flow as a sequence of characteristic slug and bubble units has led to steady state unit cell slug flow models [7, 9]. The repeating unit cells combine models for bubbly flow in the slug region and separated flow in the bubble region where the two regions are related by mass balance equations. These models can be solved as a point model and integrated into dynamic simulators. Periodic unit wave models have also been derived for the roll wave regime, based on discontinuous numerical solutions of the mass and momentum balance equations in both phases [17]. Unit cell methods give adequate predictions of average holdup and pressure drop but do not include slug or wave dynamics

such as growth or decay.

The similarities observed experimentally between large amplitude roll waves and slug flow [24, 12] suggest that roll waves can be incorporated into a tracking scheme in similar fashion to slugs. The main focus of this work, therefore, is on the problem of large roll waves in a slug tracking scheme. To accomplish this, the following are needed: measurements on the dynamic behavior of individual waves, an integral wave model based on these experiments, and continuous transitions between slug, wave and stratified flow.

The next chapters and the research papers which follow describe the experiments, model development and its demonstration. The background of this work has already been introduced, objectives and a summary of the papers follow in this chapter. Chapter 2 on the experimental setup and chapter 3 on the implementation of the wave model supplement the included papers. Chapter 4 presents the main conclusions from the papers.

1.2 Objectives

The simple roll wave model and experimental investigations developed and conducted in this work are for gas-liquid two-phase flow in pipes. The main objective of this work is to explore ways of introducing large roll waves as computational objects into a one-dimensional computational scheme for dynamic slug tracking. The scheme is based on a moving and adaptive grid, as opposed to capturing schemes which require a fine grid to resolve sharp fronts. The roll wave model is to be dynamic, simple and allow smooth transition to slug flow and stratified flow within the framework of the slug tracking scheme. This demands an integral wave model relating pressure drop, wave amplitude and front velocity for individual waves.

The objectives of this research are as follows:

- Compare an existing steady state roll wave model and a commercial multiphase flow simulator to experimental data on a gas-condensate system so that current methods of modelling large amplitude waves can be investigated.
- Investigate and measure the pressure change across roll waves in air-water pipe flow experimentally. Due to similarities between large waves and slugs and lack of pressure data on waves in the literature [17, 24, 25, 30, 33, 12, 10], the pressure behavior of large amplitude roll waves is investigated with the data forming a basis for model development.
- Develop a simple, dynamic model for roll waves based on the air-water experimental results.
- Incorporate the roll wave model into an existing slug tracking scheme. The modelling work presented in this thesis is a continuation of work done on a slug tracking scheme at NTNU, the last implementation related to plug tracking [18].

- Demonstrate the roll wave and slug tracking scheme by comparing to available experimental data.
- Compare the tracking scheme to some particular experiments on flushing an initially empty undulating pipeline with liquid.

1.3 Summary of papers

This section summarizes the research papers produced during the course of this PhD work. These include three conference papers, one paper published in an international journal, and one paper to be submitted. The first paper discusses two existing methods of modelling large amplitude wave flow compared to experimental data from the literature. The next one covers air-water pipe flow experiments investigating the pressure behavior of large roll waves and slugs. The last three papers present and demonstrate the roll wave and slug tracking scheme as compared to experiments in-house and in the literature.

Paper 1

A steady state gas-liquid roll wave model [17] and a commercial multiphase flow simulator [6] lacking in a particular model for large amplitude wavy flow were compared to experimental data on a high pressure gas-condensate system in a pipeline [21]. Simulation results from the commercial software were provided by co-authors A. Goldszal and I. J. Monsen. These results were analyzed in combination with the simulation results from the steady state roll wave model and the experimental data. It was found that both the steady state wave model and the commercial simulator gave similarly accurate results when compared to data including large amplitude waves. Of additional value, the steady state model provides information about average wave length, speed, and height.

The work in this paper was completed so that existing modelling methods for gas-liquid flow with large amplitude waves in pipes could be investigated before the model presented in this thesis was developed.

Paper 2

This paper covers the pressure behavior of large roll waves in air-water pipe flow experiments at atmospheric pressure. The paper concluded that roll waves have a pressure variation across the front similar to slugs. The experiments and pressure variation results were discussed and a mathematical model relating the pressure variation to an orifice type relation was presented along with an estimate of the discharge coefficient used in orifice relations. The paper was based on a short conference manuscript where the experiments were first presented. It is included in Appendix A.

Paper 3

The simple dynamic roll wave model and its incorporation into the slug tracking scheme was presented and compared to the results from the air-water pipe flow experiments dis-

cussed in Paper 2. Wave and slug dynamics were demonstrated with the example of a wave growing to a slug, and a wave which grew to a slug and then decayed again. The model gave a reasonable approximation of wave speed but modelled pressure drops were sometimes low due to a difference in the number of simulated and actual waves in the pipe.

Paper 4

A detailed description of the roll wave model, the existing slug tracking scheme and how the wave model was incorporated in the slug tracking scheme was presented. The wave tracking capabilities were then further demonstrated by comparison with data on roll waves at high pressure [17]. The simulation results for both wave velocity and average pressure drop were quite good.

Papers 3 and 4 fulfilled the objectives of developing and demonstrating a simple dynamic model for roll waves in a slug tracking scheme. In these papers, the model was presented and reasonable comparisons to experimental data were made. The dynamic nature of the model was demonstrated through examples in Paper 3. The experimental and simulated results from the test cases discussed in these papers are tabulated in Appendix B.

Paper 5

The wave and slug tracking scheme was compared to experiments where an initially empty undulating pipeline was filled with water. The pipeline consisted of five upward and downward inclined segments where the formation of slugs, their decay, and bubble turning were observed experimentally and numerically. Four cases were run where one case resulted in complete flushing of the pipeline with liquid. In the other three cases, the inlet pressure was insufficient to fill the pipe completely and resulted in partial filling of the pipe segments. Simulations with the tracking scheme compared favorably with the experimental end states however comparisons of the liquid front propagation showed that it took longer for the simulated liquid front to reach the same position as in experiments.

The undulating pipeline experiments were conducted by A. N. Winnem as part of a M.Sc. work. Additional snapshots from videos taken during the experiments and from simulations are shown in Appendix C.

Chapter 2

Experimental Procedures

The experimental results discussed in Papers 2 and 5 and referred to in Paper 3 were obtained in the multiphase flow laboratory at NTNU in Trondheim, Norway. This chapter describes the experimental methods used in obtaining these results.

2.1 Experiments on roll waves and slugs

Since the roll wave flow regime was of interest, flow conditions where roll waves occur were identified. Then flow rates, liquid phase fractions (holdups), and pressure variations were recorded at the desired flow conditions. Video recordings with a time stamp were also taken for visual comparison to the measurements. The experimental materials, setup and data analysis procedure are discussed here.

2.1.1 Materials

A 16 m straight acrylic pipe test section with 0.06 m internal diameter (I.D.) was used. Its supporting beam could be inclined from -15° to $+15^\circ$ from the horizontal with a precision of $\pm 0.1^\circ$. The following instruments were used in and around the test section:

- Digital protractor (BMI ®Incli Tronic Plus) to verify the angle of pipe inclination.
- 4 pairs of conductance ring probes for measuring liquid phase fractions, built in house.
- Pressure transducer (Druck PTX 1400) with range 0 to 0.25 barg $\pm 0.15\%$ of full scale.
- Workstation with data acquisition board (PCI-6035E National Instruments).
- Video camera (Sony Digital 8 DCR - TRV510E PAL) with a resolution of 640×480 pixels at 25 fps.

Four different flow meters were used depending on flow rate and phase. They were as follows:

- Electromagnetic volume flow meter (Endress & Hauser Promag 330A) for low water volume flow rates from 0.19 to 6.4 m^3/h $\pm 0.5\%$ of reading.
- Electromagnetic volume flow meter (Fischer & Porter COPA-XM) for higher water flow rates from 3 to 60 m^3/h $\pm 0.5\%$ of reading.
- Coriolis mass flow meter (MicroMotion CMF025 Elite) for low gas flow rates from 5 to 2180 kg/h $\pm 0.05\%$ of reading.
- Vortex volume flow meter (Endress & Hauser Prowirl 77A) for higher gas flow rates from 31 to 375 m^3/h $\pm 1\%$ of reading.

Working fluids had the following properties at experimental conditions:

- Air with density 1.20 kg/m^3, and viscosity 1.80×10^{-5} $N \cdot s/m^2$ [32].
- Water with density 998.0 kg/m^3, and viscosity 1.003×10^{-3} $N \cdot s/m^2$ [32].

An in house program called LAWO was written in Labview for loop control and data acquisition. Time traces were analyzed using scripts written in Matlab.

2.1.2 Setup

The straight pipe made from acrylic was used to allow visual observations and video recordings. It is possible to run air, oil, and water in the pipe, but for these experiments oil was not used. The air-water experiments were conducted at atmospheric pressure and a temperature of 20°C. A schematic of the test section and attached instruments is shown in figure 2.1.

The fluids, air and water, enter the pipe as stratified layers with the less dense air phase on top. The fluids continue through the straight section where experimental observations are made, and exit into a pre-separator where the air is vented to the atmosphere. The liquid phase then continues to an oil-water separator, as the flow loop also has the possibility of adding a third oil phase. The water is recycled back into the flow loop in its own flow line by a frequency controlled centrifugal pump (Gustavsberg). Air is supplied from a pressurized line through a control valve. A schematic of the flow loop is shown in figure 2.2.

Four pairs of conductance ring probes made in house measured the liquid holdup (H) along the test section at 6.34 m, 8.85 m, 11.88 m, and 14.39 m from the inlet, locations shown in figure 2.1. Recording the holdup time traces at four locations allowed the evolution of waves and slugs along the pipe to be tracked and, after cross correlating the signals, the holdup time traces also provided a measure of the wave or slug speed.

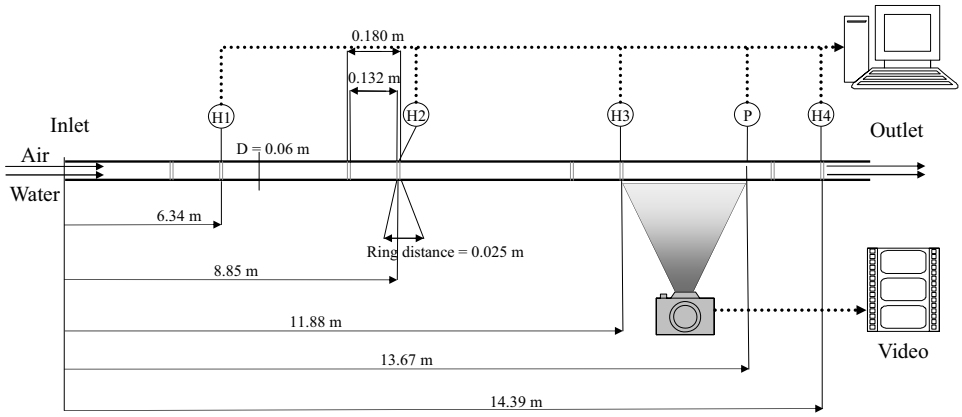

Figure 2.1: Schematic of multiphase flow test section with the position of holdup probes, pressure transducer, and video camera. H1, H2, H3, H4 - conductance ring probes measuring holdup. P - pressure transducer.

The main purpose of these experiments was to determine if roll waves have an associated pressure variation ΔP across the front similar to slugs. A pressure transducer was placed along the pipe at 13.67 m from the inlet, indicated in figure 2.1, to measure such a pressure variation between the last two conductance ring probes.

To allow identification of individual waves and slugs, the flow was recorded with a video camera at the same location as the pressure transducer, shown in figure 2.1. The video images had a time stamp which matched the corresponding holdup and pressure signals in the time traces. Whether the signal belonged to a slug or a wave could then be determined visually. The video recordings were for visualization only and were not used for further data processing. A colored dye was added to the water phase for ease of visualization.

2.1.3 Experimental procedure

Once the instrumentation was calibrated, a range of fluid flow rates and pipe inclinations were tested to determine where roll waves occur at low frequencies, and to control that this behavior matched with previous transition experiments observed in the multiphase flow laboratory. When several waves or slugs are present at the same time in the pipe, it becomes difficult to interpret the dynamics of the pressure recordings. After the initial screening, measurements of holdup and pressure as well as video recordings were taken at the flow conditions listed in table 2.1.

For each experiment, the holdup was measured by conductance probes at the four locations shown in figure 2.1. Pressure measurements and video recordings were taken simultaneously between the last two conductance probes. The angles of inclination were verified with a digital protractor.

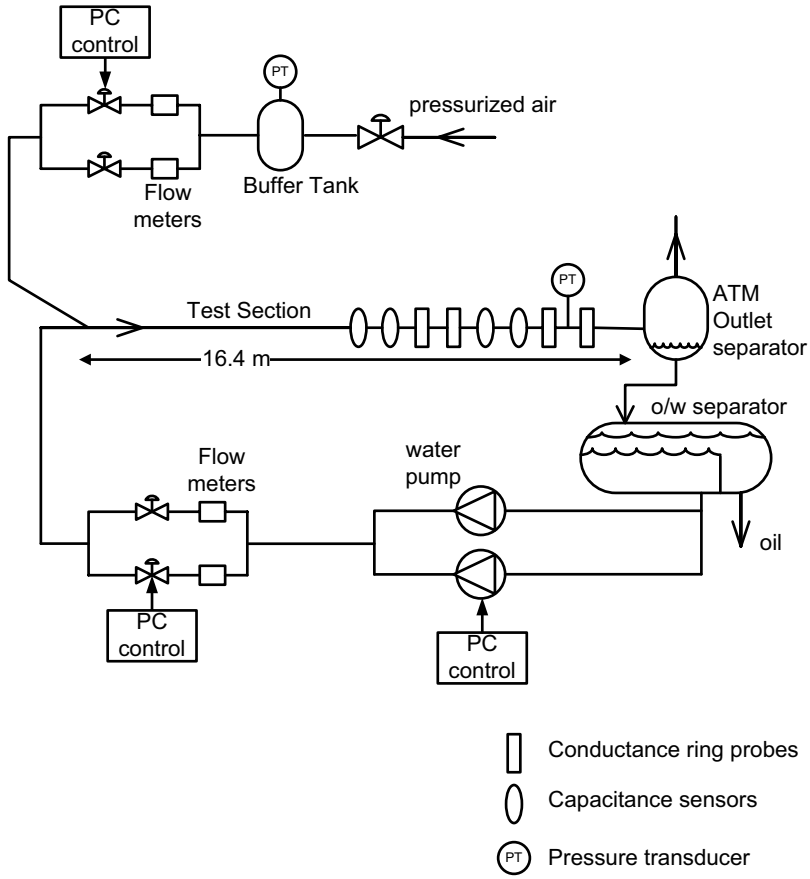

Figure 2.2: Schematic of the multiphase flow loop including the 0.06 m I.D. test section used for experiments.

Inclination (degrees)	U_{sl} (m/s)	U_{sg} (m/s)
-1.0	0.25, 0.29, 0.30, 0.45, 0.52	3.63, 5.86, 8.37, 11.51
0.0	0.17, 0.20, 0.22, 0.25, 0.26, 0.62, 0.33, 0.34, 0.35	1.53, 2.33, 3.38, 3.79, 3.84, 4.08, 4.65, 4.74, 4.87, 5.32, 5.56, 5.89, 6.01, 6.34, 6.43, 8.53
1.0	0.13, 0.14, 0.19, 0.20, 0.26, 0.27, 0.34, 0.42	2.35, 3.31, 3.47, 3.89, 4.09, 4.22, 4.32, 4.34, 5.15, 5.87, 6.20, 6.21, 6.45
2.0	0.11, 0.12, 0.17, 0.18, 0.29, 0.37, 0.39	2.62, 3.45, 4.24, 4.40, 4.82, 5.70, 6.09, 8.35
2.8	0.04, 0.05, 0.06, 0.11, 0.13, 0.18, 0.23, 0.35	3.09, 4.61, 5.02, 5.04, 5.05

Table 2.1: Combinations of inclination and phase superficial velocities (volume flow per pipe area) run in experiments.

Flow rates and data acquisition of holdup and pressure were controlled through a Labview program which also allowed the user to specify pump and valve settings. Air and water flow rates were measured before the phases were mixed at the inlet of the test section. Measurements from the four conductance probes and the pressure transducer were taken through the data acquisition board as voltage signals and converted to holdup and pressure units respectively after calibration. Data was sampled at 100 Hz and logged over 80 seconds for each experiment. Logging was initiated once flow stabilized after adjusting flow rates and angle of inclination.

The holdup and pressure time traces logged during the data acquisition process were then taken over to Matlab scripts for further analysis and comparison to the video recordings.

2.1.4 Data analysis procedure

Time series were analyzed semi-automatically using Matlab scripts developed for this purpose. The scripts were used to plot the four holdup time traces and the pressure time trace so that holdup and pressure peaks associated with waves and slugs lined up with each other.

The automatic analysis of individual waves turned out to be difficult because waves can decay or grow between the conductance probes, making them difficult to track from one probe to the next. Therefore, a simplified analysis was made. An averaged wave velocity was obtained from cross-correlating the four holdup time traces, giving three average velocity measurements.

Cross-correlation gives an indication of how similar two signals are as a function of the time delay between them. The cross-correlation function $R_{xy}(d)$ for two signals $x(i)$ and

$y(i)$ can be defined as in equation (2.1) where $i = 0, 1, 2, ..., N-1$ and N is the total number of samples. In this case, experiments run for 80 sec with a sampling frequency of 100 Hz produced a signal made up of 8000 samples.

$$R_{xy}(d) = \sum_i (x(i) - \overline{x})(y(i+d) - \overline{y}) \quad \text{for } d = 0, 1, 2, ..., N-1 \tag{2.1}$$

where $\overline{x}$ and $\overline{y}$ and the mean values of signals $x(i)$ and $y(i)$.

The cross correlation function is calculated for all delays d. The maximum value of $R_{xy}(d)$ indicates maximum correlation while a value of zero indicates no correlation. The goal of cross-correlating two signals is to find the delay d_{max} when $R_{xy}(d)$ has a maximum peak. Dividing d_{max} by the sampling frequency 100 Hz gives the characteristic time delay between signals, τ_{max}, in seconds.

Here, signals $x(i)$ and $y(i)$ are replaced with the signals from adjacent holdup probes. Since there are four holdup probes along the pipe, the first through fourth probes can be represented with signals $H1$, $H2$, $H3$, and $H4$. Signal H1 belongs to the first holdup probe and so on. The three cross correlation functions are then R_{H1H2}, R_{H2H3}, and R_{H3H4}.

The average velocity U of the waves or slugs between pairs of holdup probes separated by Δx is then:

$$U = \Delta x / \tau_{max} \tag{2.2}$$

Four holdup probes give three values of U.

The 95% percentile values of the time series were taken as characteristic holdup peaks and pressure variations in waves and slugs. The 95% percentile value means that 95% of all samples fall below this value. Pressure drops (in Pa/m) were estimated for use in Paper 3 assuming atmospheric pressure at the outlet of the pipe and dividing the measured gauge pressure by the length from the pressure transducer to the outlet. These results were used in developing and for comparison to the roll wave model presented in this thesis.

2.2 Experiments in an undulating pipeline

2.2.1 Materials and setup

The undulating pipeline test section consisted of the following components:

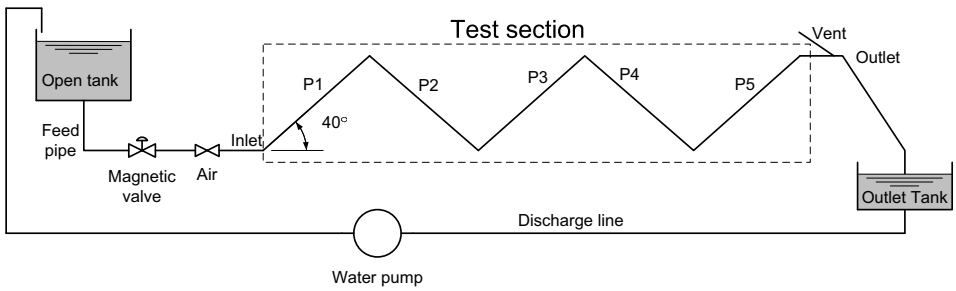

Figure 2.3: Schematic of the undulating pipeline experimental setup. The inclined pipe segments are numbered P1 through P5.

- 5x 0.016 m I.D. rigid acrylic pipe segments inclined at 40° from the horizontal, either upward or downward. The first segment was 0.91 m long and the others each 0.83 m long.

- 5x 0.016 m I.D. clear flexible hoses connecting the inclined segments, forming bends, each 0.155 m long.

- 1x 0.016 m I.D. outlet segment open to the atmosphere through a vent, 0.085 m long.

Constant inlet pressure was obtained by attaching a large tank of room temperature tap water with a constant liquid level at the inlet. The inlet pressure was determined by the weight of the liquid column above it. The tank volume was large compared to the volume of the undulating pipeline so that variation in the tank liquid level was negligible during pipe flushing. The liquid level above the inlet was varied by raising the tank on a manual jack.

The tank was connected to the test section through a feed pipe. Liquid flow into the test section was actuated through a magnetic valve (ASCO Magnetic Diafragma). After the experiment, water remaining in the test section was cleared by compressed air entering through a T-junction. The compressed air line remained closed during the experiment. The water discharged from the pipe was pumped back into the tank through a discharge line. A schematic of the experimental setup is shown in figure 2.3.

The flushing of the test section with water was recorded at 25 fps using a high definition video camera (Sony HDR-UX7W) with a resolution of 1920×1080 pixels. To enable better visualization of the water phase, fluorescent green dye (Merck Natrium and Sodium) was added and a black sheet was mounted behind the test section.

2.2.2 Procedure

Four inlet pressures were tested, corresponding to the following liquid column heights in the tank:

- 0.450 m above the inlet.
- 0.675 m above the inlet.
- 0.750 m above the inlet.
- 0.825 m above the inlet.

First, the camera was placed so that the entire test section could be filmed and this location was marked for future reference. The tank was then adjusted to the desired height with the manual jack. Additional water was added to the tank manually to fine tune desired elevation. Before actuating the magnetic valve, the video camera was started and water flowing into the initially empty undulating test section was recorded. Once the liquid in the test section reached equilibrium or the test section was flushed completely with liquid, the video camera was switched off and the magnetic valve was closed. End states were reached in less than 12 sec and so recorded videos were about this long. If the test section was not flushed completely, the equilibrium height of liquid column in each pipe segment was measured. The test section was then cleared of water and dried with compressed air and the water was pumped back into the tank, ready for the next experiment. Experiments at each elevation above the inlet were repeated at least twice.

2.2.3 Data analysis

The position of the liquid front in the test section was extracted from the video using Matlab scripts for digital image analysis. Since the water was dyed green, the areas filled with liquid were determined based on the green color intensity. If the green intensity was above a certain threshold, then liquid was present. The front most green area was then picked out and its location in each video frame was saved.

The green color intensity ranges from 0 at the lightest to 255 at the darkest. The pixels corresponding to green liquid in the video generally had a green intensity of 75. The threshold intensity was set to 50. Above this value, the region of the test section in the image frame was identified as liquid. To locate the liquid front, the green pixels furthest from the inlet were picked out and saved with the matching time stamp.

Positions in the video frames were converted from number of pixels to meters by comparing a reference length measured on the test section to the number of pixels the same reference occupied in a video frame. The horizontal and vertical displacement of the liquid front from the inlet were then determined in meters. Since each frame had a corresponding time stamp, the position of the liquid front at a given time was known. The

transient progress of the liquid front in the test section was then plotted and later compared to simulation results.

2.3 Other experimental results used

In Papers 1 and 4, experimental data conducted by others has been compared to simulation data. These experiments are described briefly in this section.

2.3.1 Gas-condensate data

In Paper 1, experimental data from a gas-condensate system at 80 bar was compared to a previously developed numerical model [17] and commercial software [6]. The experimental data was obtained at Statoil Hydro Oil and Energy Research Centre in Norway and included a total of 84 experiments conducted in a 0.078 m I.D. pipe [20]. Pipe inclinations ranged from -6° to 10° from the horizontal, U_{sg} from 0.3 to 9 m/s, and U_{sl} were 0.146 and 0.292 m/s. The gas density and viscosity were 73 kg/m^3 and 1.4×10^{-5} Pa·s, and condensate density and viscosity were 660 kg/m^3 and 7.0×10^{-4} Pa·s respectively at 80 bar and $30°C$ [20]. The relevant experimental information available for comparison were the identification of the flow regime, total pressure drop, and average liquid holdup [21, 20].

2.3.2 Large amplitude wave data at 8 bar

In Paper 4, the tracking scheme is compared to experimental data on roll waves at 8 bar [17]. These experiments were run at the Institute for Energy Technology in Norway and include a total of 984 experiments in a 0.1 m I.D. pipe. Working fluids were sulfurhexafloride (SF6) gas and water at 8 bar and $20°C$. At these conditions, the gas density and viscosity were 50 kg/m^3 and 1.61×10^{-5} Pa·s, and water density and viscosity were 998 kg/m^3 and 1×10^{-3} Pa·s respectively [17]. Pipe inclinations ranged from 0 to 5° upward, U_{sg} from 0.5 to 4.5 m/s, and U_{sl} from 0.1 to 0.6 m/s. Each experimental case was run for 100 sec in a 25 m long test section. Results for wave velocity and average pressure drop were of interest for comparison.

Chapter 3

Model Description and Implementation

This chapter describes how the mass and momentum balance equations in the wave and slug tracking scheme are discretized, the propagation of moving objects, and the model implementation in the C++ programming language. The discretization and implementation follow from previous documentation on the slug tracking scheme [18]. Further details of the roll wave model and other correlations necessary for the tracking scheme are presented in Paper 4.

3.1 Nomenclature

A	Cross-sectional area	m^2
D	Pipe diameter	m
g	Acceleration of gravity	m/s^2
H	Liquid holdup	(-)
h_l	Liquid height	m
L	Section length	m
$m = M/AL$	Mass per volume	kg/m^3
M	Mass	kg
P	Pressure	Pa
S	Wetted perimeter	m
t	Time	sec
Δt	Time step size	sec
T	Temperature	K
U	Velocity	m/s
V	Volume	m^3

Greek symbols

α	Area fraction	(-)
λ	Friction factor	(-)
θ	Angle of pipe inclination	deg
ρ	Density	kg/m^3
τ	Shear stress	N/m^2
ψ	Volume error term	m^3/sec

Subscripts

b	Border
$front$	Front of a wave or slug section
g	Gas phase
i	Interface
j	Spatial index
J	Spatial index
k	Phase k, either liquid or gas
l	Liquid phase
mix	Mixture
n	Neighboring phase, opposite of phase k
$strat$	Stratified
$tail$	Tail of a wave or slug section

Superscripts

$\widehat{()}$	Upwind quantity $()$
$\cdot$	Time rate of change of a quantity
n	Current time step
$n+1$	Next time step
s	Source

3.2 Model equations

This section reviews how the one-dimensional mass and momentum balance equations are discretized for use in the slug tracking scheme. As discussed in Papers 3, 4 and 5, the slug tracking scheme consists of slug units separated by stratified regions: the bubbles. In the stratified regions, the two-fluid model is solved on a staggered grid. A mixture momentum equation is solved for the slug regions with moving boundaries. Similarly, the wave front objects added to the scheme in the course of this thesis work have moving boundaries and require integral gas and liquid momentum balance equations of their own.

The mass and momentum balance equations are integrated over a control volume called V_k which is occupied by phase k, either liquid or gas. The boundaries of V_k are moving with boundary velocities denoted U_b, this is zero for stationary boundaries. The positive direction is from left to right.

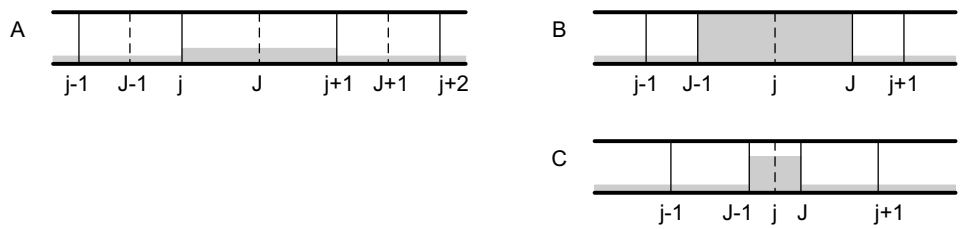

Figure 3.1: Index notation in A. stratified regions, B. slug regions, and C. waves. Solid lines indicate section borders. Dashed lines indicate section centers.

The spatial grid notation used in the discretized equations is explained in figure 3.1, as used in Paper 4. Lower case letters j denote the boundaries of stratified sections and the center of slug and wave sections. Upper case letters J denote stratified section centers and the moving boundaries of waves and slugs. For discretization in time, the superscript n indicates the current time step and superscript $n+1$ indicates the next time step.

Variables with a hat e.g. $\hat{M}$ are treated as upwind. Other variables are either well defined at their index location or determined as an averaged value. For example, at a stratified section center pressure P_J is well defined but phase velocity $U_{k,J}$ is determined as an average of the two velocities defined at the section's borders $U_{k,j}$ and $U_{k,j+1}$.

Derivatives with respect to time $\partial()/\partial t$ are discretized as $\frac{()^{n+1}+()^n}{\Delta t}$ where Δt is the size of the time step. Spatial derivatives $\partial()/\partial x$ are discretized as $\frac{()_J+()_{J-1}}{L_j}$ where L is the length corresponding to section or border j.

3.2.1 The mass balance equations

The one-dimensional mass balance equation for either phase is as follows:

$$\frac{\partial \rho}{\partial t} + \frac{\partial(\rho U)}{\partial x} = \dot{\rho^s} \tag{3.1}$$

Following integration over V_k, equation 3.1 gives the following [18]:

$$\frac{\partial M_k}{\partial t} + \oint_{A_k} \rho_k (U_k - U_b) dA = \dot{M}_k^s \tag{3.2}$$

In stratified regions

The mass balance equation for phase k is solved at grid cell centers. In stratified sections, the equation is solved implicitly. The discretized mass balance equation for stratified cell

J is as below:

$$\frac{M_{k,J}^{n+1} - M_{k,J}^{n}}{\Delta t} + \frac{\hat{M}_{k,j+1}^{n+1}}{\hat{L}_{j+1}^{n}}\left(U_{k,j+1}^{n+1} - U_{b,j+1}^{n+1}\right) - \frac{\hat{M}_{k,j}^{n+1}}{\hat{L}_{j}^{n}}\left(U_{k,j}^{n+1} - U_{b,j}^{n+1}\right) = \dot{M}_{k,J}^{s} \quad (3.3)$$

In slugs and waves

For slugs and waves, mass balances are solved explicitly so that the slug lengths and wave heights are consistent with the masses [18]. The equation for phase k in a wave or slug is discretized as follows:

$$\frac{M_{k}^{n+1} - M_{k}^{n}}{\Delta t} = \frac{M_{k}^{n}\left(U_{k}^{n+1} - U_{tail}\right)}{L} - \frac{M_{k}^{n}\left(U_{k}^{n+1} - U_{front}\right)}{L} \quad (3.4)$$

3.2.2 The pressure equation

Deriving the pressure equation for the two-fluid model in stratified sections begins with expanding equation (3.2) using $M_k = \rho_k V_k$ and then dividing by the phase density ρ_k. The result is the following equation:

$$\frac{V_k}{\rho_k}\frac{\partial \rho_k}{\partial t} + \frac{\partial V_k}{\partial t} + \frac{1}{\rho_k}\oint_{A_k} \rho_k (U_k - U_b) dA = \frac{\dot{M}_k^s}{\rho_k} \quad (3.5)$$

The term $\frac{\partial \rho_k}{\partial t}$ is expanded using the equation of state to give:

$$\frac{\partial \rho_k}{\partial t} = \left(\frac{\partial \rho_k}{\partial P}\right)_{T_k}\frac{\partial P}{\partial t} + \left(\frac{\partial \rho_k}{\partial T}\right)_{P}\frac{\partial T_k}{\partial t} \quad (3.6)$$

Putting expansion (3.6) into equation (3.5) gives:

$$\frac{V_k}{\rho_k}\left[\left(\frac{\partial \rho_k}{\partial P}\right)_{T_k}\frac{\partial P}{\partial t} + \left(\frac{\partial \rho_k}{\partial T}\right)_{P}\frac{\partial T_k}{\partial t}\right] + \frac{\partial V_k}{\partial t} + \frac{1}{\rho_k}\oint_{A_k} \rho_k (U_k - U_b) dA = \frac{\dot{M}_k^s}{\rho_k} \quad (3.7)$$

Adding equation (3.7) for all the phases, in this case gas and liquid phases, gives the pressure equation (3.8) [18], as follows:

$$\sum_k \frac{V_k}{\rho_k}\left[\left(\frac{\partial \rho_k}{\partial P}\right)_{T_k}\frac{\partial P}{\partial t} + \left(\frac{\partial \rho_k}{\partial T}\right)_{P}\frac{\partial T_k}{\partial t}\right] + \frac{\partial V}{\partial t} + \sum_k \frac{1}{\rho_k}\oint_{A_k} \rho_k (U_k - U_b) dA = \sum_k \frac{\dot{M}_k^s}{\rho_k} \quad (3.8)$$

The discretized version of equation (3.8) is resolved at grid cell centers in stratified regions. For cell J, the discretized pressure equation is as follows:

$$\sum_k \frac{V_{k,J}^n}{\rho_{k,J}^n}\left[\left(\frac{\partial \rho_{k,J}^n}{\partial P}\right)_{T_k}\frac{P_J^{n+1}-P_J^n}{\Delta t}\right] + A\left(U_{b,j+1}^{n+1}-U_{b,j}^{n+1}\right) \tag{3.9}$$
$$+\sum_k \frac{1}{\rho_{k,J}^n}\left[\hat{m}_{k,j+1}^n A\left(U_{k,j+1}^{n+1}-U_{b,j+1}^{n+1}\right)-\hat{m}_{k,j}^n A\left(U_{k,j}^{n+1}-U_{b,j}^{n+1}\right)\right]=\sum_k \frac{\dot{M}_{k,J}^s}{\rho_{k,J}}+\psi_{s,J}$$

The variation of temperature over time is neglected assuming an isothermal system. As equation (3.9) is not formulated in a mass-conservational manner, a source term $\psi_{s,J}$ is added in the following time step to ensure that mass is conserved over time. The source term is the discrepancy between the masses from the mass balance equation and the masses according to the pressure and equations of state. This source term is as follows:

$$\psi_{s,J}=\frac{AL_J}{\Delta t}\left(\frac{m_{l,J}}{\rho_{l,J}}+\frac{m_{g,J}}{\rho_{g,J}}-1\right) \tag{3.10}$$

3.2.3 The momentum balance equations

The one-dimensional momentum balance equation for either gas or liquid phase is as in the following equation:

$$\frac{\partial(\rho U)}{\partial t}+\frac{\partial(\rho U^2)}{\partial x}=-\frac{\partial P}{\partial x}+\frac{\partial \tau}{\partial x}-\rho g sin\theta \tag{3.11}$$

If equation (3.11) is integrated over V_k, the momentum balance equation for phase k becomes:

$$\frac{\partial(M_k U_k)}{\partial t}+\oint_{A_k}\rho_k U_k(U_k-U_b)dA=-V_k\frac{\partial P_k}{\partial x}+\oint_{A_k}\tau_k dA-M_k g sin\theta \tag{3.12}$$

In stratified regions

For the case of gas-liquid stratified flow, P_k is related to a common pressure P at the interface between phases through the following equation [18]:

$$\frac{\partial P_k}{\partial x}=\frac{\partial P}{\partial x}+\rho_k g cos\theta\frac{\partial h_l}{\partial x} \tag{3.13}$$

The discretized version of equation (3.12) for phase k at a border j in stratified regions using relation (3.13) is given below:

$$\begin{aligned}
&M_{k,j}^n \frac{U_{k,j}^{n+1} - U_{k,j}^n}{\Delta t} + m_{k,J}^n A \left(U_{k,J}^n - U_{b,J}^n\right) \left(\hat{U}_{k,J}^{n+1} - U_{k,j}^{n+1}\right) \\
&-m_{k,J-1}^n A \left(U_{k,J-1}^n - U_{b,J-1}^n\right) \left(\hat{U}_{k,J-1}^{n+1} - U_{k,j}^{n+1}\right) = -\alpha_{k,j}^n A \left(P_J^{n+1} - P_{J-1}^{n+1}\right) \quad (3.14) \\
&-M_{k,j}^n g cos\theta \frac{h_{l,J}^n - h_{l,J-1}^n}{L_j^n} - \frac{1}{8} S_{k,j}^n L_j^n \lambda_{k,j}^n \rho_{k,j}^n \left|U_{k,j}^n\right| \left(U_{k,j}^{n+1}\right) \\
&-\frac{1}{8} S_{i,j}^n L_j^n \lambda_{i,j}^n \rho_{g,j}^n \left|U_{k,j}^n - U_{n,j}^n\right| \left(U_{k,j}^{n+1} - U_{n,j}^{n+1}\right) - M_{k,j}^n g sin\theta
\end{aligned}$$

The phase velocity U_k is solved for at the cell border j. The friction relation used is introduced in Paper 4. M_j, α_j and L_j^n are the averaged values of the phase mass, area fraction and section length at the border. $\hat{U}_{k,J}^{n+1}$ and $\hat{U}_{k,J-1}^{n+1}$ are upwind quantities.

In slugs

In slugs, a mixture momentum balance equation is solved by summing the gas and liquid momentum balance equations. In combination with a slip relation, the liquid and gas phase velocities in a slug can be obtained. The integrated mixture momentum equation in a slug is as in the following equation:

$$\begin{aligned}
&\frac{\partial (M_g U_g + M_l U_l)}{\partial t} + \oint_{A_g} m_g U_g (U_g - U_b) dA + \oint_{A_l} m_l U_l (U_l - U_b) dA \\
&\qquad = -V_s \frac{\partial P}{\partial x} + \oint_{A_s} \tau_{mix} dA - (M_l + M_g) g sin\theta \quad (3.15)
\end{aligned}$$

If no gas entrainment into the slug is assumed, the liquid fraction in the slug goes to unity and gas mass goes to zero. In that case, equation (3.15) takes the form of the liquid momentum balance equation, as follows:

$$\frac{\partial (M_l U_l)}{\partial t} + \oint_{A_l} m_l U_l (U_l - U_b)) = -V_l \frac{\partial P}{\partial x} + \oint_{A_l} \tau_l dA - M_l g sin\theta \quad (3.16)$$

The discretized version of equation (3.16) is the one used in the slug tracking scheme. This equation is solved for the liquid velocity in a slug j:

$$\begin{aligned}
&M_{l,j}^n \frac{U_{l,j}^{n+1} - U_{l,j}^n}{\Delta t} + m_{l,J}^n A \left(U_{l,J}^n - U_{b,J}^n\right) \left(\hat{U}_{l,J}^{n+1} - U_{l,j}^{n+1}\right) \\
&-m_{l,J-1}^n A \left(U_{l,J-1}^n - U_{b,J-1}^n\right) \left(\hat{U}_{l,J-1}^{n+1} - U_{l,j}^{n+1}\right) \\
&= -H_j^n A \left(P_J^{n+1} - P_{J-1}^{n+1}\right) - \frac{1}{8} S_{l,j}^n L_j^n \lambda_{l,j}^n \rho_{l,j}^n \left|U_{l,j}^n\right| \left(U_{l,j}^{n+1}\right) - M_{l,j}^n g sin\theta \quad (3.17)
\end{aligned}$$

Correlations for the moving slug and wave boundaries are laid out in Paper 4.

In waves

The addition of a wave model to the slug tracking scheme is the subject of the present work and the details of how the wave momentum equations are arrived at are discussed in Papers 3 and 4. The mixture momentum equation is not solved in wave objects since the gas phase flows over the liquid phase, but the same discretized equation (3.17) is used for the liquid momentum balance in a wave front. A discretized gas momentum balance equation for wave fronts including an orifice type relation is laid out in Paper 4. The phase momentum equations are coupled to each other through assuming that the pressure variation across a wave front is the same in the liquid phase as it is in the gas phase.

3.3 Moving boundaries

Both slugs and waves are modelled as moving objects in the slug tracking scheme. At a front boundary liquid is absorbed while at a tail boundary liquid is shed.

3.3.1 The front velocity

Slug and wave fronts move with a velocity determined from the mass balance across the front. The following equation is the liquid mass balance across the front of a slug or wave j.

$$H_j(U_{l,j} - U_{front}) = H_{strat}(U_{l,strat} - U_{front}) \tag{3.18}$$

Rearranging equation (3.18) gives an expression for the front velocity, U_{front}:

$$U_{front} = \frac{H_j U_{l,j} - H_{strat} U_{l,strat}}{H_j - H_{strat}} \tag{3.19}$$

If section j is a slug without gas entrainment, the holdup H_j goes to unity and the liquid velocity in the slug $U_{l,j}$ goes to the mixture velocity.

3.3.2 The slug tail velocity

The slug tail velocity (the bubble nose velocity) is determined using equation (3.20) with relations for C_o and U_o proposed by Bendiksen [7, 5].

$$U_{tail} = C_o U_{mix} + U_o \tag{3.20}$$

U_{mix} is the local mixture velocity in the slug. The coefficient C_o and the drift velocity U_o are defined as follows:

$$C_o = 1.05 + 0.15sin^2\theta \qquad U_o = U_{ov} + U_{oh} \qquad \text{if } |U_{mix}| < 3.6\sqrt{gD}/cos\theta$$
$$C_o = 1.2 \qquad U_o = U_{ov} \qquad \text{if } |U_{mix}| > 3.6\sqrt{gD}/cos\theta$$
$$U_{ov} = 0.35\sqrt{gD}sin\theta \qquad U_{oh} = \pm 0.54\sqrt{gD}cos\theta$$

In the case with low mixture velocities, $|U_{mix}| < 3.6\sqrt{gD}/cos\theta$, the bubble nose is close to the upper pipe wall where local liquid velocities are lower. In the high mixture velocity case, $|U_{mix}| > 3.6\sqrt{gD}/cos\theta$, the bubble nose moves to the center of the pipe where liquid velocity is a maximum. In the tracking scheme, values for C_o and U_o are chosen to give the largest U_{tail}.

3.3.3 The direction of slug propagation

The direction of slug propagation is determined by the direction of the pressure gradient in the pipe. It is assumed that large bubbles between slugs move in the opposite direction to the pressure gradient [18] i.e. towards areas of low pressure. A bubble turning criterion based on the direction of the pressure gradient is implemented in the slug tracking scheme.

The turning criterion is arrived at by considering the steady state liquid momentum balance equation in a slug where convection has been neglected. This gives a pressure gradient composed of a friction component and a gravity component, as follows:

$$\frac{\partial P}{\partial x} = -\frac{1}{2}\frac{\lambda_l}{D}\rho_l |U_l| U_l - \rho_l g sin\theta \tag{3.21}$$

The turning criterion is the point where the friction and gravity terms in equation (3.21) balance and the pressure gradient is zero [16, 26]. If the pressure gradient is negative, bubbles will propagate to the right (positive direction) and the slug's left border will be a bubble nose while its right border will be a slug front. If the pressure gradient then becomes positive, the bubbles will turn.

3.3.4 The wave tail velocity

For the wave tail velocity (appearing only in the wave mass balance equations), the following correlation allows continuous transition to the slug tail velocity as the holdup in the wave approaches unity:

$$U_{tail} = 1.2U_l \tag{3.22}$$

As the liquid holdup in the wave increases, U_l approaches the mixture velocity and the wave tail velocity approaches the slug tail velocity with coefficient $C_o = 1.2$.

Although velocities are determined for both a wave front and a wave tail, the wave object itself is of fixed length and propagates with the front velocity U_{front}. The wave tail velocity in equation (3.22) is used in the wave mass balance equations to determine the holdup in the wave. A difference in U_{tail} and U_{front} for waves leads to a change in the wave front liquid height. In slugs, this difference leads to a variation in slug length.

3.4 Model Implementation

The tracking scheme has been developed in the C++ programming language using object oriented techniques. Object oriented programming promotes code reuse through inheritance and enhances modularity which reduce complexity of the program and allow changes to be made more easily. Physical objects such as slugs and waves can be represented as computational objects in the code through the use of classes. The model implementation following from [18] is reviewed briefly here.

3.4.1 Data structure

The computational domain consists of a list of consecutive pipe objects represented by a pipe class which stores information about the pipe geometry. These are further divided into section and border classes representing the numerical grid and storing information about the fluid phases. Sections and borders are connected to each other using pointers in a linked list arrangement of alternating grid cells and cell boundaries [18].

The section class is made up of several subclasses representing slugs or stratified regions which inherit from the section class. Wave and slug computational objects are represented using the same slug class since they have many similarities. The two are differentiated through an indicator which identifies the computational object as a wave if true or a slug if false. The section class contains quantities, such as pressures and masses, that are solved at section centers using the staggered grid arrangement. The section class and its subclasses are mapped out in figure 3.2.

Similarly the border class is further subdivided into different types of section borders corresponding to, for example, the pipe inlet or the boundary between a slug section and a stratified section. The border class contains information on phase velocities which are resolved at section borders as well as the axial position of the border. The border class hierarchy is laid out in figure 3.3.

3.4.2 Section management

The computational grid used in the tracking scheme is adjusted dynamically as slug and wave objects move. Stratified sections which have become too small i.e. less than a user

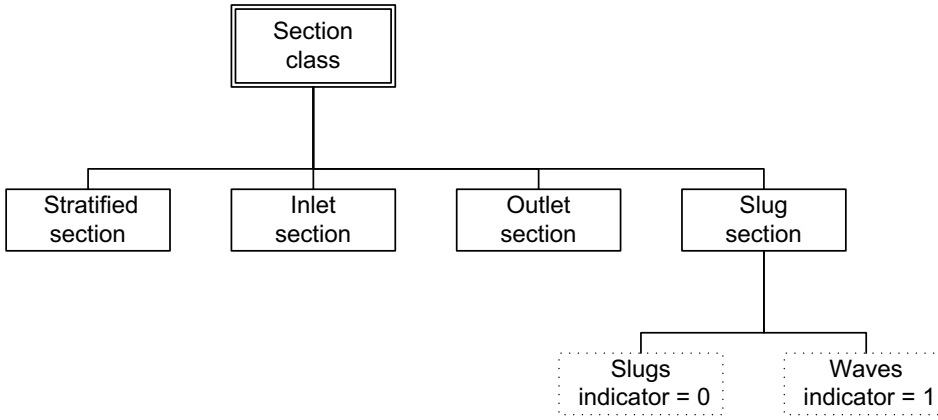

Figure 3.2: Section class structure.

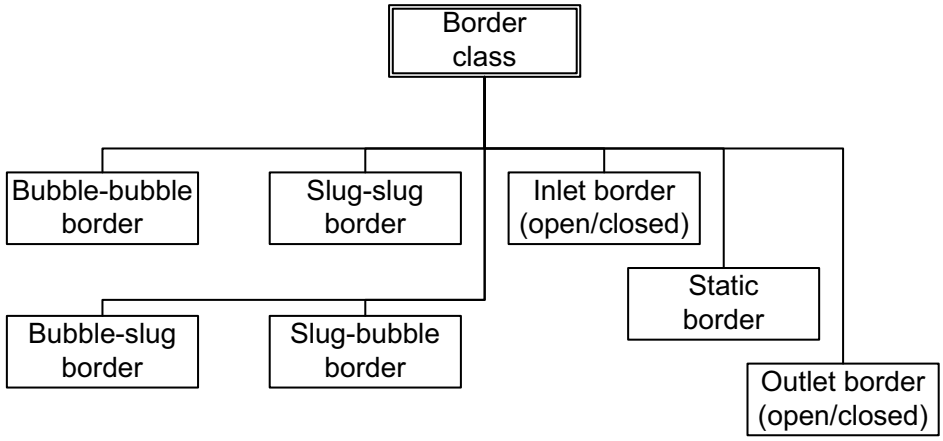

Figure 3.3: Border class structure.

specified minimum grid length are merged with a neighboring section. Those that have exceeded a user defined maximum grid length are split into two identical sections.

Slugs are inserted when the holdup in a stratified section exceeds a maximum value and the slugs are converted to waves when they become too small. Waves can be inserted either based on an initiation criteria or based on a given frequency. Waves are converted to slugs when their holdup exceeds a maximum value or two of them merge. They are deleted when their holdup approaches the holdup in the surrounding stratified sections.

A special case occurs when a single stratified section is located between two slugs or waves. If the section is large enough, it is split in two (even if it does not exceed the maximum stratified grid size) so that the two-fluid model can be solved on a staggered grid over the two neighboring stratified sections. If the section becomes too small, because the slug behind it is moving faster than the slug in front of it, then the two slugs are merged and it means the slower slug has been overtaken.

3.4.3 Inlet and outlet boundary conditions

Inlet and outlet boundaries can be either closed with fixed phase velocities or constant pressure. For closed inlets superficial velocities and inlet holdup are specified and used to determine phase velocities at the inlet border. For the case of constant pressure, the user can define a constant pressure at the inlet or outlet. The specified pressure is then used in the momentum balance equations to determine inlet or outlet phase velocities.

3.4.4 Computational Sequence

The mass, momentum, and pressure equations have been formulated implicitly for increased stability and linearized in terms of the unknown variables so that they can be solved by direct Gauss elimination [18]. Equations are also represented computationally using a generic class structure including a mass balance equation class and a momentum balance equation class. Since the gas and liquid mass and momentum balance equations have the same general structure, this avoids having a separate formulation for each phase. The equation class contains an array to store the equation coefficients. Each array corresponds to a row in a sparse system of linear equations. The coefficient arrays are collected, joined in a condensed matrix, and solved. The computational sequence in a given time step is shown in the flow chart in figure 3.4.

At the beginning of a time step, the coefficients of computational section border velocities are determined. This is followed by solving the system of pressure and momentum equations by Gauss elimination. From there, phase velocities and pressures are determined. Border velocities are updated using the new phase velocities and border velocity coefficients determined in step 1. Then, in step 4, phase masses are determined. The phase mass equations in each stratified section are built into a system of equations which are also

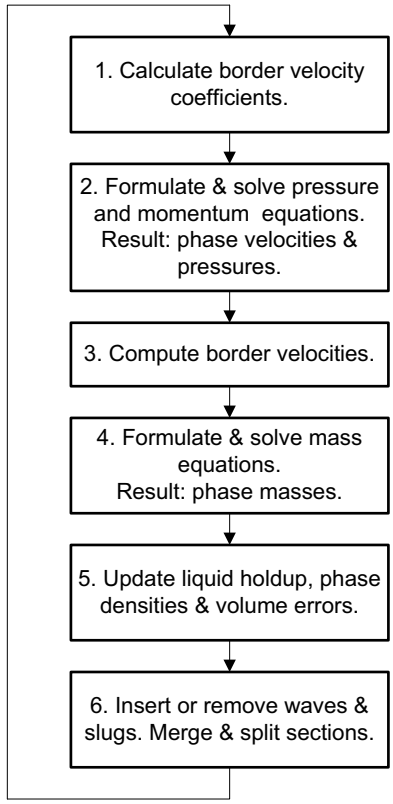

Figure 3.4: Flow chart of the computational sequence in a single time step.

solved by Gauss elimination. In slugs and waves, mass balances are solved explicitly. In step 5, liquid holdup, phase densities, and the volume error term appearing in equation (3.8) are updated. Lastly, section management is taken care of. Sections are inserted and removed as necessary. Stratified sections that are too long are split in two and those that are too short are merged with their neighbors. The simulation then proceeds to the next time step.

3.4.5 Model output

The results from a simulation with the wave and slug tracking scheme can be output as a text file listing quantities of interest for all sections at each time step. This information includes:

- The type of border, its position in the pipeline, and its velocity.
- The type of section (stratified, slug, or wave) and its length.
- The liquid holdup in a section.
- The pressure in a section.
- The gas and liquid phase velocities.

This output can then be animated using in house visualization code or used for further analysis and plotting.

Chapter 4

Conclusions

Summary

This work has focused on a roll wave and slug tracking scheme and has been presented in five papers. Existing methods of modelling large roll waves were investigated by comparing a steady state roll wave model, a commercial simulator, and experimental gas-condensate data at high pressure and various pipe inclinations. The pressure behavior in roll waves was investigated at atmospheric pressure in near horizontal pipes using air and water. Those measurements became the basis for developing a simple dynamic roll wave model, which was then incorporated in an existing slug tracking scheme. The wave and slug tracking scheme was then demonstrated in comparison with the experimental data obtained at atmospheric pressure and data on roll waves at high pressure. The tracking scheme was also compared to experiments on liquid filling of an initially empty undulating pipeline.

Evaluation of existing steady-state models

Comparison of simulations from the steady state roll wave model, the commercial multiphase flow simulator OLGA®which does not include a particular model for wavy flow, and large roll wave data from the gas-condensate experiments resulted in similarly accurate predictions from both simulation methods. Since the steady state model gave similar results to the commercial simulator and experimental data, it was concluded that the steady state model performed well.

Experiments

Pipe flow experiments were conducted with air and water at horizontal and near horizontal inclinations at atmospheric pressure. The aim was to study the details of the pressure response related to large amplitude waves, as this data was lacking in the literature. Time

traces from four liquid holdup probes, one pressure transducer and synchronized video recordings showed that large amplitude roll waves were associated with a pressure jump. These results then formed the basis for following modelling efforts: approaching roll wave modelling in a similar way as to slug flow.

After further analysis, average wave and slug velocities were obtained as well as characteristic pressure variations across waves and slugs. As expected, resulting average wave velocities were smaller than slug velocities as well as mixture velocities. The observed pressure variation across large amplitude waves was similar to slugs but of lesser magnitude.

Roll wave model in a slug tracking scheme

These pressure measurements and other similarities between roll waves and slugs led to the idea of modelling waves in a tracking scheme: as moving objects with a pressure variation across them. A mathematical model relating the losses in a wave to the pressure variation was proposed where the same pressure variation corresponds to acceleration at the wave front in the liquid phase and to an orifice type loss in the gas phase. Estimates of the loss coefficient in the orifice type relation for waves lay between 0.2 and 0.4.

The effect of grid refinement on tracking simulations was discussed. Running the scheme with a coarse grid allowed for faster computational times and simulation in longer pipes but meant that waves and slugs were modelled as square objects without trailing tails. A finer grid allowed a more physical representation of waves with tails at the expense of computational speed. The flow dynamics such as a wave growing to a slug or a slug decaying to a wave were also demonstrated.

The model for large roll waves was implemented and tested in an existing slug tracking scheme. The wave model also introduced a simplified relationship for wave speed which allowed for smooth transition to slug flow.

Comparison with data

Computations were demonstrated in comparison to the experimental data obtained at atmospheric pressure. The model gave a reasonable approximation of wave speeds and pressure drops for flow with large roll waves. Modelled pressure drops were sometimes low compared to experimental values due to a difference in the number of waves and slugs in the pipe.

The wave and slug tracking scheme was then compared with available experimental data for roll waves at high gas densities where the simulated waves were initiated at the experimental frequencies. The resulting comparison between computed wave velocities and pressure drops were good with average percentage differences of 8% and 17% respectively.

Other flow cases

Finally, comparing the tracking scheme simulation results with experimental data related to flushing an undulating pipeline with water gave qualitatively similar results. The upward and downward pipe segments were either partially filled at lower inlet pressures where flow stopped completely or flushed with water at sufficient inlet pressure. The final water levels resting in the partially filled pipe segments were similar in experiments and simulations but the simulations differed from the experiments by about 50% sec in the time to reach the final state.

The position of the propagating liquid front was plotted against time and simulated liquid front positions were very similar to experiments in the first pipe segment. However after that the front positions lagged behind the experimental results. Slug formation, decay and bubble turning were also observed in the simulations similar to the behavior in the experiments.

Bibliography

[1] P. Andreussi, A. Minervini, and A. Paglianti. Mechanistic model of slug flow in near-horizontal pipes. *AIChE Journal*, 39(8):1281–1291, 1993.

[2] N. Andritsos and T. J. Hanratty. Influence of interfacial waves in stratified gas-liquid flows. *AIChE Journal*, 33(3):444–454, 1987.

[3] N. Andritsos, L. Williams, and T. J. Hanratty. Effect of liquid viscosity on the stratified-slug transition in horizontal pipe flow. *Int. J. Multiphase Flow*, 15(6):877–892, 1989.

[4] D. Barnea and Y. Taitel. Kelvin-helmholtz stability criteria for stratified flow: Viscous versus non-viscous (inviscid) approaches. *Int. J. Multiphase Flow*, 19:639–649, 1993.

[5] K. H. Bendiksen. An experimental investigation of the motion of long bubbles in inclined tubes. *Int. J. Multiphase Flow*, 10:467–483, 1984.

[6] K. H. Bendiksen, D. Malnes, R. Moe, and S. Nuland. The dynamic two-fluid model olga: Theory and application. In *SPE Production Engineering*, 1991.

[7] K. H. Bendiksen, D. Malnes, and O. J. Nydal. On the modelling of slug flow. *Chem. Eng. Comm.*, 141-142:71–102, 1996.

[8] M. Bonizzi and R. I. Issa. A model for simulating gas bubble entrainment in two-phase horizontal slug flow. *Int. J. Multiphase Flow*, 29:1685–1717, 2003.

[9] J. Fabre and A. Line. Modeling of two-phase slug flow. *Annu. Rev. Fluid Mech.*, 24:21–46, 1992.

[10] Z. Fan, Z. Ruder, and T. J. Hanratty. Pressure profiles for slugs in horizontal pipelines. *Int. J. Multiphase Flow*, 3:421–437, 1993.

[11] T. J. Hanratty and A. Hershmann. Initiation of roll waves. *AIChE Journal*, 7:488–497, 1961.

[12] G. Hanyang and G. Liejin. Experimental investigation of slug development on horizontal two-phase flow. *Chinese Journal of Chemical Engineering*, 16:171–177, 2008.

[13] H. Holmås. *Numerical simulation of waves in two-phase pipe flow using 1D two-fluid models*. PhD thesis, University of Oslo, 2008.

[14] B. Hu, C. Stewart, P. D. Manfield, P. M. Ujang, C. P. Hale, C. J. Lawrence, and G. F. Hewitt. A model for tracking the evolution of slugs and waves in straight pipelines. In *6th International Conference on Multiphase Flow*, Leipzig, Germany, 2007.

[15] R. I. Issa and M. H. W. Kempf. Simulation of slug flow in horizontal and nearly horizontal pipes with the two-fluid model. *Int. J. Multiphase Flow*, 29:69–95, 2003.

[16] M. Johansen. *An experimental study of bubble propagation velocity in 3-phase slug flow*. PhD thesis, Norwegian University of Science and Technology, 2006.

[17] G. W. Johnson. *A study of stratified gas-liquid pipe flow*. PhD thesis, University of Oslo, 2005.

[18] J. Kjølaas. *Plug propagation in multiphase pipelines*. PhD thesis, Norwegian University of Science and Technology, 2007.

[19] O. Kristiansen. *Experiments on the transition from stratified to slug flow in multiphase pipe flow*. PhD thesis, Norwegian University of Science and Technology, 2004.

[20] H. Kvandal, G. Elseth, and S. Munaweera. Inclined pipe project. gas/condensate campaign. experimental results and model prediction from 2-phase gas condensate tests. Report. Oil and Energy Research Centre Porsgrunn, Norway., 2003.

[21] H. Kvandal, S. Munaweera, G. Elseth, and H. Holm. Two-phase gas-condensate flow in inclined pipes at high pressure. In *SPE 77505, ATCE*, San Antonio, USA, 2002.

[22] M. Larsen, E. Hustvedt, and T. Straume. Petra: A novel computer code for simulation of slug flow. In *SPE Annual Technical Conference and Exhibition*, San Antonio, Texas, 1997.

[23] P. Y. Lin and T. J. Hanratty. Prediction of the initiation of slugs with linear stability theory. *Int. J. Multiphase Flow*, 12:79–98, 1986.

[24] P. Y. Lin and T. J. Hanratty. Detection of slug flow from pressure measurements. *Int. J. Multiphase Flow*, 13:13–21, 1987.

[25] M. Miya, D. E. Woodmansee, and T. J. Hanratty. A model for roll waves in gas-liquid flow. *Chemical Engineering Science,*, 26:1915–1931, 1971.

[26] O. J. Nydal. Experiments in downwards flow on stability of slug fronts. In *Third International Conference on Multiphase Flow*, Lyon, France, 1998.

[27] O. J. Nydal and S. Banerjee. Dynamic slug tracking simulations for gas-liquid flow in pipelines. *Chem. Eng. Comm.*, 141-142:13–39, 1996.

[28] M. Ottens, K. Klinkspoor, H. C. J. Hoefsloot, and P. J. Hamersma. Correlations predicting liquid hold-up and pressure gradient in steady-state (nearly) horizontal co-current gas-liquid pipe flow. *Trans IChemE,*, 79:581–592, 2001.

[29] F. Renault. *A Lagrangian slug capturing scheme for gas-liquid flows in pipes*. PhD thesis, Norwegian University of Science and Technology, 2007.

[30] A. Soleimani and T.J. Hanratty. Critical liquid flows for the transition from the pseudo-slug and stratified patterns to slug flow. *Chemical Engineering Science*, 29:51–67, 2003.

[31] P. M. Ujang, C. J. Lawrence, C. P. Hale, and G. F. Hewitt. Slug initiation and evolution in two-phase horizontal flow. *Int. J. Multiphase Flow*, 32:527–552, 2006.

[32] F. M. White. *Fluid Mechanics*. McGraw Hill, Boston, 5th international edition, 2005.

[33] B. D. Woods, Z. Fan, and T. J. Hanratty. Frequency and development of slugs in a horizontal pipe at large liquid flows. *Int. J. Multiphase Flow*, 32:902–925, 2006.

[34] B. D. Woods, E. T. Hurlburt, and T. J. Hanratty. Mechanism of slug formation in downwardly inclined pipes. *Int. J. Multiphase Flow*, 26:977–998, 2000.

Paper 1

Comparison of two phase pipe flow experiments with a roll wave model and a commercial simulator

A. De Leebeeck, O. J. Nydal, G. W. Johnson, J. I. Monsen and A. Goldszal

Presented at the 6th North American Conference on Multiphase Technology, Banff, Canada, June 4-6 2008

Comparison of two phase pipe flow experiments with a roll wave model and a commercial simulator.

A De Leebeeck, O J Nydal
Department of Energy and Process Engineering, Norwegian University of Science and Technology, Norway
G W Johnson
Statoil Hydro, Norway
J I Monsen, A Goldszal
TOTAL E&P NORGE AS, Norway

1 NOTATION

g gravity, 9.81 m/s^2

h local liquid depth

A cross sectional area of pipe

A_g cross-sectional area occupied by the gas

A_l cross-sectional area occupied by the liquid

C wave celerity

$H = A_l / A$ average liquid holdup

$H_l = A_l / S_i$

N denominator in equation (1)

$\frac{\partial P_i}{\partial X}$ pressure gradient

S_g gas wetted perimeter

S_i width of interface in cross-sectional plane

S_l liquid wetted perimeter

T numerator in equation (1)

U_g area averaged gas velocity

U_l area averaged liquid velocity

Usg superficial gas velocity

Usl superficial liquid velocity

X stream-wise position referred to a coordinate system moving with C

θ angle of pipe inclination from horizontal

$\Delta\rho = \rho_l - \rho_g$ difference in liquid and gas density

ρ_g gas density

ρ_l liquid density

τ_g gas wall shear stress

τ_i interfacial shear stress

τ_l liquid wall shear stress

2 ABSTRACT

A model for roll waves was compared with two-phase flow data from experiments with a gas-condensate system at high pressure in upward and downward inclined pipes, and with commercial multiphase flow simulator software OLGA® which does not include a particular model for wavy flow. Wavy flow in the commercial simulator is treated as averaged stratified flow. The roll wave model without any tuning to the data and the commercial simulator gave similarly accurate results for experiments with large amplitude waves. The roll wave model also provided additional information on large roll wave flow such as wave length, speed and height.

3 INTRODUCTION AND LITERATURE SURVEY

Commercial multiphase flow modelling software such as OLGA® does not currently predict large amplitude wavy flows. Slug flow is treated as averaged flow, on the basis of a “unit cell model”. In stratified flow the gas-liquid interaction is made through effective friction models. In a previous paper [1], it was observed that the commercial simulator predicted either slug or stratified flow for a whole range of pipe flow experiments. Modelling large roll waves is of interest because they have been observed in experiments [2] and they are not as yet accounted for in commercial software. Doing so would provide a more complete picture of the flow regimes possible in a pipe. The

ability to model such waves could also be of interest for studying flow regime transitions or for studying slug precursors or decayed slugs.

A model for roll waves was developed for two-phase flows in inclined pipes where roll waves occur and has been previously shown to give good results in high pressure inclined pipe flow [2]. This model was based on physical assumptions and was not tuned against any particular dataset. Predictions for liquid holdup and pressure gradient using the commercial simulator, when waves were present, were compared with the roll wave model of [2]. The roll wave model can also provide additional information on wave height, length and speed which the commercial simulator cannot.

The experimental data used for comparison were obtained at Statoil Hydro Oil and Energy Research Centre in Norway under a JIP involving Norsk Hydro, Total E&P Norge AS and the Ormen Lange license [3]. The purpose of the experiments was to acquire data on high pressure gas-condensate systems in inclined flow and validate the commercial software with the data [1]. This data set was used in the development of the commercial simulator along with many others [4]. This experimental data set has also been previously used in a comparison with results from another flow model, LedaFlow® [5]. Of the 84 experiments, 19 cases with large amplitude waves were observed.

In this paper, a model for roll waves was compared with commercial multiphase flow modelling software and with two-phase flow data from high pressure experiments in upward and downward inclined pipes. Predictions of average liquid holdup and pressure drop with the commercial simulator were compared with the roll wave model when waves were present. In addition, the roll wave model was compared with all 84 experiments.

4 THE ROLL WAVE MODEL

A 1-D model for roll waves in two-phase gas liquid pipe flow has previously been developed and compared to high pressure flow experiments at the Institute for Energy Technology (IFE) [2]. Based on the two-fluid equations for stratified flow, the model is capable of modelling flow in upward and downward inclined pipes. The model is not tuned against any particular data set but is based on physical assumptions. It is summarized below; a more detailed description can be found in [2].

The roll wave model provides information about wave properties, which the commercial simulator does not, such as wave speed, wave height and wave length as well as accounting for increased interface friction. It determines axial variations in gas and liquid velocities as well as the pressure gradient and the average liquid fraction which were compared with the gas-condensate experimental results and the results from the commercial model.

To solve the two-fluid equations, it was assumed that the gas and liquid phases were incompressible, flow was turbulent and velocity profiles were uniform in both phases. It was also assumed that roll waves evolved to maximum amplitude roll waves based on experimental observations conducted by [2].

The profile equation of a roll wave was modelled from the two-fluid equations as follows:

$$\frac{dh}{dX} = \frac{T(h)}{N(h)} \quad (1)$$

where

$$N = \Delta\rho g H_l \cos\theta - \rho_l (U_l - C)^2 - \rho_g \left(\frac{A_l}{A_g}\right)(U_g - C)^2 \quad (2)$$

$$T = H_l \left[-\Delta\rho g \sin\theta + \left(\frac{1}{A_l} + \frac{1}{A_g}\right)\tau_i S_i + \frac{1}{A_g}\tau_g S_g - \frac{1}{A_l}\tau_l S_l \right] \quad (3)$$

$\Delta\rho = \rho_l - \rho_g$, $H_l = A_l / S_i$, and X is a relative stream-wise coordinate moving at the wave speed, C. Equation (1) is a non-linear first order autonomous equation. The profile is discontinuous and joined together by a shock over the discontinuity.

The pressure gradient was determined as follows:

$$\frac{\partial P_l}{\partial X} = \frac{1}{A}\left(\rho_g S_i (U_g - C)^2 + \rho_l S_i (U_l - C)^2 + \tau_l S_l + \tau_g S_g + (\rho_g A_g + \rho_l A_l) g \sin\theta + \frac{\partial h}{\partial X}(\rho_g A_g + \rho_l A_l) g \cos\theta \right) \quad (4)$$

The wall friction factors for the gas and liquid were taken from single phase relations using Haaland's friction factor [6]. The ratio between the interfacial friction factor and the gas wall friction factor was determined as part of the solution by assuming that a solution with maximum amplitude waves was reached. The friction factor ratio is equal to one on a smooth interface between the gas and the liquid where the interfacial friction factor is equal to the gas wall friction factor. This is not the case, however for wavy interfaces where the friction increases. In the model solution, the friction factor ratio should always be greater than 1.

The roll wave model is limited to two phase pipe flow with separate gas and liquid phases. It is intended for the roll wave regime and can provide information about what occurs between stratified and slug flow, however, it does not provide a slug solution.

5 THE EXPERIMENTAL DATA

The experimental data set was obtained at Statoil Hydro Oil and Energy Research Centre in Norway [3]. The experimental setup and procedure was presented elsewhere [1], but the flow conditions and pipe geometry are listed below.

A total of 84 experiments were conducted using a gas-condensate system at high pressure (80 bar) in pipes inclined at -6, -1, 0, 0.1, 1, 5, and 10 degrees with Usg ranging between 0.3 to 9 m/s and Usl of 0.146 and 0.292 m/s [3]. The internal pipe diameter was 78 mm. The gas density and viscosity were 73 kg/m^3 and 1.4x10^{-5} Pa·s, and condensate density and viscosity were 660 kg/m^3 and 7.0x10^{-4} Pa·s respectively [3]. Flow patterns observed during the experiments were identified as either: stratified (33 experiments), slug (4 experiments), stratified flow with large amplitude waves (19

experiments), annular (14 experiments) and a transition from stratified to annular (14 experiments) [1, 3].

The data available from the experiments included the total, static and frictional pressure gradients, and the average liquid holdup (H) [1, 3]. Experimental results used for comparison with the roll wave and commercial models included H, the total pressure gradient, and the flow regime identification.

The experiments were laid out as follows, for a total of 84 experiments [3]:

- Angles of pipe inclination were -6, -1, 0, 0.1, 1, 5, and 10 degrees
- At each angle, Usl were: 0.146 m/s and 0.292 m/s
- At each Usl and angle, Usg were approximately: 0.3, 0.6, 1.2, 2.3, 4.7, and 8.8 m/s.

The following 19 cases were identified as having a flow regime with large amplitude waves [3]:

- For Usl = 0.146 m/s:
    - At 1 degrees, Usg = 0.59, 1.17 m/s
    - At 5 degrees, Usg = 0.58, 1.17, 2.34 m/s
    - At 10 degrees, Usg = 0.29, 0.59, 1.19, 2.34 m/s
- For Usg = 0.292 m/s:
    - At 1 degrees, Usg = 0.58, 1.17, 2.34 m/s
    - At 5 degrees, Usg = 0.58, 1.18, 2.33 m/s
    - At 10 degrees, Usg = 0.29, 0.59, 1.16, 2.33 m/s

The experimental error for most H results was up to 5%, error in pressure gradient was within 10% [3]. The measurement error was higher than 5% at lower liquid levels, especially at the highest Usg values [3].

6 RESULTS

Both the roll wave model and the commercial simulator were used to predict the experimental gas-condensate results for experiments identified as large amplitude waves and the accuracy of both models was compared. The experimental flow rates and pipe inclination were needed as input for simulations. In addition, the roll wave model was compared with the remaining experimental data which contains other flow regimes: stratified, slug, annular, and a transition from stratified to annular.

There were two quantities available in the experimental data for comparison with numerical models: H and the total pressure gradient. The error between the calculated H and the experimental H was calculated as a global percentage difference: 100*(H from model – experimental H). The relative percentage error in pressure gradient was calculated as: 100*(model pressure gradient – experimental pressure gradient)/experimental pressure gradient. A negative percentage error indicates that the model under-predicted the value and a positive percentage error indicates model overprediction.

6.1 Comparison for large amplitude wave experiments

There were 19 experiments identified with large amplitude waves and they occurred at pipe inclinations of 1, 5, and 10 degrees. Figure 1 shows plots of H and pressure

gradient against Usg for these experiments. Results from the roll wave model, the commercial simulator, and the experiments are plotted together for each combination of angle of inclination and Usl. A legend is given in the figure caption.

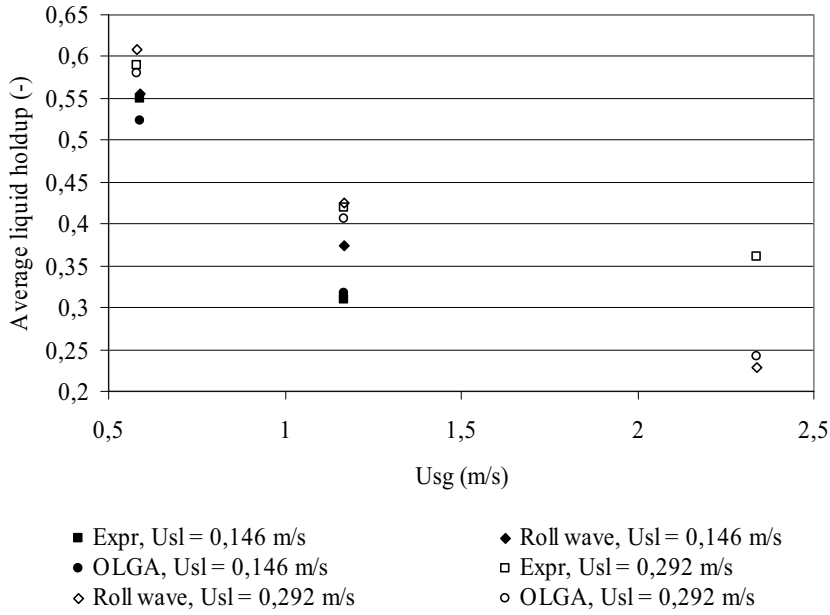

a) 1 degrees H

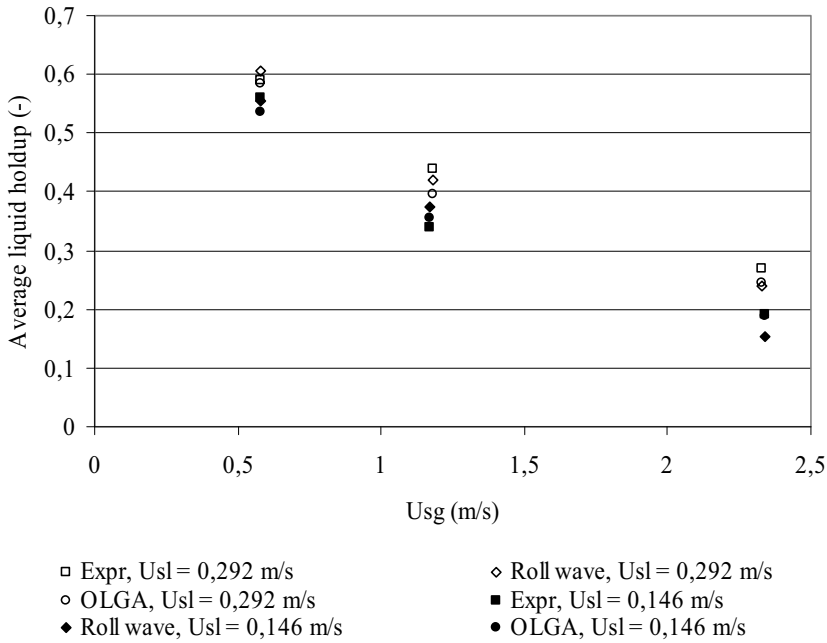

b) 5 degrees H

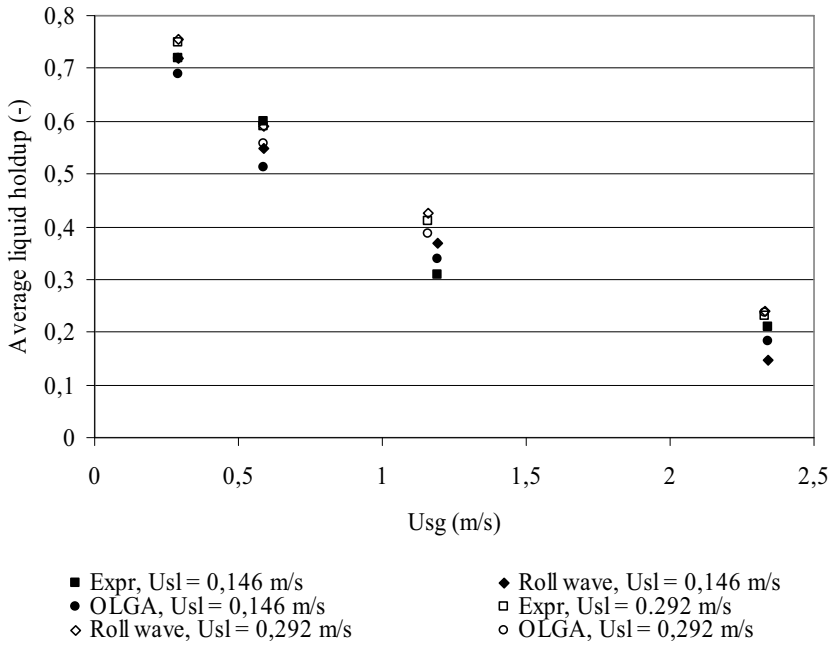

c) 10 degrees H

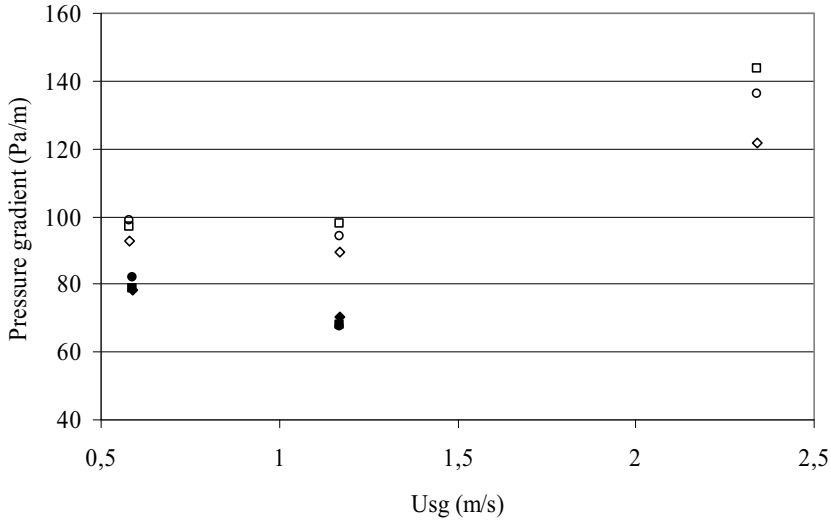

d) 1 degrees pressure gradient

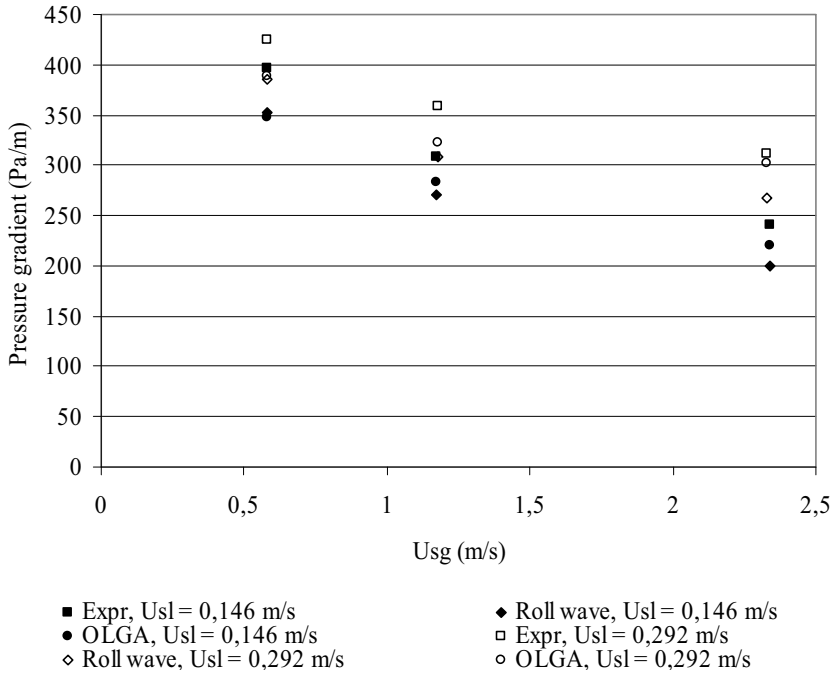

e) 5 degrees pressure gradient

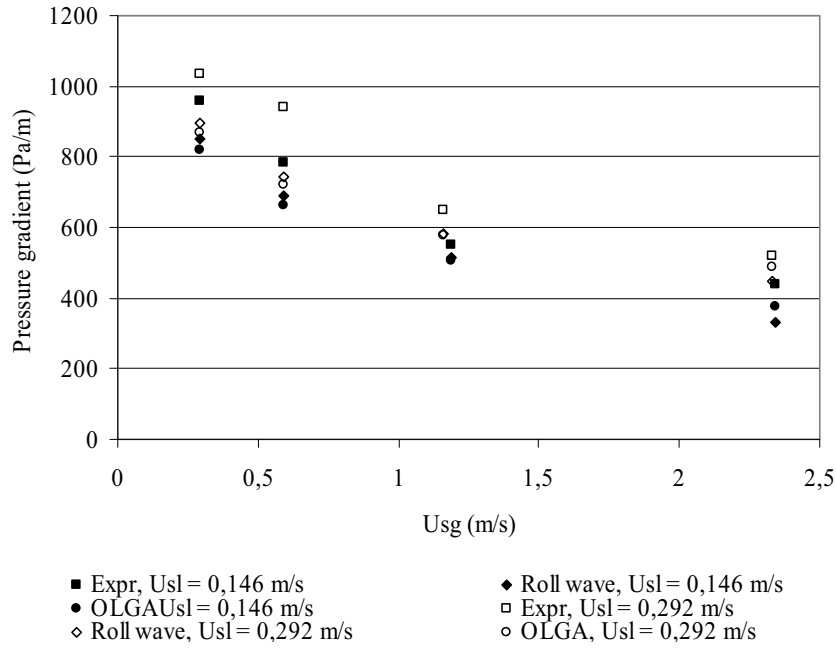

f) 10 degrees pressure gradient

Figure 1. Average liquid holdup or pressure gradient in Pa/m vs. Usg, in m/s for large amplitude wave experimental (■, □), commercial simulator OLGA® (●, ○) and the roll wave model (♦, ◊) results. Filled symbols (■, ●, ♦) are for Usl = 0.146 m/s, and open symbols (□, ○, ◊) are for Usl = 0.292 m/s.

In general, the two numerical models predicted similar results for both H and pressure gradient. Predictions from both models were accurate but they tended to under-predict the experimental pressure gradient.

In figures 1a through 1c, results for H are plotted at 1, 5 and 10 degrees respectively. The roll wave model and commercial simulator gave similar results which were very close to the experimental H. Agreement from both models was quite good for H, however at Usl = 0.292 m/s and large Usg both models under-predicted H.

Figures 1d through 1f show the pressure gradient results for 1, 5, and 10 degrees respectively. The plots showed that both models under-predicted the pressure gradient. Both gave about the same result for the lowest Usg value but at higher Usg, the commercial simulator was slightly more accurate.

The average percentage errors from the roll wave model and the commercial simulator were quantified and compared in Table 1.

Table 1. Average percentage errors between the roll wave model, commercial simulator OLGA®, and the experimental results.

	% Error in liquid holdup, H		% Error in pressure gradient	
	Roll wave	OLGA®	Roll wave	OLGA®
Overall average	-0.53	-2.3	-11.4	-8.6
Minimum	-13.1	-11.8	3.5	3.8
Maximum	6.4	2.8	-24.4	-23.4
Average for 1 degree	-0.76	-3.2	-5.0	-0.73
Average for 5 degrees	-0.66	-1.4	-13.1	-8.4
Average for 10 degrees	-0.28	-2.5	-14.1	-13.7
Average for Usl = 0.146 m/s	0,09	-1.7	-10.3	-8.6
Average for Usl = 0.292 m/s	-1.9	-2.9	-12.4	-8.6

The overall average percentage error between the experimental measurements and the roll wave model for H was -0.53%. This average percentage error was within the 5% experimental error in H [3] and was less than half the average percentage error of -2.3% from the commercial model. The maximum was 6.4% and the minimum was -13.1%. The minimum percentage error of -13.1% occurred at 1 degree pipe inclination, Usg = 2.34 m/s and Usl = 0.292 m/s. This deviation was quite a bit larger than the other data points with Usg = 2.34 m/s.

Both models tended to under-predict experimental H on average. The roll wave model performed slightly better overall but the maximum error for the roll wave model was larger than the commercial simulator. Looking at average error by angle, the roll wave model agreed slightly better for all angles and both models were within the 5% experimental error [3]. Looking at average error for each of the Usl 0.146 m/s and 0.292 m/s, the roll wave model had the smaller average percentage error.

The pressure gradients obtained from both models were quite similar, especially at 10 degrees, but the commercial simulator was slightly more accurate on average with -8.6% average error compared to -11.4% from the roll wave model and an experimental error of 10% [3]. The range in minimum to maximum error for both models was similar as seen in Table 1. The minimum error in the roll wave model belonged to the 10 degrees, Usg = 2.34 m/s, Usl = 0.146 m/s case. This case also had a poor agreement with experimental H. Since the classification of large amplitude waves includes other types of waves in addition to roll waves, it could be that in this particular case another type of large amplitude wave occurred and so the large percentage difference. The minimum percentage error in pressure gradient for the commercial model occurred at 10 degrees, Usg = 0.59 m/s, and Usl = 0.292 m/s. One reason for this could be that the commercial simulator was unable to account for large amplitude waves. Mostly however, the results from both models for pressure gradient were within 20% of the experiments.

At all angles 1, 5 and 10 degrees the commercial simulator agreed slightly better with the experimental pressure gradient than the roll wave model, however at 10 degrees the error was about the same in both. The commercial simulator also agreed better with experiments for both Usl, with a consistent -8.6% error.

6.2 Comparison of roll wave model to all experiments

During the gas-condensate experiments there were several flow regimes observed: stratified, slug, large amplitude wave, annular, and a transition from stratified to annular. The roll wave model was compared with all experiments and average percentage errors for each flow regime were calculated. Assuming that large amplitude wave experiments contained roll waves, the roll wave model could be most accurate for that flow regime. The average error between the roll wave model and the experiments for the large amplitude wave regime could therefore be a reference number to compare the average errors from other flow regimes.

The roll wave model's performance for the stratified, slug, annular, and transition stratified-to-annular experiments is discussed first. Then the model's performance at each angle of inclination is discussed.

6.2.1 Comparison by flow regime

The 14 experiments with largest Usg around 8.8 m/s were identified as the annular flow regime at all angles of inclination. Differences in liquid height were less than 3.5% and 0.53% on average. Agreement in pressure gradient was poor, with percentage error greater than 35% because the assumptions for modelling the roll wave regime did not apply to annular flow.

Experiments, 14 in total, with a gas flow rate around 4.7 m/s were classified as a transition between stratified flow and annular at all angles of inclination. The difference between experiments and the roll wave model for 0, 1, 5, 10, and 0.1 degrees was less than 18% in pressure gradient and less than 4.0% (-1.6% on average) in H for all angles. Agreement in pressure gradient for negative angles was poor, especially at -6 degrees with error greater than 60%. The transition of stratified to annular flow might have contained large waves, possibly at the positive angles which had better agreement than negative angles in pressure gradient.

The average percentage error in H between stratified flow experiments, 33 experiments in total, and the model was 4.7% which was larger than the -0.53% average error for the large amplitude wave cases. Agreement in H for the largest H values was poorest, for example, at 0.1 degrees, Usg = 0.29 m/s, Usl = 0.146 m/s the error was 19.0% where H = 0.53, most likely because this stratified flow experiment did not contain roll waves which the model was intended for. Agreement in pressure gradient was good with average percentage error -2.3% compared to an average error of -11.4% for the large amplitude wave experiments. The roll wave model might perform well in calculating the pressure gradient for this flow regime because it was based on the two-fluid equations for stratified flow.

For slug flow experiments, the roll wave model predicted H within 3.5% and total pressure gradient within -5.5% on average for a total of 4 experiments. Average error in H was larger than the large amplitude wave cases, but agreement in pressure gradient was better. A possible explanation for the roll wave model's success in modelling slug flow was that the slugs were just touching the top of the pipe and perhaps were not too far from being large roll waves. However the roll wave model's success in modelling

slug flow would need to be investigated further as it was only compared to 4 experiments.

6.2.2 Comparison by angle

The regimes which occurred for horizontal flow included stratified and annular flow, but not large amplitude waves. The pressure gradient agreement was 3.0% on average and ranged from -31 % to over 45% for annular flow experiments when Usg was 8.8 m/s. Most of the stratified experiments had a percentage error less than 20% in pressure gradient for intermediate velocities. For H agreement between model and experiment was 1.4% on average, slightly larger than that the large amplitude wave experiments. Agreement in H was a bit better for Usl = 0.292 m/s, -1.9% on average compared to 4.7% when Usl = 0.146 m/s. At 0 degrees, the roll wave model was better at predicting pressure gradient for stratified flow. As mentioned earlier, this was probably because the roll wave model was based on the two-fluid equations for stratified flow.

Several experiments at 1 degree of inclination were identified as large amplitude waves. For all experiments at 1 degree, the agreement in pressure gradient was good, 7.0% on average, and most errors under 20% except for the highest Usg value in the annular flow regime which was overpredicted by more than 45%. For H, the average percentage error was 0.53%, the same as that for large amplitude waves. The roll wave model gave good agreement with most experimental cases at 1 degree, probably because several of the experiments contained large amplitude waves.

For experiments inclined at 5 degrees, several were identified as large amplitude waves. The average error in pressure gradient was 0.2% and for most experiments error was less than 20% except for the largest Usg which had an error greater than 45%. These were the annular flow experiments. The average percentage error in H for 5 degrees was 1.2%, slightly larger than that for large amplitude waves. The roll wave model predicted most experiments at 5 degrees reasonably well most likely because several of the experiments were identified with large amplitude waves.

At 10 degrees, most of the experiments were identified as large amplitude waves but also included some annular flow at largest Usg. As with 0, 1 and 5 degrees, the largest Usg case was overpredicted by at least 35%. Average percentage error was -3.6% an improvement over the large amplitude wave average. The majority of errors were under 20%. The average error in H was 0.4%, a bit less than the large amplitude wave average. The roll wave model predicted most of the 10 degrees experiments accurately since most were identified as having large amplitude waves.

For 0.1 degrees inclination, there might have been a hydraulic gradient that affected the experimental results [3]. The model followed the trend of the experimental pressure gradient well with average error of 17%, except the largest Usg which was annular flow. This was overpredicted by more than 55%. H was overpredicted for low Usg where H was larger than 0.3, then agreement improved at larger Usg values. The average error in H was 6.5%. At the larger H values, with the lowest Usg values, the differences were between 9.0% and 18% in H. The roll wave model assumptions might not apply to calculating large H values in stratified flow.

The roll wave model predicted a ratio of interface friction factor to gas wall friction factor. This quantity should be always positive, however, for both -1 and -6 degrees, negative friction factor ratios were calculated. This happened when a negative pressure gradient occurred experimentally and flow was stratified. Downward inclined stratified

flow with negative pressure gradients seemed to be outside the applicability of the roll wave model. Results with negative friction factors were not considered since negative friction factors are not physical. The roll wave model, however, did produce physical results with a positive friction factor ratio for the three highest Usg in the downward inclined experiments.

The average error in pressure gradient for -1 degrees was 21.8%, for -6 degrees it was 43.1%. For Usg around 8.8 m/s, i.e. annular flow, error in pressure gradient was greater than 55%. Average error in H for -1 degrees was -2.0% and -0.32% for -6 degrees for the cases where the model calculated positive friction factors. None of the downward inclined experiments, however, were identified with large amplitude waves.

7 CONCLUSIONS

When comparing to the large amplitude wave experiments, the roll wave model and the commercial simulator OLGA® gave similar results which compared accurately with the experimental data. It was expected that the commercial simulator would compare well with the gas-condensate data set which was used partly in the development of the software. The fact that the roll wave model, without any model tuning, gives similar results to both the commercial simulator and the experimental data indicates that that the roll wave model performed well.

For all experiments with annular flow, the pressure gradient was greatly overpredicted by the roll wave model because the roll wave model assumptions did not apply to annular flow. Predictions for cases with slug flow, large amplitude wave flow, stratified wavy flow and the transition stratified to annular were generally within 20%. The model gave the best predictions in H for the large amplitude wave and annular experiments and the best prediction in total pressure gradient for stratified flow.

The predictions from the roll wave model for horizontal and positive inclinations were more accurate than the negative inclinations on average, however none of the experiments at negative inclinations were identified with large amplitude waves and may have been outside the applicability of the roll wave model. The best performance of the model occurred at 1, 5, and 10 degrees because several of the experiments at these inclinations contained large amplitude waves, likely including roll waves, which the model was intended for.

The roll wave model was not tuned to the experimental data, so potentially if the model were tuned it could give even more accurate results. The model did not compare as well to negative inclinations, however none of these experiments were identified with large amplitude waves. To give a better idea of how the model performs for negative inclinations, it should be compared against experiments with roll waves in downward inclined pipes.

8 ACKNOWLEDGEMENTS

Financial support from Total E&P Norge AS is gratefully acknowledged by A. De Leebeeck.

9 REFERENCES

[1] Kvandal, H., Munaweera, S., Elseth, G. and Holm, H. (2002) "Two-phase Gas-Condensate Flow in Inclined Pipes at High Pressure", SPE 77505, ATCE, San Antonio, USA.

[2] Johnson, G. W. (2005) "A study of stratified gas liquid pipe flow". Dissertation. Mechanics Division, Department of Mathematics, University of Oslo, Norway.

[3] Kvandal, H., Elseth, G., Munaweera, S. (2003), "Inclined pipe project. Gas/condensate campaign. Experimental results and model prediction from 2-phase gas condensate tests". Report. Oil and Energy Research Centre Porsgrunn, Norway.

[4] OLGA® 5 User Manual, SPT Group.

[5] Goldszal, A., Monsen, J. I., Danielson, T. J., Bansal, K. M., Yang, Z. L., Johansen, S. T., Depay, G. (2007) "LedaFlow 1D: Simulation results with multiphase gas/condensate and oil/gas field data", BHRG.

[6] Haaland, S. E. (1983), "Simple and explicit formulas for the friction factor in turbulent pipe flow," Journal of Fluids Engineering, Vol. 105, pp. 89-90.

Paper 2

Experiments on large roll waves in air-water pipe flow at atmospheric pressure

A. De Leebeeck and O. J. Nydal

To be submitted to the International Journal of Multiphase Flow

Experiments on large roll waves in air-water pipe flow at atmospheric pressure.

A. De Leebeeck and O. J. Nydal
Norwegian University of Science and Technology (NTNU)

January 10, 2010

Abstract

Two-phase air-water flow experiments have been conducted in inclined pipes at atmospheric pressure, with emphasis on the roll wave regime. The background for this work is in computational front tracking methods, where data on propagation velocities and pressure losses are needed. Pressure and liquid fraction time traces are obtained, together with video recordings. The results show that large amplitude roll waves have a pressure variation across the front similar to slugs, suggesting the possibility of modelling large amplitude waves in a similar way to slug flow. A mathematical relation for the observed pressure variation across waves is also discussed.

1 Introduction

Multiphase flow simulators are important tools for the design and operation of sub-sea pipelines carrying mixtures of oil and gas. Design considerations include both steady operation related to pressure drop, liquid content and temperatures, and dynamic flow conditions such as operational transients and unstable flows. The basic flow models in these simulators are one dimensional, and as the closure relations cover averaged physical phenomena they are normally empirically determined. Experimental data at realistic flow conditions then become an important basis for the modelling work.

In slug flow, liquid slugs block the pipe cross-section and they normally exceed 10 pipe diameters in length. Slug fronts advance over a liquid layer, which is absorbed and accelerated to the liquid phase velocity in the slug front. Liquid is then shed at the tail of the slugs (bubble nose), and decelerated along the trailing bubble.

Previous experiments have looked at measuring slug properties such as their propagation velocity, pressure variation, length and frequency [8, 10, 19, 27, 28]. Some of the slug flow experiments have resulted in mathematical correlations, for example bubble nose velocity [4], which have been used in later numerical models [5, 6, 12, 15, 16, 21].

Flow with large amplitude roll waves occurs in particular for high pressure systems corresponding to high gas densities. Although this regime has some similarities with slug flow, it is often treated as averaged stratified flow in one-dimensional flow models.

Similarities between flows with large amplitude roll waves and slug flow include the sharp propagating front which overruns a liquid layer and a sloping tail as the liquid shed behind the wave decelerates. Roll waves also transport liquid and propagate at a velocity greater than the liquid phase velocity.

Typical differences between the two flow regimes are in the length scales and the magnitude of the front velocities. Wave fronts are on the order of a few pipe diameters long as opposed to tens of diameters for typical slug lengths. Wave front velocities are much slower than slug

velocities. The roll wave regime is also more irregular, with a larger spread in velocities and amplitudes. Waves can be seen to collapse and to merge with other waves, or grow to slugs. The wave regime can perhaps be thought of as a transitional regime towards slug flow. Many experimental studies have focused on the transition to wavy flow or to slug flow [2,3,9,18,25] and many experimental studies of slug flow have been made in the past, for example [8,10,19,25,27]. Much less experimental work has been presented for roll waves. One reason may be that this regime is more dominant in high pressure systems than in low pressure [14].

Slug flow can be modelled as an average flow ('unit cell model') and there are several variations of such models presented by [24]. Wavy flow is also often treated as an extension of stratified flow, with closure laws adjusted accordingly. Front tracking models resolve the dynamics on the scale of slugs [12, 15, 16, 21]. When waves are on a similar scale as slugs, it would be consistent to include a wave tracking model, in particular when the transition from stratified to slug flow is through the regime of large amplitude waves.

The objective of this work is to determine if large roll waves have a pressure variation across the front similar to slugs and to measure some of their characteristic quantities: pressures, wave heights, and propagation velocities. An experimental study has been made on roll waves before in a 0.1 m internal diameter (I.D.) pipe with high gas densities [14] measuring their characteristic quantities. The added value of the present experiments is in the investigation of the pressure response of individual waves, which is information lacking in most other previous experimental studies [14, 19, 20, 27, 28]. The experiments are conducted in an atmospheric flow loop with air and water. An interpretation of the measured pressure variation across roll waves is also discussed in relation to a tracking model.

2 Experimental Method

Flow conditions where roll waves occur were identified in the pipe by an initial screening of pipe inclinations and flow rates. Then liquid phase fractions (holdups) and pressure variations were recorded at selected flow conditions. Video recordings with a time stamp were also taken for visual comparison to the measurements.

A straight acrylic pipe test section with 0.06 m I.D accurate to 1%, 16.4 m long, was used. The total range of pipe inclinations possible were from -15° to $+15^\circ$ from the horizontal. These angles were measured with a digital protractor.

Working fluids in the test section were air and water at atmospheric pressure and $20^\circ C$. A frequency controlled centrifugal pump circulated the water through its own line before it entered the mixing section at the inlet of the test section. Air was supplied from a pressurized line through a control valve. On exit, air was vented to the atmosphere and the water recirculated.

Water flow rates were measured with two different electromagnetic volume flow meters for low flow rates and higher flow rates. A coriolis mass flow meter was used for low gas rates while a vortex volume flow meter was used for higher gas rates.

The liquid phase fraction (holdup) was measured at four locations along the test section, as shown in figure 1, using 4 pairs of conductance ring probes built in house. The four holdup time traces later allowed the evolution of waves and slugs to be tracked and their speed to be determined. The pressure variation over waves and slugs was measured with an absolute pressure transducer, location shown in figure 1. To allow visual identification of waves and slugs, video was taken at 25 fps using a video camera. A colored dye was added to the water phase for ease of visualization.

All flow rates, liquid phase fractions, and pressures were recorded on a workstation with a data acquisition board. An in house Labview program controlled the data acquisition.

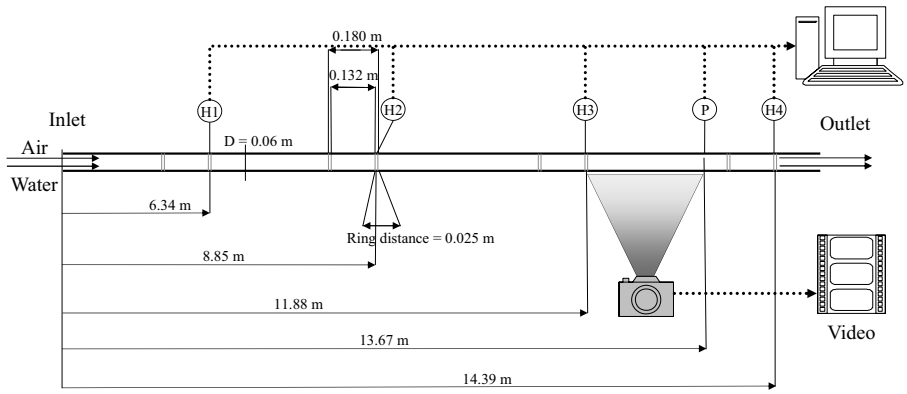

Figure 1: Schematic of multiphase flow test section with the position of holdup probes, pressure transducer, and video camera. H1, H2, H3, H4 - conductance ring probes measuring holdup. P - pressure transducer.

After calibrating the instruments and choosing flow conditions with waves and slugs, a total of 51 experimental cases were recorded at the following inclinations and superficial phase velocities:

- Inclinations of -1, 0, 1, 2, and 2.8 degrees
- Water superficial velocities (U_{sl}) of 0.04 to 0.52 m/s
- Air superficial velocities (U_{sg}) of 1.5 to 11.5 m/s

The average velocities of waves and slugs in a given experiment were determined from cross-correlating the holdup time signals of adjacent ring probes. The cross-correlation gave the characteristic time required for a wave to travel a known distance from one probe to the next. The 95% percentile values of the time series were taken as characteristic holdup peaks and pressure variations in waves and slugs.

Selected waves that appeared to be consistent between the third and fourth conductance probes were compared with images from the video recordings to control whether waves or slugs were producing the associated peaks in the pressure signal.

3 Results and discussion

Liquid holdup and pressure time traces for a case with wave flow and a case with slug flow are shown in figures 2 and 3. The time traces have been shifted by the characteristic time delays determined from cross-correlations so that waves and slugs are aligned in the time plots. Arrows follow selected waves and slugs from one time trace to the next. Straight lines indicate where holdup peaks measured by the fourth holdup probe correspond to peaks in the pressure signal. Similarities between the case of slugs and wave include the presence of sharp peaks followed by a sloping tail and the corresponding pressure peak. Differences are in the height of the peaks. Peak holdups for waves are around 0.5 while for slugs peaks are well above that, between 0.9 and 1.0. Pressure peaks for the wave case are below 5000 Pa while most of the slug pressure peaks are above 5000 Pa.

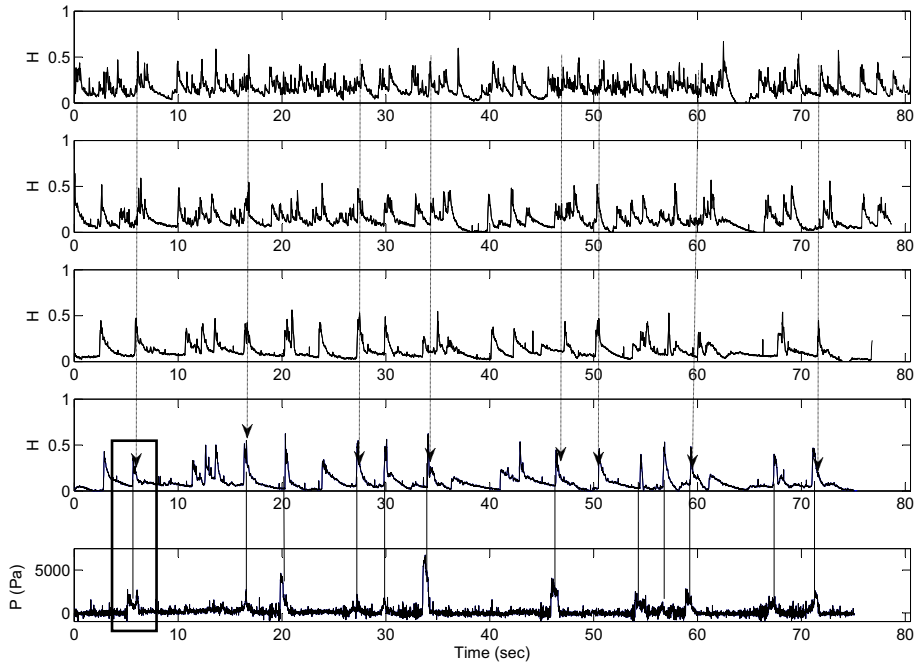

Figure 2: Holdup and pressure time traces at wave conditions. $U_{sl} = 0.17$ m/s, $U_{sg} = 5.89$ m/s, and horizontal pipe. The 1^{st} holdup trace is on top followed by the 2^{nd}, 3^{rd}, and 4^{th} holdup time traces, and the pressure time trace at the bottom.

The time traces for the wave case in figure 2 were recorded at $U_{sl} = 0.17$ m/s, $U_{sg} = 5.89$ m/s and in a horizontal pipe. The characteristic holdup, pressure peak value and wave velocity are 0.28, 1400 Pa, and 1.86 m/s respectively. The waves seem to be more consistent from the third to the fourth holdup measurement, but result from the merging of several waves seen in earlier holdup time traces.

The pressure and holdup peaks inside the box in figure 2 at 5 sec are matched to their corresponding video snapshot in figure 4. The snapshot shows the wave does not completely block the pipe as a slug would. The holdup peaks from the third and fourth holdup probe and the pressure peak are plotted overlapping and shifted in time so the peaks are aligned. This individual wave moves at 1.67 m/s, which is close to the average wave velocity for this experiment, 1.86 m/s. The time traces and matched video show that waves do in fact have a corresponding pressure variation.

The slug time traces in figure 3 were measured at $U_{sl} = 0.52$ m/s, $U_{sg} = 3.63$ m/s, and -1 degrees of inclination. Characteristic holdup, pressure peak, and slug velocity were 0.47, 4800 Pa, and 4.92 m/s respectively. As opposed to the wave case, the slug holdup peaks seem to be consistent through most of the time traces. Some of the smaller holdup and pressure peaks probably correspond to waves occurring between slugs.

The slug holdup and pressure peaks inside the box in figure 3 at 21 sec are plotted overlapped with peaks aligned and shown with their video snapshot in figure 5. The snapshot is of the slug front and shows the liquid phase completely fills the pipe in the slug. The velocity of this

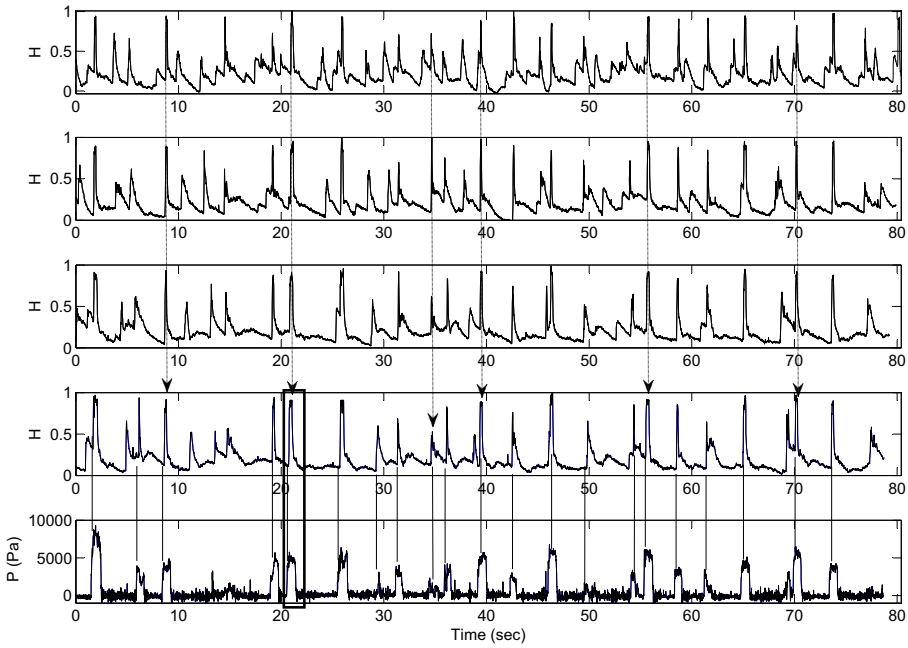

Figure 3: Holdup and pressure time traces at slug conditions. $U_{sl} = 0.52$ m/s, $U_{sg} = 3.63$ m/s, and inclination of -1 degrees from horizontal. The 1^{st} holdup trace is on top followed by the 2^{nd}, 3^{rd}, and 4^{th} holdup time traces, and the pressure time trace at the bottom.

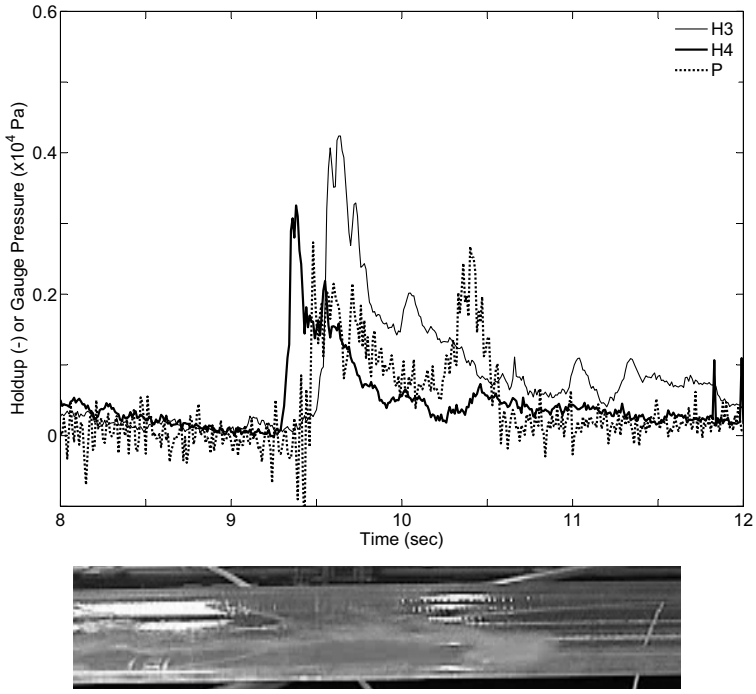

Figure 4: An individual wave: peaks from the 3^{rd} holdup time trace H3, the 4^{th} holdup time trace H4, and the pressure time trace P overlapped (top plot) and corresponding video snapshot (bottom). $U_{sl} = 0.17$ m/s, $U_{sg} = 5.89$ m/s, and horizontal pipe.

individual slug is 4.92 m/s. As expected and as described in other experiments [8,19], slugs are also observed to have a pressure variation across them.

As expected, slugs travel faster than waves. This type of behavior in wave and slug velocity has also been shown in [10,19,27]. In figure 6, the average wave and slug velocities determined from cross-correlations are plotted against the mixture velocity U_{mix}. A commonly used relationship for determining the slug velocity $U_{slug} = 1.2U_{mix}$ is also plotted for comparison. The data points grouped around this line correspond mainly to experiments with slug flow, while those with smaller velocities have majority waves. The increase in slug velocity with mixture velocity is much more apparent than with waves. The relationship between wave velocity and mixture velocity is less clear but seems to be increasing slightly.

In figure 7, the characteristic pressure variations across waves and slugs are plotted against the average wave or slug velocity. The trend is for pressure variation to increase with the wave or slug velocity as waves speed up and slugs take over. Velocities below 4 m/s correspond more readily to waves as seen in figure 6. The average pressure variation for cases with velocity less than 4 m/s is 2300 Pa while above 4 m/s it is 4700 Pa. The pressure variations fall in the range of 800 Pa to 8300 Pa and the range on wave or slug velocities is 1.39 m/s to 6.78 m/s.

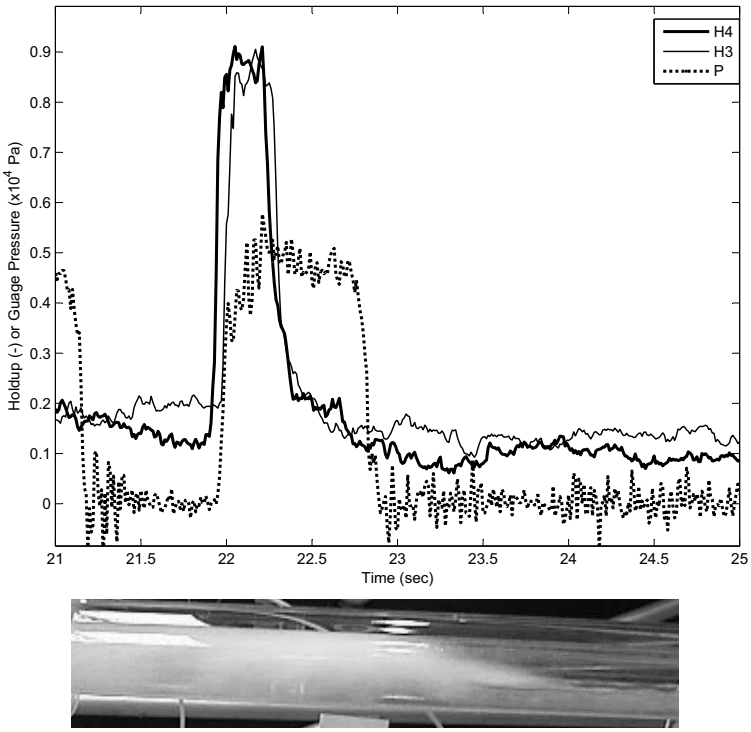

Figure 5: An individual slug: peaks from the 3^{rd} holdup time trace H3, the 4^{th} holdup time trace H4, and the pressure time trace P overlapped (top plot) and corresponding video snapshot (bottom). $U_{sl} = 0.52$ m/s, $U_{sg} = 3.63$ m/s, and inclination of -1 degrees.

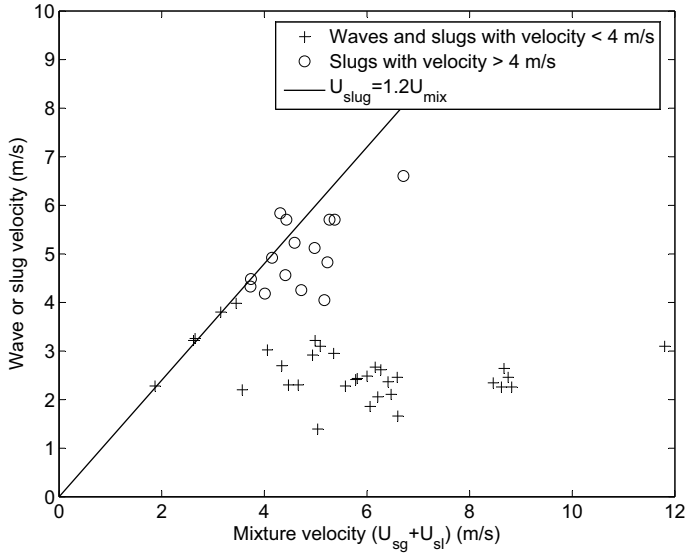

Figure 6: Experimental wave or slug velocity and theoretical slug velocity against mixture velocity. The crosses (+) appearing along the $U_{slug} = 1.2U_{mix}$ line correspond to cases with slugs.

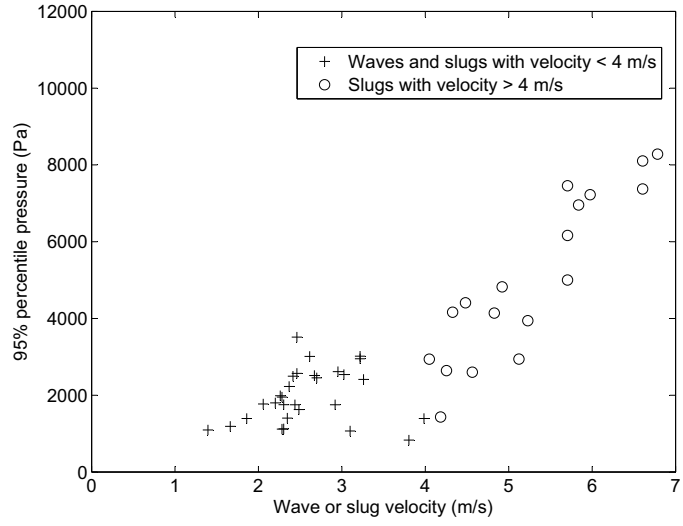

Figure 7: Experimental pressure variation against wave or slug velocity.

3.1 Towards modelling

Numerical modelling can be applied to resolve flow dynamics at length scales from a pipe diameter to systems of several hundred kilometers. At the pipe diameter length scale, individual slug and wave dynamics can be captured numerically by solving a two-phase flow model on a small grid. This has been demonstrated using a two-fluid model, with a set of conservation equations for both phases [7, 11, 13, 23]. However, such models are sensitive to the numerical scheme, and the computational times can be prohibitive for simulation in long pipelines.

Alternatively, tracking schemes [12, 15, 21] which employ a grid moving with the fronts can allow for computations with orders of magnitude fewer grid points than with a capturing scheme. The grid velocities in tracking schemes are the characteristic bubble propagation velocity in slug flow and the front velocities derived from mass balances, or could be the wave propagation velocity.

Small scale dynamics of slug or wave flow is often less important for simulation in long pipelines with lengths up to tens and hundreds of kilometers. In these cases, slug flow can be treated as a quasi-stationary flow, with averaged pressure drop and liquid fraction over several slug-bubble units. Time and length scales related to the dynamics would be on the order of transport times and riser lengths, not on diameter scales. Steady state unit cell slug flow models combine models for bubbly flow in the slug region and stratified flow in the bubble region related by mass balance equations [6]. These models can be solved as a point model and integrated into dynamic simulators. Stratified wavy flow is often modelled as averaged stratified flow assuming an average interface geometry and using empirically determined interface friction relations [1, 22]. This is probably a reasonable approach when the waves are small. For the roll wave regime, with breaking waves and significant liquid transport in the waves, improvements may be possible by using approaches similar to slug flow.

Unit wave models have also been derived for the roll wave regime, based on discontinuous numerical solutions of the gas and liquid mass and momentum balance equations [14]. A wave tracking model has also been tested in a slug tracking scheme [17].

The present experiments have shown that the pressure drop in large amplitude wavy flows is largely made up of a pressure change over the waves. This could suggest a modelling approach similar to slug flow as in dynamic tracking models. An integral wave model is then needed, including relations for the wave velocity, wave height, and pressure variation across the wave.

Assuming the pressure variation is the same in both liquid and gas phase, the gas and liquid momentum equations could be solved across a wave front. In the liquid phase, the pressure variation is mainly related to the acceleration of the liquid at the wave front. Gas flow over a large wave can be thought of as similar to gas flow through an orifice. An orifice type relation could be used to represent losses in the gas phase momentum equation.

The starting point for such a model is with the single phase gas velocity through the throat of an orifice U_t, equation 1 [26].

$$U_t = C_d A_t \left(\frac{2\Delta P_{orifice}/\rho_g}{1 - (A_t/A_{pipe})^2} \right)^{\frac{1}{2}} \tag{1}$$

C_d is the discharge coefficient, A_t is the orifice throat area, A_{pipe} is the pipe cross-sectional area, and ρ_g is the gas density.

Rewriting equation (1) to give the pressure variation across the orifice $\Delta P_{orifice}$ gives the following:

$$\Delta P_{orifice} = \frac{1}{2} \frac{1}{C_d^2} \rho_g U_t^2 \left(1 - (A_t/A_{pipe})^2 \right) \tag{2}$$

In thinking of gas flowing over a large wave front as similar to gas flow through an orifice, several modifications are made to the orifice relation in equation (2). The wave is no longer stationary so U_t is replaced with the difference between the gas phase velocity over the wave $U_{g,wave}$ and the velocity of the wave front U_{wave}.

$$U_t \Rightarrow U_{g,wave} - U_{wave} \tag{3}$$

$$U_t^2 \Rightarrow (U_{g,wave} - U_{wave}) \, |U_{g,wave} - U_{wave}| \tag{4}$$

The orifice relation is for single phase flow with only the gas phase. For two-phase flow, the gas phase occupies only a fraction of the pipe. In equation (2), the term A_{pipe} is replaced with the gas phase area in stratified regions between waves $A_{g,bubble}$. The area of the orifice throat can be thought of as the area occupied by the gas at the wave front $A_{g,wave}$ where wave height is a maximum. The ratio of the two areas can then be written in terms of gas or liquid area fractions.

$$\frac{A_t}{A_{pipe}} \Rightarrow \frac{A_{g,wave}}{A_{g,bubble}} = \frac{A_{g,wave}/A_{pipe}}{A_{g,bubble}/A_{pipe}} = \frac{1 - H_{wave}}{1 - H_{bubble}} \tag{5}$$

H_{wave} is the liquid holdup at the wave peak and H_{bubble} is the holdup in the thin liquid film between waves.

Finally the pressure loss in the gas phase for a wave is written as in equation (6).

$$\Delta P_{wave} = \left[\frac{1}{2} \frac{1}{C_d^2} \rho_g \left(1 - \left(\frac{1 - H_{wave}}{1 - H_{bubble}} \right)^2 \right) (U_{g,wave} - U_{wave}) \, |U_{g,wave} - U_{wave}| \right] \tag{6}$$

The discharge coefficient C_d is a loss coefficient [26] accounting for friction and compressibility in an orifice. Empirical relations for C_d have been determined, depending on the ratio of the orifice throat to pipe diameter, Reynolds number, and the type of taps (corner taps or flanges for example) in the orifice [26]. The typical range of values for C_d is from 0.59 to 0.66 [26] in an orifice. This loss coefficient then needs to be found for the case of waves.

Rough estimates of C_d have been made using equation (6) where ΔP_{wave} was the measured pressure variation, U_{wave} is the measured wave velocity, H_{wave} is the wave peak holdup, and H_{bubble} is the holdup of the thin liquid film between waves. A range of wave peak holdups between 0.4 and 0.8 were used. The wave gas phase velocity $U_{g,wave}$ was estimated from a known U_{sg} and the wave peak holdup. Experimental data used in this estimation were from cases where a majority of waves occurred.

Estimated values of C_d were scattered, but most appeared to occur between $C_d = 0.1$ and 0.5. The mean value of estimated C_d was 0.3, the lower and upper quartile estimates were 0.2 and 0.4 respectively. As a first approximation, a value of $C_d = 0.4$ was used in modelling gas flow over large waves in a front tracking scheme [17].

4 Conclusions

Experiments to measure the detailed pressure response in large amplitude waves have been carried out in air-water pipe flow at near horizontal conditions and atmospheric pressure. Time traces from four holdup probes and one pressure transducer in combination with video have been recorded and wave and slug velocities obtained from cross-correlating the holdup signals.

As expected, resulting average wave velocities were smaller than slug velocities as well as mixture velocities. From corresponding holdup, pressure and video recordings, it was observed that large amplitude waves had a pressure variation across them similar to slugs but of lesser

magnitude. These pressure measurements and other similarities suggest that roll waves could be modelled in a similar way to slugs. Interpretation of the pressure drop in terms of an orifice type relation indicate an average value of about $C_d = 0.3$.

5 Acknowledgment

Financial support from Total E&P Norge, Stavanger, Norway is gratefully acknowledged by A. De Leebeeck. The authors would like to thank Masters student A. H. Gaarder for his help in running the experiments.

References

[1] N. Andritsos and T. J. Hanratty. Influence of interfacial waves in stratified gas-liquid flows. *AIChE Journal*, 33(3):444–454, 1987.

[2] N. Andritsos, L. Williams, and T. J. Hanratty. Effect of liquid viscosity on the stratified-slug transition in horizontal pipe flow. *Int. J. Multiphase Flow*, 15(6):877–892, 1989.

[3] D. Barnea and Y. Taitel. Kelvin-helmholtz stability criteria for stratified flow: Viscous versus non-viscous (inviscid) approaches. *Int. J. Multiphase Flow*, 19:639–649, 1993.

[4] K. H. Bendiksen. An experimental investigation of the motion of long bubbles in inclined tubes. *Int. J. Multiphase Flow*, 10:467–483, 1984.

[5] K. H. Bendiksen, D. Malnes, R. Moe, and S. Nuland. The dynamic two-fluid model olga: Theory and application. In *SPE Production Engineering*, 1991.

[6] K. H. Bendiksen, D. Malnes, and O. J. Nydal. On the modelling of slug flow. *Chem. Eng. Comm.*, 141-142:71–102, 1996.

[7] M. Bonizzi and R. I. Issa. A model for simulating gas bubble entrainment in two-phase horizontal slug flow. *Int. J. Multiphase Flow*, 29:1685–1717, 2003.

[8] Z. Fan, Z. Ruder, and T. J. Hanratty. Pressure profiles for slugs in horizontal pipelines. *Int. J. Multiphase Flow*, 3:421–437, 1993.

[9] T. J. Hanratty and A. Hershmann. Initiation of roll waves. *AIChE Journal*, 7:488–497, 1961.

[10] G. Hanyang and G. Liejin. Experimental investigation of slug development on horizontal two-phase flow. *Chinese Journal of Chemical Engineering*, 16:171–177, 2008.

[11] H. Holmås. *Numerical simulation of waves in two-phase pipe flow using 1D two-fluid models*. PhD thesis, University of Oslo, 2008.

[12] B. Hu, C. Stewart, P. D. Manfield, P. M. Ujang, C. P. Hale, C. J. Lawrence, and G. F. Hewitt. A model for tracking the evolution of slugs and waves in straight pipelines. In *6th International Conference on Multiphase Flow*, Leipzig, Germany, 2007.

[13] R. I. Issa and M. H. W. Kempf. Simulation of slug flow in horizontal and nearly horizontal pipes with the two-fluid model. *Int. J. Multiphase Flow*, 29:69–95, 2003.

[14] G. W. Johnson. *A study of stratified gas-liquid pipe flow*. PhD thesis, University of Oslo, 2005.

[15] J. Kjølaas. *Plug propagation in multiphase pipelines*. PhD thesis, Norwegian University of Science and Technology, 2007.

[16] M. Larsen, E. Hustvedt, and T. Straume. Petra: A novel computer code for simulation of slug flow. In *SPE Annual Technical Conference and Exhibition*, San Antonio, Texas, 1997.

[17] A. De Leebeeck and O. J. Nydal. Simulation of large amplitude waves in a slug tracking scheme compared to roll wave experiments at high pressure. *Int. J. Multiphase Flow*, 36:40–50, 2010.

[18] P. Y. Lin and T. J. Hanratty. Prediction of the initiation of slugs with linear stability theory. *Int. J. Multiphase Flow*, 12:79–98, 1986.

[19] P. Y. Lin and T. J. Hanratty. Detection of slug flow from pressure measurements. *Int. J. Multiphase Flow*, 13:13–21, 1987.

[20] M. Miya, D. E. Woodmansee, and T. J. Hanratty. A model for roll waves in gas-liquid flow. *Chemical Engineering Science,*, 26:1915–1931, 1971.

[21] O. J. Nydal and S. Banerjee. Dynamic slug tracking simulations for gas-liquid flow in pipelines. *Chem. Eng. Comm.*, 141-142:13–39, 1996.

[22] M. Ottens, K. Klinkspoor, H. C. J. Hoefsloot, and P. J. Hamersma. Correlations predicting liquid hold-up and pressure gradient in steady-state (nearly) horizontal co-current gas-liquid pipe flow. *Trans IChemE,*, 79:581–592, 2001.

[23] F. Renault. *A Lagrangian slug capturing scheme for gas-liquid flows in pipes*. PhD thesis, Norwegian University of Science and Technology, 2007.

[24] Y. Taitel and A. E. Dukler. A model for slug frequency during gas-liquid flow in horizontal and near horizontal pipes. *Int. J. Multiphase Flow*, 3:585–596, 1977.

[25] P. M. Ujang, C. J. Lawrence, C. P. Hale, and G. F. Hewitt. Slug initiation and evolution in two-phase horizontal flow. *Int. J. Multiphase Flow*, 32:527–552, 2006.

[26] F. M. White. *Fluid Mechanics*. McGraw Hill, Boston, 5th international edition, 2005.

[27] B. D. Woods, Z. Fan, and T. J. Hanratty. Frequency and development of slugs in a horizontal pipe at large liquid flows. *Int. J. Multiphase Flow*, 32:902925, 2006.

[28] B. D. Woods, E. T. Hurlburt, and T. J. Hanratty. Mechanism of slug formation in downwardly inclined pipes. *Int. J. Multiphase Flow*, 26:977–998, 2000.

Paper 3

Large amplitude waves in a slug tracking scheme

A. De Leebeeck and O. J. Nydal

Presented at the 5th International Conference on Multiphase Flow, New Forest, UK, June 15-17 2009 and published in *Computational Methods in Multiphase Flow V*, Editors A. A. Mamoli and C.A. Brebbia, pp. 99-109, Copyright 2009. Reproduced with permission from WIT Press, Southampton, UK

Large amplitude waves in a slug tracking scheme

A. De Leebeeck and O. J. Nydal
Department of Energy and Process Engineering, Norwegian University of Science and Technology (NTNU), Norway.

Abstract

Large amplitude roll waves are incorporated into a previously developed slug tracking scheme for two phase gas-liquid pipe flow. The applicability of the tracking scheme to large amplitude waves is demonstrated with a simplified model for the waves. The waves are modelled analogous to slugs on a moving grid with corresponding wave velocities and a pressure variation determined using an orifice type relation. Slugs and waves in the tracking scheme are separated by regions of stratified flow, which are modelled on a stationary grid using the two-fluid model. The computational scheme is described, compared to experimental data on roll waves, and some wave dynamics such as waves developing to slugs and slugs decaying to waves are demonstrated.

Keywords: roll waves, tracking, two phase pipe flow, modelling.

1 Introduction

In two phase gas-liquid pipe flow, different flow regimes occur depending on gas and liquid phase velocities, fluid properties, and pipe geometries. Various numerical strategies exist for the different flow regimes in dynamic models. Slug flow, for example, can be treated with unit cell models (Bendiksen et al. [2]), in slug capturing (Bonizzi et al. [3], Issa et al. [7], Renault [12]), or in tracking schemes [Taitel et al. [13], Nydal et al. [11]). Although capturing schemes (Issa et al. [7], Bonizzi et al. [3]) can model the initiation of slugs and roll waves, they require the use of fine grids which are computationally expensive and the large computational times are prohibitive for simulation in long pipelines. Tracking schemes, however, use orders of magnitude fewer grid

points. Tracking schemes can also be suitable for plug simulations (Kjølaas [9]). A combination of capturing and tracking has also been tested by Renault [12].

Large roll waves can have similar scales and behavior to slug flow in that they transport liquid and have a propagating front. A simple model treating waves as moving objects in a similar way as for slugs is therefore desired in the tracking scheme. Similarities between slugs and roll waves such as a propagating front and a sloping tail have been observed experimentally in, for example, Johnson [8]. Pressure variations across wave fronts similar to slugs have also been measured (De Leebeeck et al. [4]). These experiments are used to develop a wave model including the observed pressure variation.

The slug tracking scheme of Kjølaas [9] is the starting point for incorporating wave tracking capabilities into a slug tracking scheme. Slug flow is modelled as alternating liquid slugs and bubbles with stratified flow. The two-fluid model is solved on a stationary staggered grid in bubbles, while integral momentum equations are solved in slugs on a moving grid. Before the addition of wave tracking, decaying slugs were replaced immediately with stratified flow. With the addition of wave tracking, slugs can decay into waves, modelled analogous to slugs with integral momentum equations and their own front and tail velocities.

The tracking scheme of Hu et al. [6] includes wave tracking with a liquid height profile behind waves and slugs, solving the two-fluid model in combination with modelling the wave front as a hydraulic jump (Hu et al. [6]). Other models for roll waves include, for example, Johnson [8] and Holmås [5] who solve the two-fluid model with modified friction terms in roll waves. Johnson [8] assumes a sequence of repeating “maximum amplitude” waves with a sharp front and includes a unique interfacial friction factor as part of a steady state solution. The model of Holmås [5] model is dynamic and includes increased turbulence at the wave front using a modified Biberg friction model.

In our scheme, we simplify waves and slugs as square objects that can be modelled dynamically on a coarse grid. The dynamics of the waves and slugs are determined from mass and momentum balances. The stratified gas regions between waves and slugs are solved with a two fluid model. A large grid gives square shaped bubbles. Slug and wave tails can be reproduced by refining the grid in the bubble region.

2 Description of the model

The wave tracking model builds on a slug tracking scheme (Kjølaas [9]) which is coded in C++ using object oriented programming techniques. Slug flow is represented in one dimension with alternating slug objects that completely fill the pipe and stratified sections including both phases as shown in figure 1A. In stratified sections, the two-fluid model is solved on a stationary staggered grid where phase velocities are determined at section borders while pressure and masses are determined at section centers. Slug sections are modelled as moving objects where liquid phase velocity, slug length, front and tail velocities are determined from mass and momentum balances.

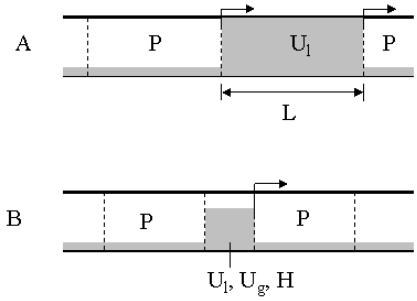

Figure 1. Schematic of models for A. slug flow and B. wave flow in the tracking scheme. The arrows indicate direction of flow. Dashed lines represent section borders. Gray – liquid phase. White – gas phase.

Waves, shown in figure 1B, are modelled in a similar way to slugs as moving objects and include a pressure variation due to liquid acceleration at the wave front. In the gas phase, the pressure variation across the wave front is modelled with an orifice type relation. Assuming that the pressure variation is the same in both phases, the phase velocities in the wave can be determined from the momentum balance equations. Front and tail velocities and liquid holdup are also determined in the wave assuming a fixed length as opposed to slugs which have a variable length.

Gas flow in a slug is modelled using a slip relation, however, in a wave the gas phase flows through a gap between the liquid phase and the upper pipe wall. In this way, gas flow over a large wave can be thought of as similar to gas flow through an orifice, and therefore an orifice type relation is used in the gas momentum balance eqn (1) for waves. The orifice type relation, the second term in eqn (1), replaces the gas wall and interfacial friction terms. Eqn (1) is then used to determine the gas velocity in a wave by relating it to the pressure variation across the wave front.

$$\begin{aligned} &\frac{M_g}{\Delta t}\Delta U_g \\ &+(1-H)A\frac{1}{2}\frac{1}{C_d^2}\rho_g\left(1-\left(\frac{1-H}{1-H_R}\right)^2\right)\cdot(U_g^{n+1}-U_{front})\left|U_g^n-U_{front}\right| \\ &=(1-H)A(P_L-P_R)-M_g g\sin\theta \end{aligned} \tag{1}$$

Using the same pressure variation across a wave front as in eqn (1), the liquid momentum balance eqn (2) is used to determine the liquid phase velocity in a wave. In the liquid phase, the main component giving pressure variation is the acceleration of the liquid at the wave front. There is also a contribution from liquid wall friction and gravity.

$$\frac{M_l}{\Delta t}\Delta U_l + H\rho_l A(U_l^n - U_{front})(U_{lR}^n - U_l^{n+1}) = HA(P_L - P_R) + (-\tfrac{1}{8}LS_l\lambda_l\rho_l\left|U_l^n\right|U_l^{n+1}) - M_l g\sin\theta \quad (2)$$

Slugs are modelled as objects with moving boundaries, the front of a slug moves with a front velocity determined from a mass balance across the front while the tail moves with a bubble nose velocity. If the front velocity is greater than the tail velocity, the slug will grow in length, otherwise its length will decrease. Similarly, waves are modelled as moving objects but they have a fixed length of one to two pipe diameters and move with the wave front velocity. The front velocity of a wave is determined from the mass balance across the front, eqn (3), and given in eqn (4).

$$H(U_l^{n+1} - U_{front}) = H_R(U_{lR}^n - U_{front}) \quad (3)$$

$$U_{front} = \frac{H}{H - H_R}U_l^{n+1} - \frac{H_R}{H - H_R}U_{lR}^n \quad (4)$$

One of the aims of the wave tracking scheme was to have a simplified model, therefore a simple wave tail speed relationship was desired. The wave tail speed is given in eqn (5).

$$U_{tail} = 1.2U_l \quad (5)$$

The factor of 1.2 allows for continuous transition between wave and slug flow. When the liquid holdup in a wave approaches unity, the liquid phase velocity in the wave approaches the mixture velocity. The bubble nose velocity or wave tail velocity is commonly related to the mixture velocity by a factor of 1.2.

The mass balance equations in a wave or slug are the same, where the change in mass in a given time step is the difference in mass flux in and out. Eqns (6) and (7) are the liquid phase and gas phase mass balance equations respectively. The liquid holdup is given in eqn (8).

$$\frac{\Delta M_l}{\Delta t} = \left(M_l^n(U_l^{n+1} - U_{tail})/L - M_l^n(U_l^{n+1} - U_{front})/L\right) \quad (6)$$

$$\frac{\Delta M_g}{\Delta t} = \left(M_g^n(U_g^{n+1} - U_{tail})/L - M_g^n(U_g^{n+1} - U_{front})/L\right) \quad (7)$$

$$H = \frac{M_l^{n+1}}{AL\rho_l} \quad (8)$$

Since wave fronts are modelled with a fixed length and they move at the wave front velocity, the wave tail velocity only appears in the mass balance eqns (6) and (7). If the front speed is larger than the tail speed the liquid mass in the wave will increase and vice versa. Therefore waves can grow or decay in amplitude.

2.1 Transitions and wave insertion

Waves can be formed from stratified flow or they can form from decayed slugs. At the transition from stratified flow waves are inserted according to the

inviscous Kelvin Helmholtz stability criteria, eqn (9). Neglecting surface tension and viscous effects, stratified flow is stable if (Barnea et al. [1], Lin et al. [10]):

$$\left(\frac{A_l}{\rho_l S_i}+\frac{A_g}{\rho_g S_i}\right)(\rho_l-\rho_g)g\cos\theta-(U_g-U_l)^2>0 \tag{9}$$

On the other hand, if a wave is dying, it will be removed when the holdup in the wave approaches the holdup in the stratified section in front of it.

A decaying slug will be converted to a wave when its length goes below a user defined minimum, i.e. one or two pipe diameters in length. In the reverse case where a wave grows to a slug, a wave will be converted to a slug if its holdup goes above a user defined maximum, e.g. a holdup of 0.99. Slugs can also form if two waves merge or a slug overtakes a slower moving wave.

3 Results and discussion

The roll wave tracking model has been compared with experiments that were conducted in the multiphase flow laboratory at NTNU in a 16 m long, 0.06 m I.D. pipe using air and water at atmospheric pressure (De Leebeeck [4]). The experiments included pipe inclinations from -1 to 3 degrees, Usg from 2 to 11.5 m/s, and Usl from 0.04 to 0.52 m/s where a mixture of waves and slugs occurred. Data for comparison include liquid holdup and pressure time traces, average wave velocities from cross correlation between holdup time traces, and pressure drop. One purpose of doing the experiments was to measure the pressure variation over a wave, as this is an assumption in the tracking model. This was confirmed in the experiments, and led to an estimate of the discharge coefficient in the orifice relation in eqn (1) of C_d = 0.2 to 0.4.

The simulations discussed here used a fixed grid size of 2 pipe diameters in wave fronts, a minimum of 20 and maximum of 100 pipe diameters in stratified sections. Pipe length, diameter, fluid properties, and a simulation time of 80 sec were as in the experiments. A discharge coefficient giving the best approximation of experimental wave speed and pressure variation with value C_d = 0.2 was used in the gas momentum equation for waves. The waves were inserted at a similar frequency to the experiments.

Figure 2 shows a plot of wave or slug velocity for all experiments and wave velocity from the model plotted against mixture velocity. The largest velocities are associated with slugs which have larger velocities than waves. The experiments with lower velocities contained more waves than slugs. Looking at the data qualitatively, the model gives wave velocities in the same range as the experiments.

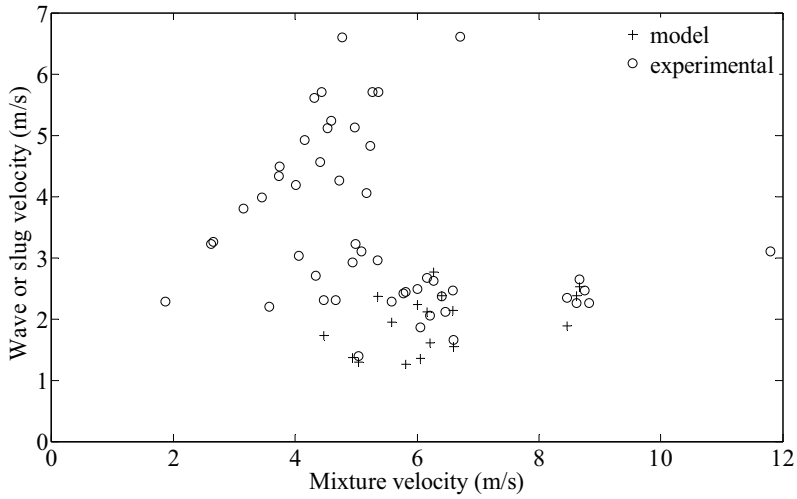

Figure 2. Experimental velocities compared with wave velocities from dynamic wave tracking simulations. For Umix < 4 m/s: mainly slug flow. Umix > 4 m/s: a mixture of waves and slugs.

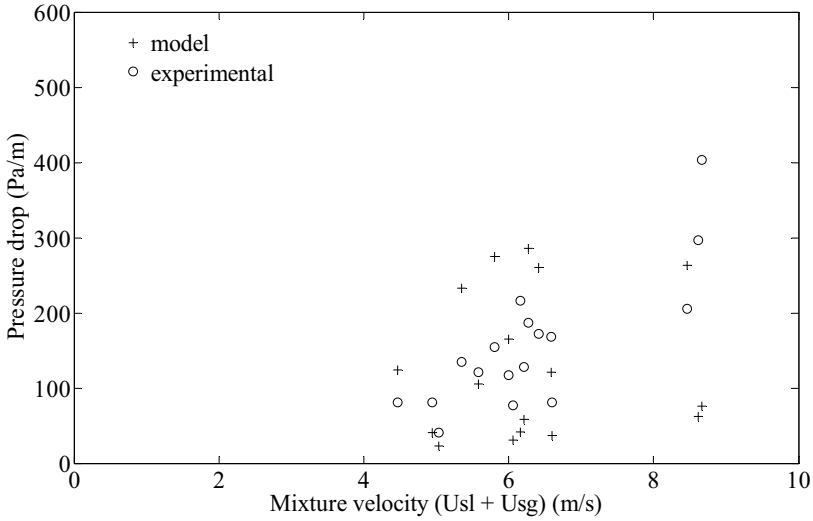

Figure 3. Experimental pressure drop compared with averaged pressure drop from tracking simulations.

In figure 3, the experimental and modelled pressure drops are compared. Although all of the simulations reproduced a pressure variation in waves, some of the pressure drops tended to be low compared to the experimental values. The magnitude of the pressure drop depends on the number of waves and slugs in the experiment or simulation. An experiment with more slugs will have a larger pressure drop than one with fewer. All the experiments contained a mixture of waves and slugs but some of the simulations, especially downward inclined, reproduced waves which did not grow to slugs resulting in low pressure drops.

One advantage of modelling waves in a tracking scheme is that coarse grids can be used allowing for longer pipe systems to be modelled. Using a coarse grid means that waves and slugs are modelled as square objects corresponding to the plots figure 4A, using a maximum stratified section length of 100 pipe diameters. Finer grids can be used, however, allowing for waves with more apparent tails, shown in figure 4B, as occurs in the experimental time traces, for example figure 4C.

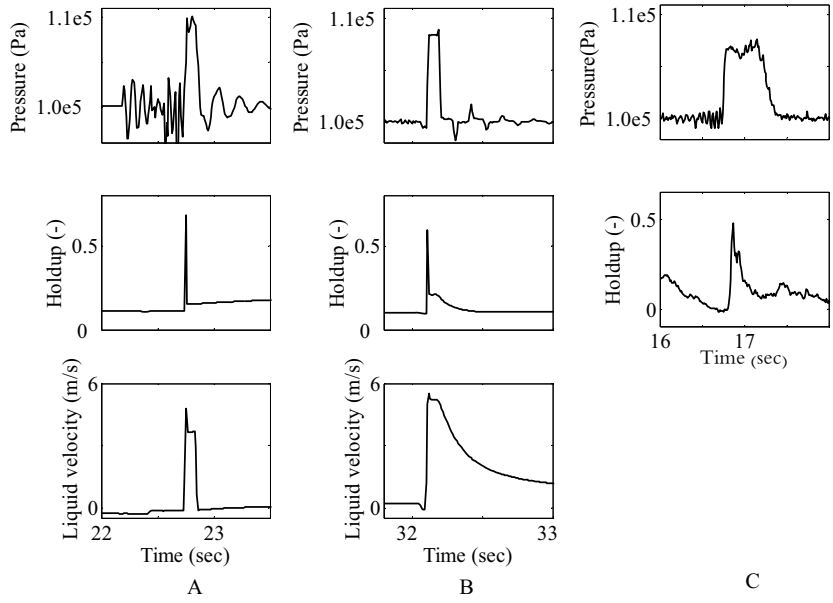

Figure 4. Pressure, holdup and liquid velocity time traces where a wave passes at a given location in the pipe. A. a coarse grid with maximum length 100 pipe diameters. B. a fine grid with maximum length 10 pipe diameters. C. Experimental. Usg = 8.0 m/s, Usl = 0.1 m/s, θ = 1 degree.

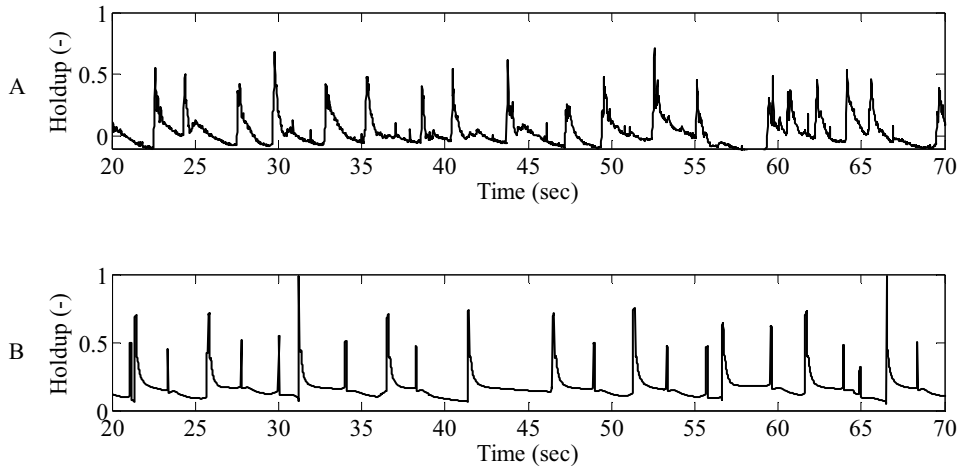

Figure 5. Holdup time traces A. experimental and B. simulation using a fine grid with maximum length 10 pipe diameters. Usg = 6.09 m/s, Usl = 0.18 m/s, $\theta = 2$ degrees.

Figure 5 shows how an experimental holdup time trace compares to a simulated time trace on a fine grid at the same Usg, Usl and pipe inclination. The model time trace in figure 5B shows a mixture of slugs and waves of various sizes occurring in the pipe as well as the shape of the waves.

Wave dynamics such as waves growing to slugs, or slugs decaying to waves is inherent in the tracking model. Examples of a wave growing to a slug and a wave which becomes a slug and then decays into a wave again are shown in figures 6 and 7 respectively. The pressure variation across the wave, liquid holdup and velocity in the wave object as it moves are plotted against time in both figures. When a wave becomes a slug the pressure variation across it and the liquid velocity increase, and the holdup approaches one. In figure 7, when the slug decays again, pressure variation, liquid velocity and holdup decrease. The time traces are cut off when the wave or slug exits the pipe.

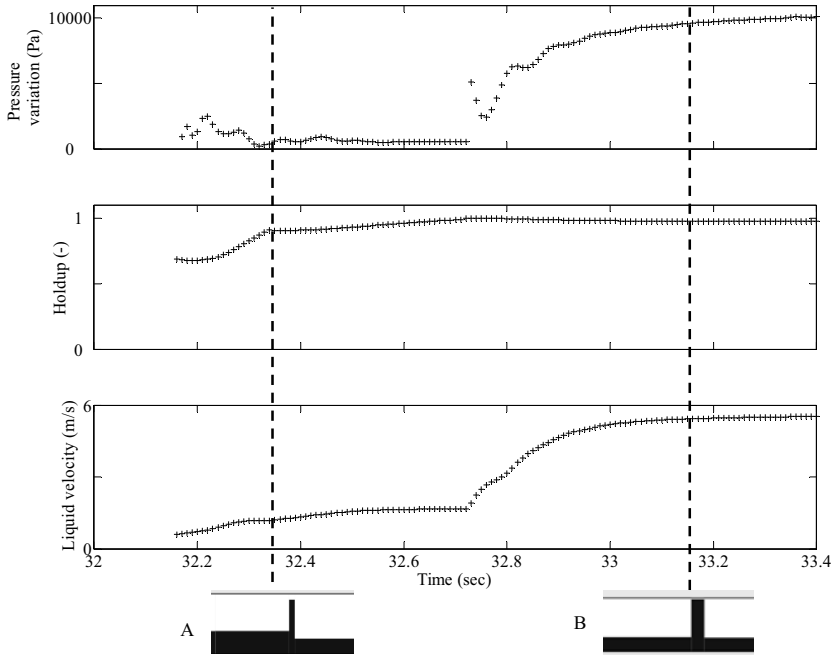

Figure 6. Pressure variation, liquid holdup and liquid velocity in a wave vs. time for A. a wave growing to B. a slug. Usg = 6.01 m/s, Usl = 0.2 m/s, horizontal pipe.

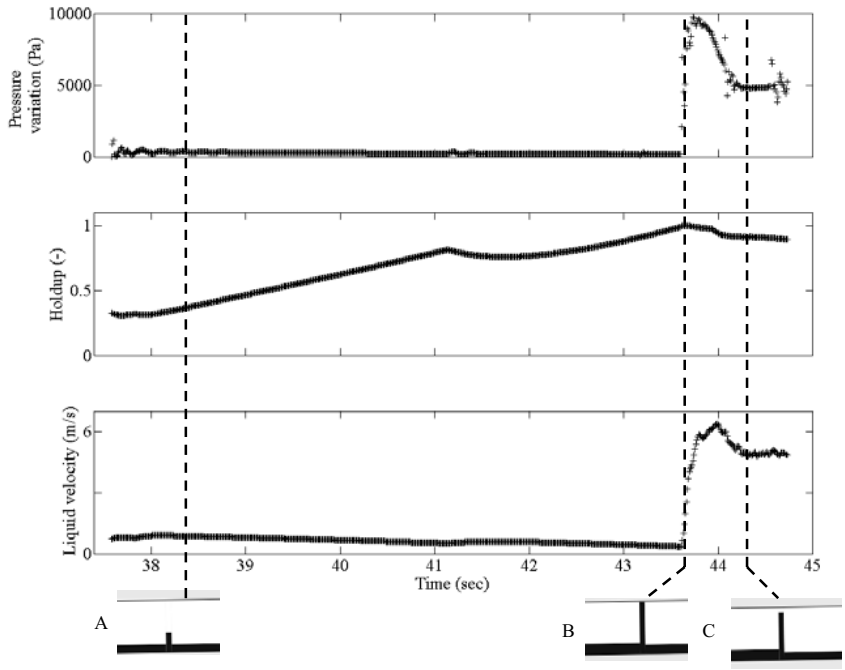

Figure 7. Pressure variation, liquid holdup, and liquid velocity in a wave vs. time for A. a wave growing to B. a slug and then decaying to C. a wave again. Usg = 5.87 m/s, Usl = 0.13 m/s, θ = 1 degrees.

4 Conclusions

A model for large roll waves has been implemented and tested in a slug tracking scheme. The model introduces an orifice type relation for pressure variation across the wave front and a simplified relationship for wave speed in a similar way as for slug flow. Computations have been demonstrated in comparison to experimental data on roll waves in two-phase air-water pipe flow at atmospheric pressure. The model gives a reasonable approximation of wave speed and pressure variations in waves. Looking at pressure drops, modelled pressure drops are sometimes low compared to experiments due to a difference in the number of waves and slugs in the pipe.

The tracking scheme can run with a coarse grid which allows simulation in longer pipes but means that waves and slugs are modelled as square objects without tails. A finer grid allows a more physical representation of waves with

tails. The model includes wave dynamics such as a wave growing to a slug or a slug decaying to a wave.

5 Acknowledgement

Financial support from Total E&P Norge is gratefully acknowledged by A. De Leebeeck.

6 List of Symbols

A	area, m^2
C_d	discharge coefficient
g	gravity, 9.81 m/s^2
H	liquid holdup
I.D.	internal diameter
L	length of section, m
M	mass, kg
P	pressure, Pa
S	wetted perimeter, m
t	time, sec
U	velocity, m/s
$Umix$	mixture velocity, m/s
Usg	superficial gas velocity, m/s
Usl	superficial liquid velocity, m/s

Greek symbols

Δ	change in a given quantity
λ	friction factor
θ	angle of pipe inclination, degrees
ρ	density, kg/m^3

Superscripts

n	current time step
n+1	next time step

Subscripts

front	front of a wave or slug
g	gas phase
i	interface
l	liquid phase
L	left section
R	right section

tail tail of a wave of slug

References

[1] Barnea, D. & Taitel, Y., Kelvin-Helmholtz stability criteria for stratified flow: Viscous versus non-viscous (inviscid) approaches, *International Journal of Multiphase flow,* **19**, pp. 639-649, 1993.

[2] Bendiksen, K.H., Malnes, D. & Nydal, O.J., On the modelling of slug flow, *Chemical Engineering Communications,* **141,** pp. 71-102, 1996.

[3] Bonizzi, M. & Issa, R.I., A model for simulating gas bubble entrainment in two-phase horizontal slug flow, *International Journal of Multiphase flow,* **29**, pp. 1685-1717, 2003.

[4] De Leebeeck, A., Gaarder, A.H. & Nydal, O.J., Experiments on Roll Waves in Air-Water Pipe Flow, *16th Australasian Fluid Mechanics Conference*, Gold Coast, Australia, 2007.

[5] Holmås, H., *Numerical simulation of waves in two phase pipe flow using 1D two-fluid models,* Doctoral dissertation, University of Oslo, 2008.

[6] Hu, B., Stewart, C., Manfield, P.D., Ujang, P.M., Hale, C.P., Lawrence, C.J. & Hewitt, G.F., A Model for Tracking the Evolution of Slugs and Waves in Straight Pipelines, *6th International Conference on Mulitphase Flow*, Leipzig, Germany, 2007.

[7] Issa, R.I. & Kempf, M.H.W., Simulation of slug flow in horizontal and nearly horizontal pipes with the two-fluid model, *International Journal of Multiphase flow,* **29**, pp. 69-95, 2003.

[8] Johnson, G.W., *A Study of Stratified Gas-Liquid Pipe Flow,* Doctoral dissertation, University of Oslo, 2005.

[9] Kjølaas, J., *Plug propagation in multiphase flow,* Doctoral thesis, Norwegian University of Science and Technology, 2007.

[10] Lin, P.Y. & Hanratty, T.J., Prediction of the initiation of slugs with linear stability theory, *International Journal of Multiphase flow,* **12**, pp. 79-98, 1986.

[11] Nydal, O.J. & Banerjee, S., Dynamic slug tracking simulation for gas-liquid flow in pipes, *Chemical Engineering Communications,* **141-142,** pp. 13-39, 1996.

[12] Renault, F., *A Lagrangian slug capturing scheme for gas-liquid flows in pipes,* Doctoral thesis, Norwegian University of Science and Technology, 2007.

[13] Taitel, Y. & Barnea D., Effect of gas compressibility on a slug tracking model, *Chemical Engineering Science,* **53(11),** pp. 2089-2097, 1998.

Paper 4

Simulation of large amplitude waves in a slug tracking scheme compared to roll wave experiments at high pressure

A. De Leebeeck and O. J. Nydal

International Journal of Multiphase Flow, Vol. 36, pp. 40-50

International Journal of Multiphase Flow 36 (2010) 40–50

Contents lists available at ScienceDirect

International Journal of Multiphase Flow

journal homepage: www.elsevier.com/locate/ijmulflow

Simulation of large amplitude waves in a slug tracking scheme compared to roll wave experiments at high pressure

A. De Leebeeck *, O.J. Nydal

Department of Energy and Process Engineering, Norwegian University of Science and Technology, NO-7491 Trondheim, Norway

ARTICLE INFO

Article history:
Received 18 April 2009
Received in revised form 2 September 2009
Accepted 3 September 2009
Available online 8 September 2009

Keywords:
Slug tracking scheme
Roll waves
Two-phase flow
Numerical simulation

ABSTRACT

Due to the similarities between large amplitude roll waves and slug flow in two-phase gas–liquid pipe flow, a slug tracking scheme is presented with the addition of a simplified model for roll waves. The waves are treated in a similar way to slugs, modelled as objects moving at the wave velocity and with a pressure variation across them. The two-fluid model is solved on a stationary staggered grid in stratified sections between moving waves and slugs. The model is dynamic meaning that the growth and decay of waves and slugs can be simulated. The wave model implementation within the tracking scheme is discussed and demonstrated in comparison to existing experimental data on wave velocities and averaged pressure drops. The results from the tracking scheme compared well to the experiments when waves were initiated with the experimental frequency. Wave initiation remains as a modelling challenge.

© 2009 Elsevier Ltd. All rights reserved.

1. Background

In two-phase gas–liquid pipe flow, different flow regimes occur depending on gas and liquid phase velocities, fluid properties, and pipe geometries. Various numerical strategies exist for the modelling of flow regimes at different scales. Slug flow and flow with large amplitude waves can be treated in an averaged manner using repeating unit cells (Bendiksen et al., 1996; Johnson, 2005) assuming steady, fully developed flow. The steady state roll wave model of Johnson (2005) assumes a sequence of repeating "maximum amplitude" waves with a sharp front and includes a unique interface friction factor accounting for increased friction in wavy flows. Unit cell methods give adequate predictions of average holdup and pressure drop but do not include slug or wave dynamics such as growth or decay. Johnson's (2005) model gives more information about the waves such as their velocity, amplitude and the length from one wave peak to the next in addition to average holdup and pressure drop but does not include wave dynamics. Alternatively, slugs and waves can be resolved individually in capturing (Andreussi et al., 2008; Bonizzi and Issa, 2003; Issa and Kempf, 2003; Renault, 2007; Holmås, 2008) or tracking (Taitel and Barnea, 1998; Nydal and Banerjee, 1996; Kjølaas, 2007; Hu et al., 2007) schemes.

Capturing techniques use a two-fluid model on a fine grid much smaller than the characteristic slug length to model slug flow (Renault, 2007; Issa and Kempf, 2003; Bonizzi and Issa, 2003) or flow with large amplitude waves (Holmås, 2008). Slug or wave initiation can be captured but the required refined grid becomes computationally expensive in long pipe systems. Holmås's (2008) model, however, uses a more efficient numerical method, the pseudo-spectral Fourier method, to capture the growth of roll waves but the solution breaks down for slug flow.

Tracking schemes are preferred for this work because coarser grids are possible, reducing the computational expense associated with more refined grids. In a tracking scheme, stratified sections between slugs are modelled on a coarse fixed grid while slugs are modelled as moving objects. Slugs, or similar moving objects, have boundaries corresponding to sharp fronts thus avoiding numerical diffusion and the need for excessive grid refinement (Kjølaas, 2007). Front physics such as bubble nose velocities or gas entrainment can also be implemented. Tracking schemes have also been tested for plug simulations where plugs are treated as rigid moving objects (Kjølaas, 2007). A combination of capturing for slug initiation and tracking has also been tested (Renault, 2007). The slug tracking scheme of Hu et al. (2007) includes the liquid height profile (tail) behind waves and slugs, solving the two-fluid model in combination with modelling the wave front as a hydraulic jump.

Flow with large amplitude roll waves shows some similarities to slug flow (De Leebeeck et al., 2007; Lin and Hanratty, 1987; Hanyang and Liejin, 2008) which would suggest that roll waves can be incorporated into a tracking scheme in similar fashion to slugs. These similarities include transport of liquid, a propagation velocity, sharp fronts and a sloping tail (Johnson, 2005; Ottens et al., 2001; Hanyang and Liejin, 2008; Soleimani and Hanratty, 2003; Andritsos and Hanratty, 1987). Measurements also suggest that waves have a pressure variation across them due to

* Corresponding author. Tel.: +47 73593898; fax: +47 73593580.
E-mail address: angela.de.leebeeck@ntnu.no (A. De Leebeeck).

0301-9322/$ - see front matter © 2009 Elsevier Ltd. All rights reserved.
doi:10.1016/j.ijmultiphaseflow.2009.09.002

acceleration of liquid at the wave front (De Leebeeck et al., 2007). The focus of this work, therefore, is on a tracking scheme including the problem of large amplitude roll waves. To accomplish this an integral wave model and continuous transitions between slug, wave and stratified flow are needed.

In this work, a simple model for roll waves as moving objects similar to slugs has been incorporated in an existing slug tracking scheme following the latest implementation by Kjølaas (2007). Experiments that have measured wave speed and pressure variation across waves (De Leebeeck et al., 2007; De Leebeeck and Nydal, 2009) have formed the basis for modelling waves as moving objects with an associated pressure variation. A simple model for wave velocity is suggested, allowing for transition to and from slug flow and we propose to model gas flow and pressure variation over a large wave as similar to gas flow through an orifice. The wave tracking scheme is then demonstrated by comparing to experimental data on wave velocity and averaged pressure drop in roll waves (Johnson, 2005).

2. Model description

The wave model is an addition to an existing slug tracking code following the latest implementation by Kjølaas (2007). In Kjølaas's (2007) implementation of the scheme, the two-fluid model is solved in stratified sections and hydrate plug tracking capabilities have been added. The tracking concept is now applied to other moving objects in the pipe, roll waves. The numerical model for slugs on a moving grid and stratified regions on a stationary grid has already been developed (Kjølaas, 2007) but is reviewed here to show how the simplified wave tracking model has been incorporated with the existing scheme. The model for slugs implemented by Kjølaas (2007) and the model for waves implemented here are summarized in Tables 1 and 2, respectively.

The wave and slug tracking scheme uses a one-dimensional finite volume method and applies to two-phase gas–liquid flow in a pipe. For the purposes of wave tracking, flow is assumed isothermal so the energy equation can be neglected. It is also assumed that there is no mass transfer between the phases through evaporation or condensation. Gas entrainment can be included in slugs but is not modelled in stratified regions or waves. Droplets in the gas phase are also neglected.

2.1. Geometry

Pipeline geometry is listed as a sequence of pipes with a length, angle of inclination, internal diameter, and roughness for

Table 1
Slug model summary.

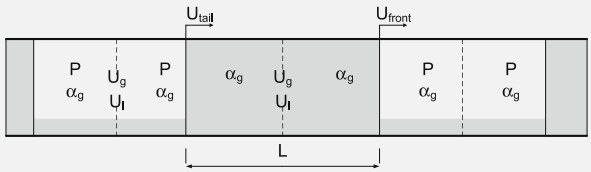

Slug sections	U_l	Mixture momentum balance equation (8)
	U_g	Slip relation equation (9)
	α_g	Gas entrainment correlation, if any
	L	Mass balance equations (22) and (23)
Stratified sections	P	Equations of state (5)
	α_g	Mass balance equation (7)
	U_l	Liquid momentum equation (4)
	U_g	Gas momentum equation (4)
Borders	U_{tail}	Bubble nose or slug tail velocity equation (11)
	U_{front}	Mass balance across slug front equation (10)

Table 2
Wave model summary.

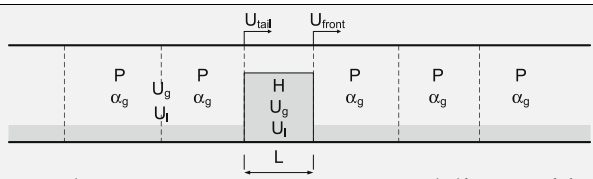

Wave sections	U_l	Liquid momentum balance equation (19) with front acceleration, friction, gravity and pressure drop
	U_g	Gas momentum balance equation (18) with orifice type loss, gravity and pressure drop
	H	Mass balance equations (22) and (23)
	L	Fixed length of wave front
Stratified sections	P	Equations of state (5)
	α_g	Mass balance equation (7)
	U_l	Liquid momentum equation (4)
	U_g	Gas momentum equation (4)
Borders	$U_{tail} = 1.2U_l$	Continuous to bubble nose velocity when $H = 1$, Eq. (21)
	U_{front}	Mass balance across wave front, Eq. (20)

calculating the frictional shear stress at the pipe walls. The pipeline can consist of one or more pipes of varying length and/or inclination, and include bends. At the boundaries between two pipes (bends) mass is free to flow in either direction.

2.2. Fluid properties

For wave tracking, the ideal gas law is used to determine the gas density. Other fluid properties such as viscosities, liquid density, and the molecular mass of the gas phase are specified by the user. The constant temperature of the fluids and outlet, inlet and initial pressure are specified so that the gas density can be calculated from the ideal gas law. The only reason for specifying the inlet pressure is so that the gas density at the inlet can be determined. It does not have any other mechanical consequences. Inside the pipe, gas density varies according to the simulated pressure.

2.3. Grids and time steps

The sequence of pipes is divided into sections including stratified sections, slug sections, and large roll wave sections. The sections are the computational grid. The boundary between a section and its neighbor is termed the section border. Since the grid is dynamic, three grid sizes are specified: a maximum and minimum grid size for stratified sections, and a minimum grid size for slugs around 1 or 2 pipe diameters. When a stratified section exceeds maximum length it is split into two smaller sections, or merged with a neighboring section if it is less than the minimum length. When slugs reach minimum length they decay to waves. The wave front is modelled as an object with a short fixed length equal to the minimum slug length.

In stratified sections, the gas and liquid phases are separate and the two-fluid model is solved on a stationary staggered grid. In the staggered grid arrangement, phase velocities are determined at section borders, while pressure, area fraction, and other quantities are determined at section centers. The staggered arrangement avoids checkerboard oscillations that would occur if pressure and velocities were determined at the same location (Ferziger and Perić, 2001).

Slug and wave sections, however, are modelled with moving borders. These section borders move with a border velocity and their position is updated at each time step. The border velocities are greater than the liquid phase velocity in stratified sections. Liquid slug sections completely fill the pipe and they may or may not contain entrained gas depending on the modelling of the gas entrainment rate at the slug front. Slug front and tail borders move with separate velocities allowing the slug to grow or shrink in length. Wave fronts are modelled in similar fashion to slugs, except gas is allowed to flow over them and they have a fixed length. The wave moves at the wave front velocity and if the wave tail velocity is different from the front velocity, the holdup in the wave front will either increase or decrease according to the mass balance over the front. Thus the wave grows or decays in amplitude.

Fig. 1 illustrates the spatial index convention used in stratified sections and slugs. The convention for slugs is also applied to waves. In stratified sections, index J represents the section center indicated with a dashed line while index j indicated with a solid line is the border to the left of section J. In moving slugs and waves, index j is the center of the slug or wave (dashed line) while index J is its right border (solid line).

Start and end times as well as the desired simulation time step are given by the user. Time steps are indicated by superscripts where n represents the current time step and $n+1$ represents the next time step. Quantities with superscript n are known at the current time step while those with superscript $n+1$ need to be determined.

2.4. Friction models

Frictional shear stress at the wall is expressed using a friction factor as follows:

$$\tau = \frac{1}{8}\lambda\rho|U|U \tag{1}$$

where τ is the shear stress, ρ is the phase density, U is the phase velocity, and λ is the Darcy friction factor.

The shear stress at the interface, τ_i, for smooth stratified flow is normally written as:

$$\tau_i = \frac{1}{8}\lambda_g\rho_g|U_g - U_l|(U_g - U_l) \tag{2}$$

where λ is the Haaland friction factor (Haaland, 1983) for phase k determined from:

$$\frac{1}{\sqrt{\lambda_k}} = -1.8\log\left(\frac{6.9}{Re_k} + \left(\frac{\epsilon}{3.7D_{h,k}}\right)^{1.11}\right) \tag{3}$$

where Reynolds number for phase k is $Re_k = \rho_k D_{h,k} U_k/\mu_k$, μ is the viscosity, and ϵ is the pipe wall roughness. Phase k can be either liquid indicated by subscript l or gas, subscript g. Hydraulic diameters D_h for the gas phase and liquid phase are:

$$\text{Gas phase} \quad D_{h,g} = \frac{\pi D^2}{S_g + S_i}$$

$$\text{Liquid phase} \quad D_{h,l} = \frac{\pi D^2}{S_l}$$

where S_g and S_l are the wetted wall perimeters and S_i is the interface length. D is the pipe diameter.

2.5. Two-fluid equations for stratified flow sections

In stratified sections, the two-fluid model consisting of the gas and liquid momentum equations, the pressure equation, and the gas and liquid mass balance equations are solved on a staggered grid adopting the notation as shown in Fig. 1. The discretized version of these equations as in Kjølaas (2007) are reviewed. For the

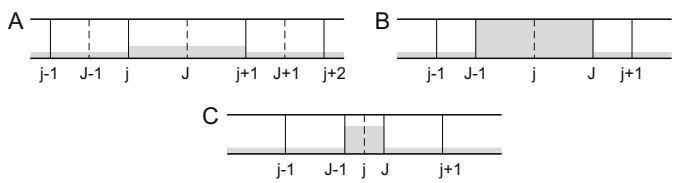

Fig. 1. Index notation in (A) stratified sections, (B) slug sections, and similar to slugs, (C) wave sections. Solid lines represent section borders, while dotted lines mark section centers.

differential form of the mass, momentum and pressure equations before discretization, see Electronic Annex 1.

The discretized momentum balance equation for phase k is given as:

$$M^n_{kJ}\frac{\Delta U_k}{\Delta t}+\dot{m}^n_{kJ}A\left(U^n_{kJ}-U^n_{bJ}\right)\left(\widehat{U}^{n+1}_{kJ}-U^{n+1}_{kJ}\right)-\dot{m}^n_{kJ-1}A\left(U^n_{kJ-1}-U^n_{bJ-1}\right)\times\left(\widehat{U}^{n+1}_{kJ-1}-U^{n+1}_{kj}\right)=-\alpha^n_{kJ}A\left(P^{n+1}_J-P^{n+1}_{J-1}\right)-M^n_{kJ}g\cos\theta\frac{h^n_{lJ}-h^n_{lJ-1}}{L^n_J}-\frac{1}{8}S^n_{kJ}L^n_J\lambda^n_{kJ}\rho^n_{kJ}|U^n_{kJ}|\left(U^{n+1}_{kJ}\right)-\frac{1}{8}S^n_{iJ}L^n_J\lambda^n_{iJ}\rho^n_{gJ}|U^n_{kJ}-U^n_{nJ}|\left(U^{n+1}_{kJ}-U^{n+1}_{nJ}\right)-M^n_{kJ}g\sin\theta \tag{4}$$

where M is the phase mass, $\Delta U_k = U^{n+1}_k - U^n_k$, Δt is the time step size, $m = M/AL$ is the phase specific mass, A is the pipe cross-sectional area, S is the wetted wall perimeter, t is time, α is the area fraction, P is pressure, L is the section length, h_l is the liquid height, g is the acceleration of gravity (9.81 m/s^2), and θ is the angle of pipe inclination from the horizontal. A positive angle indicates upward inclination. The subscript b indicates a quantity associated with a border, subscript k indicates the current phase, subscript n indicates the neighboring phase, and subscript i indicates a quantity associated with the interface. Upwind discretization is used for the convection terms. Upwind quantities are indicated with a hat, e.g., the velocity $\widehat{U}^{n+1}_{kJ}$ in the above equation.

The implementation of the two-fluid model in stratified regions means that the convection terms, the second and third terms in Eq. (4), are included. This in turn means that the gradually sloping liquid height profile (tail) behind wave fronts and slugs can be resolved on a sufficiently refined grid.

The following equation, the pressure equation, is a combination of the mass balance and equations of state for both phases:

$$\sum_k \frac{V^n_{kJ}}{\rho^n_{kJ}}\left[\left(\frac{\partial\rho^n_{kJ}}{\partial P}\right)_{T_k}\frac{P^{n+1}_J-P^n_J}{\Delta t}\right]+A\left(U^{n+1}_{bJ+1}-U^{n+1}_{bJ}\right)+\sum_k\frac{1}{\rho^n_{kJ}}\left[\dot{m}^n_{kJ+1}A\left(U^{n+1}_{kJ+1}-U^{n+1}_{bJ+1}\right)-\dot{m}^n_{kJ}A\left(U^{n+1}_{kJ}-U^{n+1}_{bJ}\right)\right]=\psi_{sJ} \tag{5}$$

where V is volume, T is temperature, and $\left(\frac{\partial\rho^n_{kJ}}{\partial P}\right)_{T_k}$ is determined from the ideal gas law. The pressure equation (5) is solved simultaneously with the momentum balance equation (4) to get phase velocities defined at section borders and pressure defined at the center of stratified sections. The model can work with either an incompressible or a compressible liquid in stratified flow. When single phase liquid occurs, as in a slug, the computational domain is divided into compressible and incompressible regions. This avoids the problem of having one universal scheme to work for both compressible and incompressible cases.

The volume error term ψ_{sJ} in Eq. (5) is defined as follows:

$$\psi_{sJ}=\frac{V_J}{\Delta t}\left(\sum_k\frac{m_{kJ}}{\rho_{kJ}}-1\right) \tag{6}$$

It is included because the pressure equation is not formulated in a mass conserving manner (Kjølaas, 2007; Ferziger and Perić, 2001; Prosperetti and Tryggvason, 2007) and the use of the staggered grid can introduce a first order error from acceleration by a body force (Fletcher and Thyagaraja, 1991). Including the volume error term ensures consistency between pressure and mass over time, without iteration.

The discretized mass balance equation uses an implicit time integration which is more robust for longer time steps. Mass is determined at the centers of stratified sections using the following equation:

$$\frac{\Delta M_{kJ}}{\Delta t}+\frac{\widehat{M}^{n+1}_{kJ+1}}{\widehat{L}^n_{J+1}}\left(U^{n+1}_{kJ+1}-U^{n+1}_{bJ+1}\right)-\frac{\widehat{M}^{n+1}_{kJ}}{\widehat{L}^n_J}\left(U^{n+1}_{kJ}-U^{n+1}_{bJ}\right)=0 \tag{7}$$

The mass balance equations are solved after the pressure equation and the phase fractions are determined from the masses and densities at the new pressure. As the phase fractions may not sum to unity, the phase fractions are normalized and the error term is introduced as a source term in the pressure equation (5). Including the error term in the pressure equation allows the equations to be solved non-iteratively and reduces the computational cost, and the implicit formulation ensures stability (Kjølaas, 2007).

2.6. Slugs

The dynamics of the flow in a slug can be determined from a mixture momentum equation and a slip relation. A simplified version of the mixture momentum equation is the liquid equation without the gas interaction term. The discretized version of the liquid momentum equation in slugs takes a similar form to Eq. (4), except interface friction can be neglected (no interface), as follows:

$$M^n_{lJ}\frac{\Delta U_l}{\Delta t}+\dot{m}^n_{lJ}A\left(U^n_{lJ}-U^n_{bJ}\right)\left(\widehat{U}^{n+1}_{lJ}-U^{n+1}_{lJ}\right)-\dot{m}^n_{lJ-1}A\left(U^n_{lJ-1}-U^n_{bJ-1}\right)\left(\widehat{U}^{n+1}_{lJ-1}-U^{n+1}_{lJ}\right)=-H^n_JA\left(P^{n+1}_J-P^{n+1}_{J-1}\right)-\frac{1}{8}S^n_{lJ}L^n_J\lambda^n_{lJ}\rho^n_{lJ}|U^n_{lJ}|\left(U^{n+1}_{lJ}\right)-M^n_{lJ}g\sin\theta \tag{8}$$

The second and third terms in Eq. (8) account for pressure variation due to acceleration of the liquid in the slug front.

Gas velocity in a slug is determined using a slip relation or assuming no slip:

$$U_{g,slug}=S_d(U_{l,slug}+v_o) \tag{9}$$

In the simplest case of no slip, the distribution slip ratio S_d is unity and the averaged drift velocity v_o is zero.

The slug front velocity is determined from a mass balance across the front, as follows:

$$U_{front}=\frac{H_{slug}U^{n+1}_{l,slug}-H_{bubble}U^n_{l,bubble}}{H_{slug}-H_{bubble}} \tag{10}$$

where H is liquid holdup, the subscript *slug* indicates quantities associated with the slug while subscript *bubble* indicates quantities belonging to the stratified section neighboring the slug. For the case of a slug without gas entrainment, the holdup H_{slug} goes to 1 and the local mixture velocity in a slug goes to the liquid velocity $U_{l,slug}$.

Slug tail or bubble nose velocity is determined using the following equation, proposed by Bendiksen et al. (1996) and Bendiksen (1984):

$$U_{tail}=C_oU_{mix}+U_o \tag{11}$$

where $U_{mix}=H_{slug}U_{l,slug}+(1-H_{slug})U_{g,slug}$ is the local mixture velocity in the slug. Values for C_o and U_o which give the largest U_{tail} are applied, as follows:

$$\begin{array}{lll} C_o=1.05+0.15\sin^2\theta & U_o=U_{ov}+U_{oh} & \text{if } |U_{mix}|<3.6\sqrt{gD}/\cos\theta \\ C_o=1.2 & U_o=U_{ov} & \text{if } |U_{mix}|>3.6\sqrt{gD}/\cos\theta \\ U_{ov}=0.35\sqrt{gD}\sin\theta & U_{oh}=\pm0.54\sqrt{gD}\cos\theta & \end{array}$$

A summary of the slug model and the quantities determined is given in Table 1.

2.7. Waves

The wave model includes a pressure variation across the wave front due to liquid acceleration at the front as observed experimentally (De Leebeeck et al., 2007). The overlapped holdup

and pressure time traces corresponding to a video snapshot of a wave are plotted as an example in Fig. 2. The snapshot comes from an experiment where air and water are flowing in a 0.06 m internal diameter horizontal pipe at atmospheric conditions with superficial gas velocity $U_{sg} = 5.89$ m/s and superficial liquid velocity $U_{sl} = 0.17$ m/s. The typical wave velocities and pressure variations observed in waves during this experiment were 1.86 m/s and 1400 Pa, respectively (De Leebeeck et al., 2007).

In the wave model, it is assumed that pressures in both gas and liquid phase are equal. For a known pressure variation, the liquid phase velocity in the wave front can be determined from the liquid momentum balance equation. The gas phase however needs its own model: gas flow over a large wave can be thought of as similar to gas flow through an orifice. A schematic of a large wave compared to an orifice plate is shown in Fig. 3. The adaptation of a single phase orifice relation to gas flow over a large roll wave follows.

Starting with the single phase gas velocity through the throat of an orifice, as in the following equation (White, 2005), the orifice relation is adapted to wave flow:

$$U_t = C_d A_t \left(\frac{2\Delta P_{orifice}/\rho}{1 - (A_t/A_{pipe})^2} \right)^{\frac{1}{2}} \tag{12}$$

where C_d is the discharge coefficient, A_t is the orifice throat area, $\Delta P_{orifice}$ is the pressure variation across the orifice, and A_{pipe} is the pipe cross-sectional area.

Rewriting Eq. (12) to give the pressure variation across the orifice gives the following:

$$\Delta P_{orifice} = \frac{1}{2}\frac{1}{C_d^2}\rho U_t^2 (1 - (A_t/A_{pipe})^2) \tag{13}$$

In thinking of gas flowing over a large wave front as similar to gas flow through an orifice, the following modifications are made to the orifice relation in Eq. (13):

$$U_t \Rightarrow U_{g,wave} - U_{front} \tag{14}$$

$$U_t^2 \Rightarrow (U_{g,wave} - U_{front})|U_{g,wave} - U_{front}| \tag{15}$$

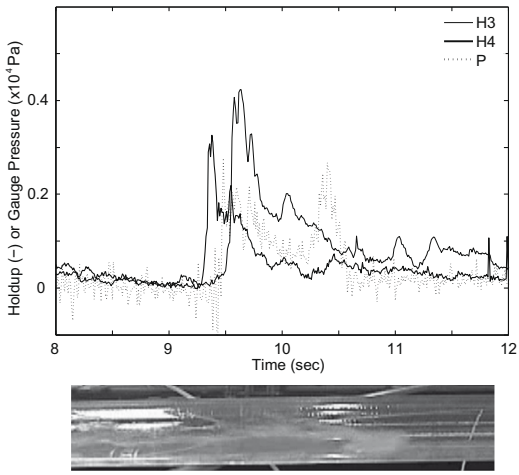

Fig. 2. Experimental pressure and holdup time traces, and corresponding image of an individual wave from air/water experiments at atmospheric pressure, horizontal pipe, $U_{sg} = 5.89$ m/s, $U_{sl} = 0.17$ m/s. The locations of holdup probes *H3* and *H4* and the pressure transducer *P* are 11.88 m, 14.39 m, and 13.67 m from the inlet of the pipe, respectively (De Leebeeck et al., 2007).

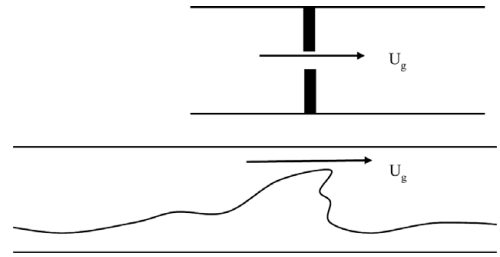

Fig. 3. Schematic of gas flow through an orifice plate (top) compared to gas flow over a large wave (bottom).

The wave is no longer stationary so U_t is replaced with the difference between the gas phase velocity over the wave $U_{g,wave}$ and the velocity of the wave front U_{front}.

The orifice relation is for single phase flow where the gas occupies the entire pipe cross section. In the case of two-phase flow, the gas phase occupies only a fraction of the pipe. In Eq. (13), the term A_{pipe} is replaced with the gas phase area ahead of the wave front $A_{g,bubble}$. The area of the orifice throat can be thought of as the area occupied by the gas at the wave front $A_{g,wave}$. The ratio of the two areas can then be written in terms of gas or liquid area fractions, as follows:

$$\frac{A_t}{A_{pipe}} \Rightarrow \frac{A_{g,wave}}{A_{g,bubble}} = \frac{A_{g,wave}/A_{pipe}}{A_{g,bubble}/A_{pipe}} = \frac{1 - H_{wave}}{1 - H_{bubble}} \tag{16}$$

where H_{wave} is the holdup in the wave front.

Finally the corresponding pressure loss to be added in the gas momentum equation for a wave is written as follows:

$$\Delta P_{wave} = \left[\frac{1}{2}\frac{1}{C_d^2}\rho_g \left(1 - \left(\frac{1 - H_{wave}}{1 - H_{bubble}} \right)^2 \right) (U_{g,wave} - U_{front})|U_{g,wave} - U_{front}| \right] \tag{17}$$

Empirical relations for the discharge coefficient C_d have been determined, depending on the ratio of the orifice throat to pipe diameter, Reynolds number, and the type of taps (corner taps or flanges for example) in the orifice (White, 2005). The typical range of values for C_d is from 0.59 to 0.66 (White, 2005) in an orifice. Since there are some differences between an actual orifice and a wave front, the question then is what should C_d be for the case of a wave? Various values of C_d can be used in simulations and compared to experimental data on waves. From there an optimal value of C_d for waves can be determined. Experimental measurements of pressure variation across a wave front (De Leebeeck et al., 2007; De Leebeeck and Nydal, 2009) led to an estimate of the discharge coefficient in the range of 0.2–0.4. These values may be lower than $C_d = 0.6$ in an actual orifice because of increased losses in the wave such as increased roughness on the wave's surface or losses due to droplet formation and air entrainment in the wave front.

The orifice type relation replaces the gas wall and interfacial shear stresses as a loss term. The following gas momentum equation for a wave front is used to determine the gas velocity by relating it to the pressure variation across the wave front:

$$\begin{aligned} &\frac{M_{g,wave}}{\Delta t}\Delta U_{g,wave} + (1 - H_{wave})A\frac{1}{2}\frac{1}{C_d^2}\rho_{g,wave}\left(1 - \left(\frac{1 - H_{wave}}{1 - H_{bubble}}\right)^2\right) \\ &\quad \times \cdot (U_{g,wave} - U_{front})|U_{g,wave} - U_{front}| \\ &= (1 - H_{wave})A(P_{J-1} - P_J) - M_{g,wave} g \sin\theta \end{aligned} \tag{18}$$

Using the same pressure variation $(P_{J-1} - P_J)$ as in Eq. (18), the following liquid momentum balance equation is used to determine the liquid phase velocity in a wave front:

$$\frac{M_{l,wave}}{\Delta t}\Delta U_{l,wave} + H\rho_{l,wave}A(U^n_{l,wave} - U_{front})(U^n_{l,bubble} - U^{n+1}_{l,wave}) = H_{wave}A(P_{J-1} - P_J) + \left(-\frac{1}{8}LS_{l,wave}\lambda_{l,wave}\rho_{l,wave}|U^n_{l,wave}|U^{n+1}_{l,wave}\right) - M_{l,wave}g\sin\theta \quad (19)$$

In the liquid phase, the main component giving pressure variation is the acceleration of the liquid at the wave front. There is also a contribution from liquid wall friction and gravity for the fixed length of the wave front.

Waves fronts are modelled as moving objects similar to slugs but they have a fixed length of 1–2 pipe diameters and move with the wave front velocity. The front velocity of a wave is determined in exactly the same way as for slugs, through a mass balance across the front. Rewriting Eq. (10) in terms of wave quantities gives:

$$U_{front} = \frac{H_{wave}U^{n+1}_{l,wave} - H_{bubble}U^n_{l,bubble}}{H_{wave} - H_{bubble}} \quad (20)$$

where subscript *wave* indicates wave related quantities.

One aim of the wave tracking scheme was to have a simplified model, therefore a simplified wave tail speed relationship was desired. The proposed wave tail speed is one which gives a continuous transition to slug flow, as in the following equation:

$$U_{tail} = C_o U_l \quad (21)$$

A factor of $C_o = 1.2$ allows for continuous transition between wave and slug flow when the liquid holdup in a wave approaches unity, assuming no gas entrained in the slug. Modifications to this relation can be done when gas entrainment is included in the slug.

The mass balance equations in a wave or slug are the same, where the change in mass in a given time step is the difference in mass flux in and out. In contrast to stratified sections, mass in waves and slugs is treated explicitly so that slug length or wave height is consistent with the masses. This is achieved automatically by integrating the wave or slug masses explicitly (Kjølaas, 2007), as in the following equations:

$$\frac{\Delta M_l}{\Delta t} = Flux_{in} - Flux_{out} = \frac{M^n_l(U^{n+1}_l - U_{tail})}{L} - \frac{M^n_l(U^{n+1}_l - U_{front})}{L} \quad (22)$$

$$\frac{\Delta M_g}{\Delta t} = Flux_{in} - Flux_{out} = \frac{M^n_g(U^{n+1}_g - U_{tail})}{L} - \frac{M^n_g(U^{n+1}_g - U_{front})}{L} \quad (23)$$

$$H = \frac{M^{n+1}_l}{AL\rho_l} \quad (24)$$

Eqs. (22) and (23) are the liquid phase and gas phase mass balance equations, respectively, in both slugs and waves. The liquid holdup can then be determined as in Eq. (24). Since wave fronts are modelled with a fixed length and they move at the wave front velocity, the tail velocity only appears in the mass balance equations (22) and (23). If the front speed is larger than the tail speed the liquid mass in the wave will increase and vice versa. Therefore wave fronts can increase or decrease in amplitude. For slugs, if the front velocity is different from the tail velocity, the slug will increase or decrease in length.

A summary of the wave model and quantities determined is given in Table 2.

2.8. Initiation and decay of slugs and waves

In principle, this scheme could be used for capturing wave initiation using the two-fluid model followed by slug tracking similar to Renault (2007) if the grid is sufficiently refined. On a coarser grid in use here, an initiation model for waves is needed. This could be implemented by testing the inviscid Kelvin–Helmholtz (K–H) criterion (Lin and Hanratty, 1986; Barnea and Taitel, 1993) at the transition from stratified flow, as follows:

$$\left(\frac{A_l}{\rho_l S_i} + \frac{A_g}{\rho_g S_i}\right)(\rho_l - \rho_g)g\cos\theta - (U_g - U_l)^2 > 0 \quad (25)$$

Waves can also be inserted in the pipe at a given frequency, as is done here. For testing in this work, they are inserted using experimentally measured frequencies.

The initiation of slugs occurs when the holdup in a wave or the liquid level in a low point exceeds a user specified maximum holdup, for example $H = 0.99$. In that case, the section will be converted to a slug. Slugs can also form if two waves merge or grow if a slug overtakes a slower moving wave.

Slugs are removed either when they exit the pipe or when their length goes below a user specified minimum of one or two pipe diameters, at which point it becomes a wave. If the wave continues to decay, it will be removed when the holdup in the wave approaches the holdup in the stratified section in front of it. This means the wave has decayed in amplitude until it reaches the stratified liquid level surrounding it.

3. Model implementation

The tracking scheme has been developed in the C++ programming language using object oriented techniques. Object oriented programming promotes code reuse through inheritance and enhances modularity which reduce complexity of the program and allow changes to be made more easily. Physical objects such as slugs and waves can be represented as computational objects in the code through the use of classes. Using list structures simplifies the grid management. Equations are also represented computationally using a generic class structure including a mass balance equation class and a momentum balance equation class. The model implementation is discussed in Kjølaas (2007).

3.1. Computational sequence

The mass, momentum, and pressure equations have been formulated implicitly for increased stability and linearized in terms of the unknown primary variables velocity U, pressure P, and specific mass m. The solution is found by using direct Gauss-elimination. The computational sequence is as follows:

1. Equation coefficients for moving borders on wave and slug sections are determined.
2. The pressure and momentum balance equation system matrix is built. This matrix is a banded system with three upper and three lower co-diagonals. The equation system is then solved giving phase velocities and pressures.
3. The mass balance equations are solved with the new velocities.
4. Phase masses, phase densities (state equation), and volume errors are updated.
5. Waves and slugs are inserted or removed, sections are merged and split as necessary.
6. The simulation moves on to the next time step, starting at step 1 again.

3.2. Grid sizes

Modelling on a coarse grid gives square shaped bubbles, slugs, and waves. However, the liquid height profile behind slugs and waves, their tails, can be reproduced by refining the grid in the

stratified region. As this only changes the resolution of stratified sections, the wave and slug velocity computations will not be affected. Fig. 4 shows how an experimental holdup time trace compares to a simulated time trace on a fine (maximum grid size 10 pipe diameters) and on a coarse grid (maximum grid size 100 pipe diameters) at the same conditions. The experiments and simulations were run for an air–water system at atmospheric pressure. The simulation ran considerably faster with the coarse grid compared with the refined grid case.

The minimum slug length corresponds to the short length of a wave front on the order of a pipe diameter. This length will determine the wave front growth rate and how soon slugs decay into waves. The effect of increasing the minimum slug length is that slugs decay to waves sooner, and the growth of wave fronts is delayed. Taking a simulation example with sulfurhexafloride (SF6) gas and water at 8 bar in a 0.1 m I.D. horizontal pipe, Table 3 shows the effect of varying the minimum slug length on the computed wave velocity and average pressure drop. The stratified section length is kept within 8–50 pipe diameters and time step size held below 0.01 s. Increasing or decreasing the minimum slug length by a factor of one or two results in a deviation from the experimental quantities of no more than 8.0%.

The time step in the model is controlled based on the Courant–Friedrichs–Lewy (CFL) condition, in stratified sections which have a stationary grid. The Courant number is as follows:

$$C = U\Delta t/\Delta x \tag{26}$$

where C is the Courant number and Δx is the length of a grid section. C is kept lower than unity for accuracy. The Courant number is tested to see if it reaches unity. If it does, the time step is changed from the user specified value so that C stays below the limit of unity. Taking the same simulation example as above, the typical liquid and gas velocities coming into a stratified grid section are 1.26 m/s and 5.14 m/s, respectively. For a time step of 0.01 s, and a minimum stratified section length of 0.8 m (or 8 pipe diameters), the Courant number for the liquid phase is 0.0158 and for the gas phase is 0.0642.

3.3. Wave and slug dynamics

Wave dynamics such as waves growing to slugs, or slugs decaying to waves is inherent in the tracking model. An example simulation of a wave which grows to a slug and then decays into a wave again is shown in Fig. 5. The pressure variation across the wave, liquid holdup and velocity in the wave object as it moves are plotted against time. When a wave becomes a slug the pressure variation across it and the liquid velocity increase, and the holdup approaches one. When the slug decays again, pressure variation, liquid velocity and holdup decrease. The time traces are cut off when the wave exits the pipe.

Table 3
An example showing the effect of varying minimum slug length on computed values. These values were computed for a 0.1 m internal diameter horizontal pipe at 8 bar with $U_{sg} = 4.5$ m/s and $U_{sl} = 0.2$ m/s. The corresponding experimental wave velocity and average pressure drop were 2.13 m/s and 181.6 Pa/m, respectively, from which percentage differences were calculated.

Minimum slug length (multiple of pipe diameter) (m/s)	Simulated values		Absolute percentage difference (%)	
	Wave velocity (m/s)	Pressure drop (Pa/m)	In wave velocity	In pressure drop
$\frac{1}{2}$	2.2	185	3.3	1.9
1	2.16	189	1.4	4.1
2	2.08	193	2.3	6.3
3	2.0	172	6.1	5.3
4	1.99	167	6.6	8.0

4. Results and discussion

Simulation results from the slug tracking scheme with incorporated wave tracking capability presented above are compared to experimental data (Johnson, 2005) specifically on roll waves.

4.1. Description of experiments

Simulations were run matching the flow conditions, fluid properties, and pipe geometry in Johnson (2005). A total of 984 experiments on two-phase roll waves were carried out at the Institute for Energy Technology (IFE) in Norway using sulfurhexafloride gas and water at 8 bar and 20 °C to simulate high pressure flows (Johnson, 2005). Pipe inclinations varied from 0 to 5 deg with gas superficial velocities, U_{sg}, ranging between 0.5 and 4.5 m/s and a variety of liquid superficial velocities, U_{sl}, in the range of 0.1–0.6 m/s at each inclination and U_{sg}. The test section was 25 m long, internal pipe diameter was 0.1 m and experiments ran for 100 s.

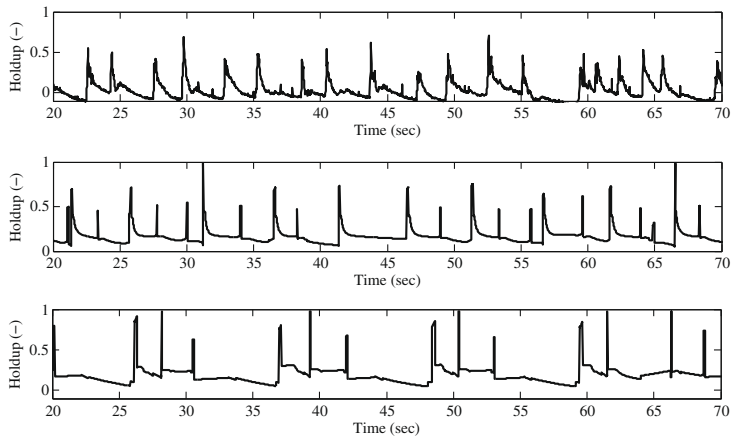

Fig. 4. Liquid holdup time traces using air and water at atmospheric pressure in a 0.06 m internal diameter pipe (De Leebeeck and Nydal, 2009). Top: experimental. Middle: simulated on a fine grid (length 10 pipe diameters). Bottom: a coarse grid (length 100 pipe diameters). $U_{sg} = 6.09$ m/s, $U_{sl} = 0.18$ m/s, $\theta = 2$ deg.

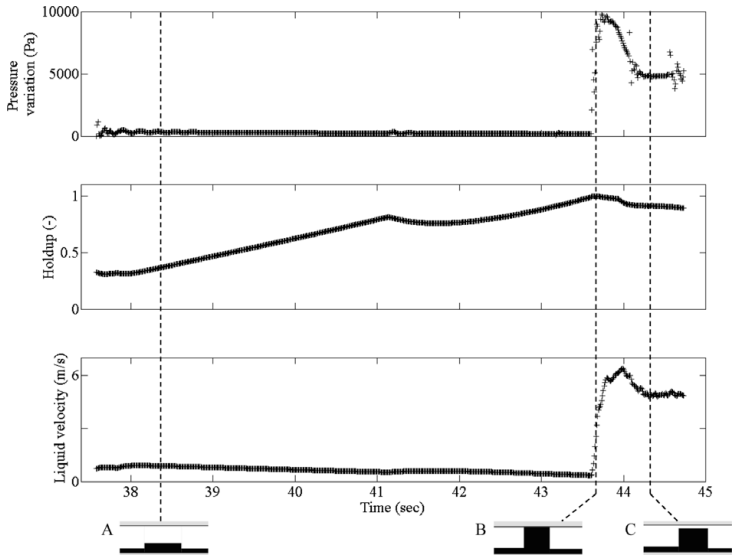

Fig. 5. Pressure variation, liquid holdup, and liquid velocity in a wave vs. time for (A) a wave growing to (B) a slug and then decaying to (C) a wave again. Simulation run at atmospheric pressure with $U_{sg} = 5.87$ m/s, $U_{sl} = 0.13$ m/s, $\theta = 1$ deg, and pipe internal diameter 0.06 m (De Leebeeck and Nydal, 2009).

The gas density and viscosity were 50 kg/m^3 and 1.61×10^{-5} Pa s, and water density and viscosity were 998 kg/m^3 and 1×10^{-3} Pa s, respectively.

The data available from the experiments included average pressure drops, superficial velocities, average liquid height, wave velocities, the length from one wave peak to the next, and wave amplitudes. Wave velocities were obtained from cross correlations between liquid height time traces. Peak to peak lengths were estimated from the dominant wave frequency and the wave velocity. Experimental results of interest for comparison with the present numerical model were in particular the wave speed and average pressure drop.

4.2. Simulations

Simulations were run using the same conditions as above. The model domain was 25 m long and each simulation was run for 100 s. Measured superficial velocities were set at the inlet boundary and the inlet source gas density was determined at 8 bar from the ideal gas law. The pressure at the outlet boundary was set to 8 bar. Various U_{sl} and U_{sg} combinations were simulated at four pipe inclinations: 0, 0.1, 0.25 and 1 deg. Grid sizes were as follows: the minimum slug length was one pipe diameter, the minimum stratified section length was 8 pipe diameters and the maximum length was 50 pipe diameters. A time step of 0.01 s was specified.

Waves were inserted at the dominating frequency determined in experiments. This frequency in combination with the wave velocity was used to find the experimental length between subsequent wave peaks but was not explicitly listed in Johnson (2005). Using the given wave velocity and experimental length, the wave frequency was calculated and used to specify a time delay between wave front insertions in the simulation. For example, the experimental case $U_{sg} = 4.5$ m/s, $U_{sl} = 0.2$ m/s, with pipe inclined at 0 deg has a corresponding length between subsequent wave peaks of 2.42 m and wave speed of 2.13 m/s (Johnson, 2005). The experimental length L_{expr} is determined as follows, knowing both dominating frequency f_d, and experimental wave velocity U_{wave} (Johnson, 2005):

$$L_{expr} = \frac{U_{wave}}{f_d} \tag{27}$$

For the stated example, the dominating frequency was 0.88 Hz or a delay of 1.1 s between waves. In the simulation of this case, waves were inserted close to the inlet every 1.1 s.

A sampling of 65 experiments were chosen as examples to compare to simulations. Simulations could have been run for all the experiments conducted but this would have been time consuming since nearly 1000 experiments were made. The smaller selection covers a range of U_{sg}, U_{sl}, and pipe inclinations summarized in Table 4. The velocities U_{sl} and U_{sg} for a given experimental case are summed together to obtain the mixture velocity, which is used in later plots.

4.3. The discharge coefficient C_d

Estimating C_d has been one of the challenges of simplification in this model. C_d is an open parameter in the simplified model using an orifice type relation that needs to be chosen. A test case with $U_{sg} = 4.5$ m/s and $U_{sl} = 0.2$ m/s in a horizontal pipe was used to determine the model's sensitivity to various values of C_d. These results are listed in Table 5. For reference, the experimentally determined wave velocity is 2.13 m/s and the pressure drop is 181.6 Pa/m. The results indicated that if C_d was doubled to 0.8 or

Table 4
Cases simulated.

Inclination (deg)	U_{sl} (m/s)	U_{sg} (m/s)
0	0.2, 0.4	1.0, 1.5, 2.0, 2.5, 3.0, 3.5, 4.0, 4.5
0.1	0.2, 0.25, 0.35, 0.4	1.0, 1.4, 1.8, 2.2, 2.6, 3.0, 3.5, 4.0, 4.5
0.25	0.2, 0.3, 0.4	1.6, 1.8 2.2, 2.4, 2.6, 3.0, 3.5, 4.0, 4.5
1	0.1, 0.2, 0.3	2.0, 2.5, 3.0, 3.5, 4.0, 4.5

Table 5
Simulated wave velocity and pressure drop for different values of discharge coefficient C_d. Simulations were run for a 0.1 m internal diameter horizontal pipe at 8 bar with $U_{sg} = 4.5$ m/s and $U_{sl} = 0.2$ m/s.

Discharge coefficient C_d	Wave velocity (m/s)	Pressure drop (Pa/m)
0.2	2.72	234
0.4	2.16	189
0.6	1.88	165
0.8	1.66	155

halved to 0.2, wave velocity and pressure drop varied by about 25%. The wave velocity and pressure drop calculated with $C_d = 0.4$ gave the most reasonable approximation to the experimental values and so $C_d = 0.4$ has been used for all other simulations.

4.4. Wave velocities

A comparison of the experimental and simulated wave velocities was made. These are plotted against the mixture velocity $(U_{sl} + U_{sg})$ in four separate graphs for each pipe inclination in Fig. 6. Since two or three different U_{sl} values in combination with a wider range of U_{sg} were simulated, there appears to be two or more data sets in each plot. For similar mixture velocities, a larger wave velocity corresponds to a larger U_{sl} value. The experimental wave speeds were smaller than the mixture velocity whereas slug velocities would be approximately 1.2 times the mixture velocity. The tracking scheme reproduced waves with velocities of the expected magnitude, that is, less than what the bubble nose velocity of a slug would be for a given U_{sg} and U_{sl} combination.

The average absolute percentage difference between model and experiment was 8.4% with maximum difference of 43% and minimum of 0.36%. There were 56 of 65 total simulated wave speeds within 20% of the experimental values, indicating good agreement. The simulated case with the largest percentage difference belonged to pipe inclination 1 deg, $U_{sg} = 2.5$ m/s, and $U_{sl} = 0.3$ m/s. Most of the waves inserted in this simulation grew to slugs. The velocity used in the percentage difference estimation was the average velocity of waves before they grew to slugs, this result is slower than what was measured experimentally. Considering the simplicity of the model, the comparison with experimental wave speeds are good.

4.5. Pressure drops

It has been observed experimentally that pressure drop in flow with large amplitude waves increases significantly compared to smooth stratified flow (Holmås, 2008; Espedal, 1998; Fernandino, 2007). Considering the assumptions in the tracking scheme, it is also expected that pressure drop will increase with the number of waves in the pipe and that if slug flow occurs pressure drop will be larger still. For comparison, a case at horizontal, $U_{sg} = 3.5$ m/s, $U_{sl} = 0.2$ m/s with a wavelength of 2.65 m corresponding to a delay of 1.5 s between waves gives an averaged pressure drop of 119 Pa/m compared with an experimental value of 121.7 Pa/m

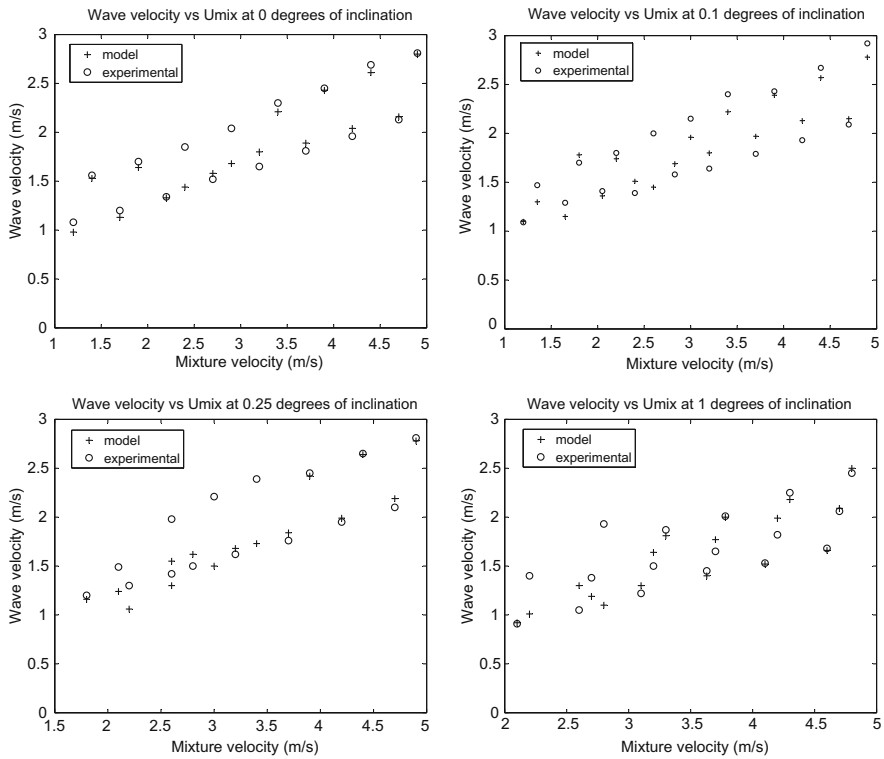

Fig. 6. Experimental wave velocities (Johnson, 2005) compared with results from dynamic tracking simulations.

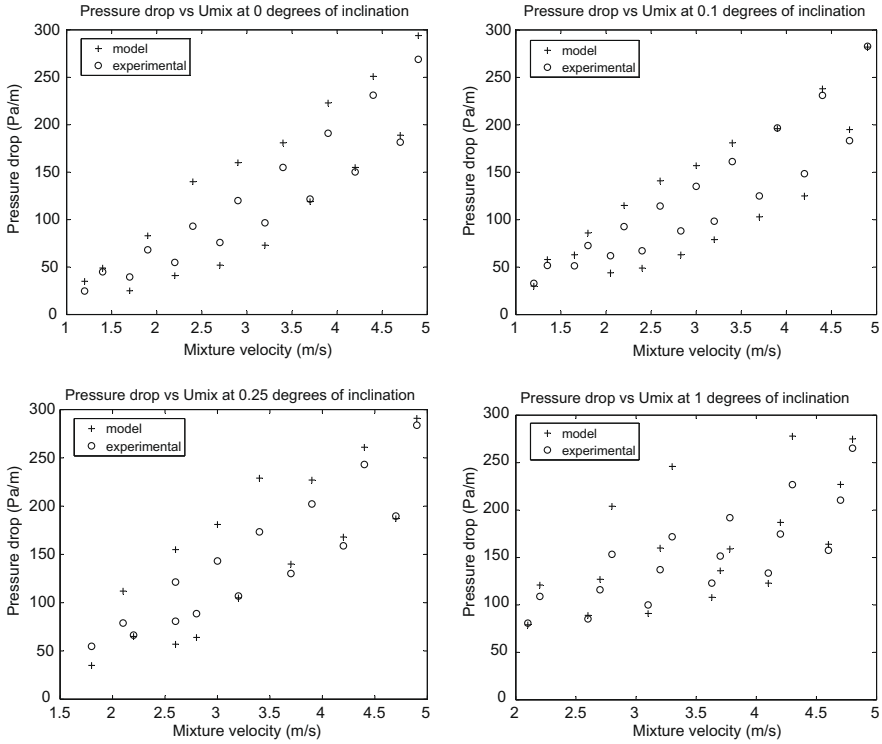

Fig. 7. Experimental pressure drops (Johnson, 2005) compared with averaged pressure drops from tracking simulations.

(Johnson, 2005), but with stratified flow (infinite time delay between waves) the pressure drop is 68 Pa/m.

Experimental pressure drops and averaged pressure drops from the tracking scheme are compared in four separate graphs for each pipe inclination in Fig. 7. As in Fig. 6, there appears to be two or more data sets in each plot. For similar mixture velocities, higher pressure drops correspond to larger U_{sl}. The model predicted pressure drops quite well, with an absolute percentage difference of 17% on average, minimum of 0.29% and maximum of 50%. Two thirds of the modelled data points were within 20% of the experimental data. In the case of the largest deviation in a horizontal pipe with $U_{sg} = 2$ m/s and $U_{sl} = 0.4$ m/s, some of the simulated waves grew to slugs. Since slugs occurred the modelled pressure drop, 140 Pa/m was larger than the experimental 93 Pa/m (Johnson, 2005). Some of the pressure predictions could be larger than expected because waves appeared too frequently in the simulation, or because some of them grew to slugs.

5. Conclusions

A simplified model for large amplitude roll waves has been implemented and tested in a dynamic slug tracking scheme. The wave model includes a simple relation for wave speed which allows for a smooth transition to slug flow. Pressure variation across wave fronts is modelled with a modified orifice type relation. The model predicts wave velocities which are less than slug velocities and pressure drops larger than in the case of stratified flow.

Dynamic flow simulations have been compared with available experimental data for roll waves at high gas densities. The waves in the simulations were initiated with a frequency similar to the experimental frequencies. The resulting comparison between computed wave velocities and pressure drops were good with average percentage differences of 8.4% and 17%, respectively. The quality of wave and slug tracking simulations depends on the initiation models. It remains as a challenge to develop grid independent initiation models for wave and slug tracking on a coarse grid.

Acknowledgment

Financial support from Total E&P Norge is gratefully acknowledged by A. De Leebeeck.

Appendix A. Supplementary data

Supplementary data associated with this article can be found, in the online version, at doi:10.1016/j.ijmultiphaseflow.2009.09.002.

References

Andreussi, P., Bonizzi, M., Lullo, A.D., Margarone, M., Scotti, A., Taddei, S., 2008. Advanced simulation of gas–liquid pipelines. In: Proceedings of the Sixth North American Conference on Multiphase Technology, Banff, Canada.

Andritsos, N., Hanratty, T.J., 1987. Interfacial instabilities for horizontal gas–liquid flows in pipelines. Int. J. Multiphase Flow 13, 583–603.

Barnea, D., Taitel, Y., 1993. Kelvin–Helmholtz stability criteria for stratified flow: viscous versus non-viscous (inviscid) approaches. Int. J. Multiphase Flow 19, 639–649.

Bendiksen, K.H., 1984. An experimental investigation of the motion of long bubbles in inclined tubes. Int. J. Multiphase Flow 10, 467–483.
Bendiksen, K.H., Malnes, D., Nydal, O.J., 1996. On the modelling of slug flow. Chem. Eng. Commun. 141–142, 71–102.
Bonizzi, M., Issa, R.I., 2003. A model for simulating gas bubble entrainment in two-phase horizontal slug flow. Int. J. Multiphase Flow 29, 1685–1717.
De Leebeeck, A., Gaarder, A.H., Nydal, O.J., 2007. Experiments on roll waves in air–water pipe flow. In: 16th Australasian Fluid Mechanics Conference, Gold Coast, Australia.
De Leebeeck, A., Nydal, O.J., 2009. Large amplitude waves in a slug tracking scheme. In: Mammoli, A.A., Brebbia, C.A. (Eds.), Computational Methods in Multiphase Flow V. WIT Press, New Forest, UK, pp. 99–110.
Espedal, M., 1998. An experimental investigation of stratified two-phase flow at small inclinations. Ph.D. Thesis, Norwegian University of Science and Technology.
Fernandino, M., 2007. Experimental and numerical characterization of turbulence structure in stratified horizontal air water duct flow. Ph.D. Thesis, Norwegian University of Science and Technology.
Ferziger, J.H., Perić, M., 2001. Computational Methods for Fluid Dynamics, third ed. Springer-Verlag, Berlin.
Fletcher, D.F., Thyagaraja, A., 1991. A finite difference error arising from the use of a staggered grid. Appl. Math. Model. 15, 496–498.
Haaland, S., 1983. Simple and explicit formulas for the friction factor in turbulent pipe flow. J. Fluid Eng. 105, 89–90.
Hanyang, G., Liejin, G., 2008. Experimental investigation of slug development on horizontal two-phase flow. Chin. J. Chem. Eng. 16, 171–177.
Holmås, H., 2008. Numerical simulation of waves in two-phase pipe flow using 1D two-fluid models. Ph.D. Thesis, University of Oslo.
Hu, B., Stewart, C., Manfield, P.D., Ujang, P.M., Hale, C.P., Lawrence, C.J., Hewitt, G.F., 2007. A model for tracking the evolution of slugs and waves in straight pipelines. In: Sixth International Conference on Mulitphase Flow, Leipzig, Germany.
Issa, R.I., Kempf, M.H.W., 2003. Simulation of slug flow in horizontal and nearly horizontal pipes with the two-fluid model. Int. J. Multiphase Flow 29, 69–95.
Johnson, G.W., 2005. A study of stratified gas–liquid pipe flow. Ph.D. Thesis, University of Oslo.
Kjølaas, J., 2007. Plug propagation in multiphase pipelines. Ph.D. Thesis, Norwegian University of Science and Technology.
Lin, P.Y., Hanratty, T.J., 1986. Prediction of the initiation of slugs with linear stability theory. Int. J. Multiphase Flow 12, 79–98.
Lin, P.Y., Hanratty, T.J., 1987. Detection of slug flow from pressure measurements. Int. J. Multiphase Flow 13, 13–21.
Nydal, O.J., Banerjee, S., 1996. Dynamic slug tracking simulations for gas–liquid flow in pipelines. Chem. Eng. Commun. 141–142, 13–39.
Ottens, M., Klinkspoor, K., Hoefsloot, H.C.J., Hamersma, P.J., 2001. Correlations predicting liquid hold-up and pressure gradient in steady-state (nearly) horizontal co-current gas–liquid pipe flow. Trans. IChemE 79, 581–592.
Prosperetti, A., Tryggvason, G., 2007. Computational Methods for Multiphase Flow. Cambridge University Press, Cambridge.
Renault, F., 2007. A Lagrangian slug capturing scheme for gas–liquid flows in pipes. Ph.D. Thesis, Norwegian University of Science and Technology.
Soleimani, A., Hanratty, T., 2003. Critical liquid flows for the transition from the pseudo-slug and stratified patterns to slug flow. Chem. Eng. Sci. 29, 5167.
Taitel, Y., Barnea, D., 1998. Effect of gas compressibility on a slug tracking model. Chem. Eng. Sci. 53, 2089–2097.
White, F.M., 2005. Fluid Mechanics, fifth ed. McGraw-Hill, Boston.

Electronic Annex 1

Extract from the dissertation of J. Kjølaas "Plug propagation in multiphase pipelines" from the Norwegian University of Science and Technology, 2007 showing the conservation equations in differential form, reproduced with permission.

Conservation equations on a moving grid

This section presents a description on how the two-fluid model equations applied in the current work have been derived. The mass- momentum- and energy equation are integrated over a control volume V_k, which by definition is exclusively occupied by the phase k. Averaged values of quantities within V_k are represented by brackets < >. It should be noted that the volume V_k is considered a moving, deformable control volume in the calculations below, leading to some additional terms in the integrated equations related to the velocity of the control volume boundaries (u_b).

Mass conservation equation

The 1D mass conservation equation is given by:

$$\partial_t \rho + \partial_x \left(\rho u \right) = \dot{\rho}^s \tag{1}$$

Here, ρ is the density, u is the velocity and $\dot{\rho}^s$ represents a mass source (kg/m^3s). Integrating (1) over the volume V_k enclosing phase k yields:

$$\partial_t M_k + \oint_{A_k} \rho_k \left(u_k - u_b \right) dS = \dot{M}_k^s \tag{2}$$

Here, M_k is the total mass within V_k ($M_k = \left\langle \rho_k \right\rangle V_k$), u_b is the velocity of the boundaries of V_k, A_k is the surface area of V_k, and $\dot{M}_k^s$ is the mass source term (kg/s).

Pressure equation

The integrated mass equation is expanded and divided by $<\rho_k>$:

$$\frac{V_k}{\left\langle \rho_k \right\rangle} \partial_t \left\langle \rho_k \right\rangle + \partial_t V_k + \frac{1}{\left\langle \rho_k \right\rangle} \oint_{A_k} \rho_k \left(u_k - u_b \right) dS = \frac{\dot{M}_k^s}{\left\langle \rho_k \right\rangle} \tag{3}$$

The transient density term is expanded using the equation of state:

$$\frac{V_k}{\left\langle \rho_k \right\rangle} \left[\left(\frac{\partial \rho_k}{\partial p} \right)_{T_k} \partial_t \left\langle p \right\rangle + \left(\frac{\partial \rho_k}{\partial T_k} \right)_p \partial_t \left\langle T_k \right\rangle \right] + \partial_t V_k + \frac{1}{\left\langle \rho_k \right\rangle} \oint_{A_k} \rho_k \left(u_k - u_b \right) dS = \frac{\dot{M}_k^s}{\left\langle \rho_k \right\rangle} \tag{4}$$

The pressure equation is obtained by adding together equation (4) for all phases k. For simplicity, the average-brackets are removed.

$$\sum_k \frac{V_k}{\rho_k} \left[\left(\frac{\partial \rho_k}{\partial p} \right)_{T_k} \partial_t p + \left(\frac{\partial \rho_k}{\partial T_k} \right)_p \partial_t T_k \right] + \partial_t V + \sum_k \frac{1}{\rho_k} \oint_{A_k} \rho_k \left(u_k - u_b \right) dS = \sum_k \frac{\dot{M}_k^s}{\rho_k} \tag{5}$$

Momentum conservation equation

The 1D momentum conservation equation is given by:

$$\partial_t\left(\rho u\right)+\partial_x\left(\rho u^2+p\right)=\partial_x\tau-\rho g\sin\varphi+\dot{\rho}^s u^s \tag{6}$$

Here, p is the pressure, $\partial_x\tau$ represents the friction term, g is the gravity acceleration, φ is the pipe inclination angle while $\dot{\rho}^s$ and u^s are the density and velocity associated with a mass source. Integrating equation (6) over a volume V_k yields:

$$\partial_t\left(M_k\left\langle u_k\right\rangle\right)+\oint_{A_k}\rho_k u_k\left(u_k-u_b\right)=-V_k\partial_x\left\langle p_k\right\rangle+\oint_{A_k}\tau_k dS-M_k g\sin\varphi+\dot{M}_k^s u_k^s \tag{7}$$

Now we assume two-phase stratified flow, and define a common pressure p for the two phases at the phase interface. The relationship between p_k and p is then:

$$\partial_x\left\langle p_k\right\rangle=\partial_x\left\langle p\right\rangle+\left\langle\rho_k\right\rangle g\cos\varphi\cdot\partial_x h_{D,l} \tag{8}$$

Here, $h_{D,l}$ is the liquid height. This yields the following momentum equation (removing the average-brackets):

$$\begin{aligned}&\partial_t\left(M_k u_k\right)+\oint_{A_k}\rho_k\left(u_k-u_b\right)u_k dS=\\&-V_k\partial_x p-M_k g\cos\varphi\cdot\partial_x h_{D,l}+\oint_{A_k}\tau_k dS-M_k g\sin\varphi+\dot{M}_k^s u_k^s\end{aligned} \tag{9}$$

Paper 5

Liquid flushing of an undulating pipeline

A. De Leebeeck, A. N. Winnem and O. J. Nydal

Submitted to the International Conference on Multiphase Flow, Tampa, FL, May 30-June 4, 2010

Liquid flushing of an undulating pipeline

A. De Leebeeck, A. N. Winnem and O. J. Nydal

December 14, 2009

Abstract

Experiments of water flushing an initially empty undulating pipeline with five upward and downward segments inclined at 40° are run in a 0.016 m I.D. pipe at atmospheric pressure. Experiments are made by opening a valve connecting the inlet to a water reservoir at constant height. Four cases with different reservoir heights are investigated. The first three cases partially fill the pipeline before the water flow stops and in the last case, the pipeline is completely flushed with water. These end states compare well to simulations from a slug tracking scheme where slugs are modelled dynamically as moving objects on a coarse grid. Time varying water front positions are obtained from video analysis of the experiments and compared with similar numerical results.

1 Introduction

When liquid starts flowing in an initially empty undulating pipeline, liquid can accumulate in low points and form slugs which completely block the pipe cross-section. As liquid flows over a bend and then downhill, stratified flow will occur where the liquid flows downwards. If enough liquid accumulates in a low point, slugs will form and eventually start propagating along the pipeline. As they flow uphill, the liquid slugs may decay again as they are penetrated by gas bubbles. If there is not sufficient inlet pressure to flush the pipe completely, large gas bubbles between slugs can turn and become trapped at high points in the pipeline. Bubbles will flow in the direction of lower pressure, usually the outlet. Laboratory experiments on water flushing in an initially empty undulating pipeline are conducted and compared with simulations from a slug tracking scheme.

In the slug tracking scheme, stratified sections between slugs are modelled on a coarse fixed grid while slugs are modelled as moving objects. Slugs, or similar moving objects, have boundaries corresponding to sharp moving fronts thus avoiding numerical diffusion and the need for excessive grid refinement [6]. Front physics such as bubble nose velocities or gas entrainment can also more easily be implemented in a tracking scheme as compared to a capturing scheme. Tracking schemes have also been tested for plug simulations where plugs are treated as rigid moving objects [6] and for large roll waves propagating in a similar way to slugs [3, 7]. The tracking scheme has also compared well with severe slugging experiments in a S-shaped riser [9].

The bubble turning process, where a bubble propagating downwards reverses direction and then moves counter-current to the liquid flow, is a key phenomenon in the flushing experiments. A turning criteria based on a critical flow rate balancing friction and gravity is used in the tracking scheme [5, 8, 10].

Four different experimental cases with inlet pressures corresponding to the weight of constant water levels at 0.450 m, 0.675 m, 0.750 m, and 0.825 m above the inlet are run in an undulating pipeline. The end state of water flow in the pipeline, whether completely flushed with liquid or blocked, is compared to simulations with the slug tracking scheme. Time varying liquid front

positions are obtained from video analysis also for comparison with corresponding numerical results.

2 Experiments

Experiments were conducted in the multiphase flow laboratory at NTNU in a 0.016 m internal diameter (I.D.) clear acrylic undulating pipeline containing two peaks and two valleys. A schematic of the experimental setup is shown in figure 1. Constant pressure was achieved at the inlet by attaching a large open water tank which was elevated with a manual jack above the inlet. The inlet pressure was determined by the weight of the liquid column above it. The tank volume was large compared to the volume of the undulating pipeline so that the tank level was essentially constant during pipe flushing. The water was allowed to flow through the initially empty pipeline by opening a magnetic valve (ASCO Magnetic Diafragma) until it came to rest. The different straight rigid pipe segments were inclined at 40 degrees upward or downward after each bend. The first segment was 0.91 m long and inclined upward to the first peak. This was followed by four alternating downward and upward segments each 0.83 m long. The rigid segments were connected with 0.16 m long clear flexible hoses at the bends. The outlet was at the top of the last upward segment. In preparation for the next experiment, pressurized air was used to empty the pipeline and the water was pumped back into the tank.

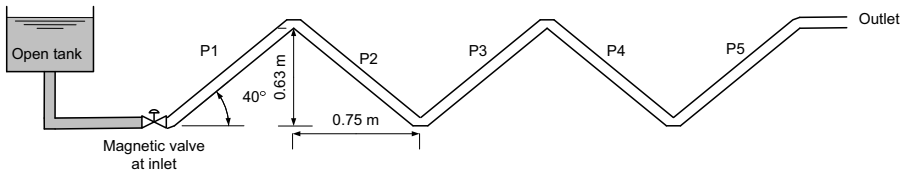

Figure 1: Schematic of the undulating pipeline setup. The test section consists of five pipe segments labeled P1 through P5 inclined at 40°. The magnetic valve allows liquid to flow into the pipeline from the open tank. Water filled areas are colored gray.

Fluorescent green dye (Merck natrium and sodium) was added to the water so that the propagating liquid front could be recorded on video with a high definition video camera (Sony HDR-UX7E) at 25 fps with a resolution of 1920×1080 pixels. The position of the green liquid front in each frame and the corresponding time stamp was then extracted from the video using image analysis scripts developed in Matlab. The video was taken for about 12 sec in each experiment, which was long enough for the water in the pipe to come to rest or for the pipe to be flushed completely with water. The end state water height in the pipe segments was also measured.

Experiments with four different water levels in the tank above the inlet were run:

- Water level at 0.450 m where liquid settled in the first upward pipe segment P1.
- Water level at 0.675 m where liquid settled in the first three pipe segments.
- Water level at 0.750 m where liquid settled in all five of the pipe segments.
- Water level at 0.825 m where the pipeline was flushed completely with water.

3 Simulations

Simulations of filling the undulating pipeline were run with a slug tracking code [3, 6, 7] which was written in C++ using object oriented programming techniques. The slug tracking scheme uses a one dimensional finite volume method with a moving grid. Slug flow is represented with alternating slug objects that completely fill the pipe cross-section with liquid and bubble regions in between slugs, where the gas flows over the liquid phase. The two-fluid model of stratified flow is solved in the bubble regions on a stationary staggered grid where phase velocities are determined at section borders, and pressure and masses are determined at section centers. Slug sections are modelled as moving objects where liquid phase velocity, slug length, front and tail velocities are determined from mass and momentum balances. A schematic of the computational objects, slugs and stratified sections, is shown in figure 2. The index notation shown at section centers and borders is used in later equations and the variables are defined below.

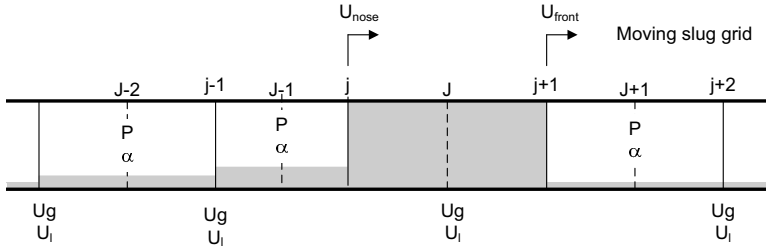

Figure 2: Schematic representation of the computational objects in the slug tracking scheme. The liquid phase is shown in gray and the gas phase in white. Dashed lines indicate section centers while solid lines indicate section borders. The index notation for section centers and borders is shown at the top. Section J is a slug between the stratified sections $J-1$ and $J+1$. Arrows indicate the movement of slug borders.

For the purposes of these simulations, flow is assumed isothermal so the energy equations can be neglected. It is also assumed that there is no mass transfer between the phases through evaporation or condensation. Gas entrainment and droplets in the gas phase are also neglected.

3.1 Stratified flow sections

The two-fluid model is applied in stratified sections on a stationary grid. Phase velocities are determined at section borders by solving the momentum balance equations. The following momentum balance equation applies to either the gas or the liquid phase at a border j:

$$\frac{\Delta U_j M_j}{\Delta t} + \Delta_j \left(\frac{M_j}{L_j} U_j \left(U_j - U_{b,j} \right) \right) = -\alpha_j A (P_J - P_{J-1}) - M_j g \cos\theta \frac{h_{l,J} - h_{l,J-1}}{L_j} - M_j g \sin\theta - \frac{1}{2} \lambda_j \rho_j \left| U_j \right| \left(U_j \right) \frac{S_j L_j}{4} - \frac{1}{2} \lambda_i \rho_{g,j} \left| U_j - U_{n,j} \right| \left(U_j - U_{n,j} \right) \frac{S_i L_j}{4} \quad (1)$$

where M_j and α_j are the averaged values of the phase mass and area fraction at the border. Δ represents a change in a quantity e.g. Δt is the time step. U is the phase velocity, U_b is the border velocity, A is area, L is length, P is pressure, θ is the angle of inclination, h_l is the liquid height, S is the perimeter, λ is the friction factor, ρ is density, and g is the acceleration of gravity. Subscripts are i for interface quantities and n for the neighboring phase.

Pressure is determined from the volumetric flow balance using a combination of mass conservation and the equations of state in both phases, as follows:

$$\left(\frac{\alpha_J}{\rho_g}\frac{\partial \rho_{g,J}}{\partial P} + \frac{1-\alpha_J}{\rho_{l,J}}\frac{\partial \rho_l}{\partial P}\right)\frac{L_J A \Delta P_J}{\Delta t} + A\left(U_{b,j+1} - U_{b,j}\right) + \sum_k \frac{1}{\rho_{k,J}}\left[m_{k,j+1}A\left(U_{k,j+1} - U_{b,j+1}\right) - m_{k,j}A\left(U_{k,j} - U_{b,j}\right)\right] = 0 \tag{2}$$

In the above equation, $m = M/AL$ is the mass per pipe volume and subscripts are g for gas phase, l for liquid phase, and k representing either phase. As equation (2) is not formulated in a mass-conservational manner, a source term is added in the following time step to ensure consistency with the mass conservation equation over time. This source term is as follows:

$$\frac{AL_J}{\Delta t}\left(\frac{m_{l,J}}{\rho_{l,J}} + \frac{m_{g,J}}{\rho_{g,J}} - 1\right) \tag{3}$$

Next, the mass balance equations are solved. The mass balance equation in a section J for either phase is given below:

$$\frac{\Delta M_J}{\Delta t} + \Delta_j\left(\frac{M_j}{L_j}\left(U_j - U_{b,j}\right)\right) = 0 \tag{4}$$

Upstream values of M_j are used in the above equation.

As the slug grid moves, stratified sections are adjusted dynamically according to the movement of slugs. Large sections are split while short ones are merged together.

3.2 Slug sections

The dynamics of the flow in a slug can be determined from a mixture momentum equation and a slip relation. A simplified version of the mixture momentum equation is the liquid momentum equation without the gas interaction term. The liquid momentum equation in a slug J takes the following form:

$$\frac{\Delta U_{l,J} M_{l,J}}{\Delta t} + \Delta_J\left(\frac{M_{l,J}}{L_J}U_{l,J}\left(U_{l,J} - U_{b,j}\right)\right) = -\alpha_{l,J}A(P_J - P_{J-1}) - M_{l,J}g\sin\theta - \frac{1}{2}\lambda_{l,J}\rho_{l,J}\left|U_{l,J}\right|\left(U_{l,J}\right)\frac{S_{l,J}L_J}{4} \tag{5}$$

The above equation has a similar form to equation (5), except interface friction can be neglected (no interface).

Gas velocity in a slug is determined using a slip relation or assuming no slip, by the following general slip equation:

$$U_{g,J} = S_d\left(U_{l,J} + v_o\right) \tag{6}$$

where S_d is the distribution slip ratio and v_o is the averaged drift velocity.

The change in mass in a slug for either phase in a given time step is the difference in mass flux in and out, determined from the same mass balance equation (4) as in stratified sections.

Slugs are modelled as objects with moving boundaries, which have either a front velocity or a bubble nose (tail) velocity. If a slug's left boundary velocity is greater than its right boundary velocity, then the slug length will grow. The front velocity is determined from a mass balance across the front as follows:

$$U_{front} = \frac{H_{slug}U_{l,slug} - H_{strat}U_{l,strat}}{H_{slug} - H_{strat}} \tag{7}$$

where H is the liquid holdup and subscripts *strat* relates to stratified sections while *slug* relates to slug sections. The bubble nose velocity is as follows [1, 2]:

$$U_{nose} = C_o U_{mix} + U_o \tag{8}$$

where $U_{mix} = H_{slug}U_{l,slug} + (1 - H_{slug})U_{g,slug}$ is the local mixture velocity in the slug. Values for C_o and U_o which give the largest U_{nose} are applied, as follows:

$$\begin{array}{lll} C_o = 1.05 + 0.15\sin^2\theta & U_o = U_{ov} + U_{oh} & \text{if } |U_{mix}| < 3.6\sqrt{gD}/\cos\theta \\ C_o = 1.2 & U_o = U_{ov} & \text{if } |U_{mix}| > 3.6\sqrt{gD}/\cos\theta \\ U_{ov} = 0.35\sqrt{gD}\sin\theta & U_{oh} = \pm 0.54\sqrt{gD}\cos\theta & \end{array}$$

The direction of slug movement and therefore whether a border is a slug front or a bubble nose is determined from a bubble turning criterion under the assumption that large bubbles between slugs will move in the direction opposite to pressure gradient [6]. The turning criterion is the point where friction and gravity balance each other and pressure gradient is zero [5, 8]. It is particularly important in downward flow where bubbles can reverse direction relative to the liquid flow.

The initiation of slugs occurs when the liquid level in a low point exceeds a user specified maximum holdup, for example $H = 0.99$. In that case, the stratified section will be converted to a slug section. Slugs are removed either when they exit the pipe or when their length goes below a user specified minimum value.

3.3 Computational Sequence

The computational sequence in a given time step begins with determining the equation coefficients on moving borders in slug sections. Next the system of pressure and momentum balance equations (equations (5) and (2)) is solved simultaneously by inverting a banded matrix. The solution is found using direct Gauss elimination and gives phase velocities and pressures. The border velocities and positions of slugs are then updated. This is followed by solving the mass balance equations, with implicit time integration in the stratified sections. In slug sections, the mass balance equations are solved explicitly. Next, phase masses, phase densities from equations of state, and volume errors are updated. Slugs are inserted or deleted and sections are merged and split according to the the movement of slug borders. Lastly, the time step is incremented and the sequence repeated.

3.4 Simulation setup

The undulating pipeline was simulated as a series of five straight pipe segments inclined at 40° degrees alternating upward and downward. Each pipe had a 0.016 m I.D. and was 0.98 m long to account for the additional length of the flexible hose at the bends. A vertical column filled with the same water height as in the inlet tank in the experiment was modelled at the inlet. A constant level of water at the top of the vertical pipe was assumed. The pipeline outlet was set at atmospheric pressure. The pipeline was initially empty and the propagating front coming in from the liquid column was simulated for a total of 60 sec. Water properties were constant and the air was treated as an ideal gas.

3.5 Effect of grid sizes

Grid sizes are adjusted dynamically according to the movement and growth of slugs. Minimum and maximum grid lengths in numbers of pipe diameters were: one diameter for the minimum

slug length at which point slugs are killed, four diameters for the minimum stratified section length when the section is merged with its neighbor, and 15 diameters for the maximum stratified section length when the section is split.

The maximum grid size will determine how quickly slugs form at low points. It takes longer for a large computational section to fill with liquid and become a slug. As an example simulations with an inlet liquid column height of 0.675 m were run with different maximum grid lengths while the minimum slug length and stratified section length were fixed at 1 and 4 diameters respectively. The end state of simulations with a maximum grid length of 5, 10, 15, and 30 diameters are shown in figure 3. The results were qualitatively similar but there was more liquid in the low point as the grid size increased to 30 diameters.

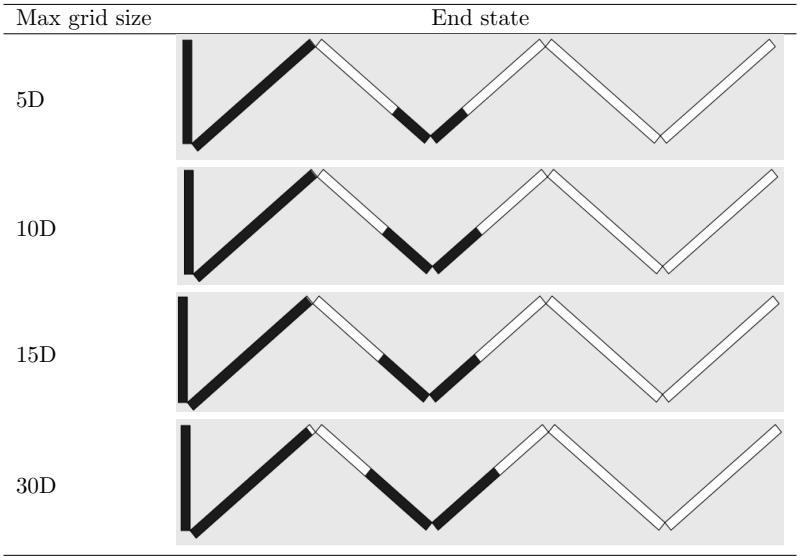

Figure 3: Images of the simulated end state in the undulating pipeline with different maximum grid sizes in multiples of pipe diameter D. The water height above the inlet is 0.675 m. Water filled areas are shown in black, white areas represent the air phase.

3.6 Pipe friction and additional losses

Frictional losses were larger in the experiments than in the first computations. Therefore an attempt was made to approach the experimental conditions by adding the component losses of bends and a valve to the simulated system. These were introduced into the simulation assuming loss coefficients K for a single phase pipeline from [11]. Table 1 lists the components causing additional losses in the experimental setup and their estimated loss coefficients assuming the pipeline is completely flushed with liquid. The total loss coefficient $\Sigma K = 13.5$ was assumed in simulations.

Pipe roughness was also specified, $\epsilon = 1 \times 10^{-5}$ m for acrylic pipe, and used in determining the pipe friction factor, as follows [4]:

$$\frac{1}{\sqrt{\lambda_k}} = -1.8\log\left(\frac{6.9}{Re_k} + \left(\frac{\epsilon}{3.7D_{h,k}}\right)^{1.11}\right) \tag{9}$$

Component	Loss coefficient
4x 90° long radius bends in $\frac{1}{2}$ inch pipe	1.0
1x 45° long radius bends in $\frac{1}{2}$ inch pipe	0.2
1x sharp inlet	0.5
1x outlet	1.0
1x T where gas can enter, line flow	0.9
1x globe valve 2 inch ID fully open	6.9
TOTAL	13.5

Table 1: Loss coefficients for various components giving additional losses in the undulating pipeline [11].

where Re is the Reynolds number and D_h is the hydraulic diameter. Head loss from pipe wall friction is as follows [11]:

$$h_f = \lambda \frac{L_{pipe}}{D} \frac{|U|\,U}{2g} \tag{10}$$

where L_{pipe} is the length of the pipeline. The head loss from additional pipe components is as follows [11]:

$$h_c = \Sigma K \frac{|U|\,U}{2g} \tag{11}$$

Head losses are related to shear stress τ as follows:

$$h_{losses} = h_f + h_c = \frac{4\tau L_{pipe}}{\rho g D} \tag{12}$$

Rearranging equations 10, 11, and 12 gives the frictional shear stress including both pipe wall friction losses and losses from additional pipe components which will appear in the momentum balance equations:

$$\tau = \frac{1}{8}\left(\lambda + \frac{\Sigma K D}{L_{pipe}}\right)\rho\,|U|\,U \tag{13}$$

Taking an example with the water height above the inlet equal to 0.675 m, the effect of additional component losses was investigated in simulations. The end state images corresponding to different total loss coefficients are shown in figure 4. The expected behavior from the experiment was that the first pipe filled completely and liquid collected in the first low point. Without the component losses or if the losses were approximately half of the estimated total $\Sigma K = 13.5$, liquid completely filled the first three pipes and accumulated in the second low point, behavior which differed from the experiment. Once component losses approached the estimated value $\Sigma K = 13.5$, the simulations produced the expected results.

4 Results and Discussion

Results from the experiments included videos, transient plots of the liquid front position, measurements of the end state liquid column heights in each pipe segment if the test section was not completely flushed, and times to reach the final state. The results from the four experimental cases run have been compared to simulations.

Total loss coefficient	End state image
0.00	
6.00	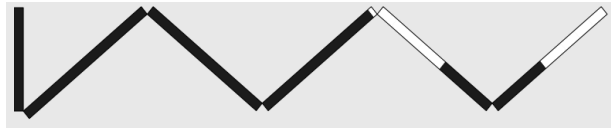
12.0	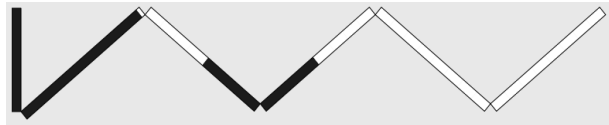
13.5	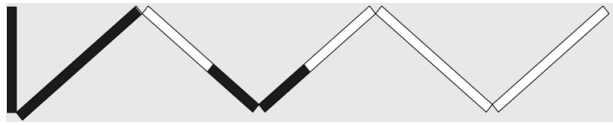

Figure 4: Images showing the effect of the total loss coefficient on the end state of simulations. The water level above the inlet is 0.675 m. Water filled areas are shown in black, air filled areas in white.

The simulations gave qualitatively similar results to the experiments when the liquid in the test section reached equilibrium or when the pipe was flushed completely. Snapshots of the end states from experiments and simulations are shown together for each experimental case in figures 5 through 8.

For the largest liquid level at 0.825 m, the pipeline was flushed completely with water. The measured height of the water column in each pipe segment at the final state and the time to reach the final state are listed in table 2 for experiments and simulations. The end states and final water heights were similar between experiments and simulations, but the time to reach the final state differed by 1 to 4 sec.

The transient behavior during pipe flushing was also investigated experimentally and numerically. Figure 9 shows snapshots at different times during filling when the liquid was 0.825 m above the inlet. In the first snapshot, the liquid has reached the top of P1. This segment was filled faster in the simulation than the experiment where the liquid reached the first peak in 1.05 sec as opposed to 1.80 sec experimentally. The liquid flowed as a stratified film down P2 into the first low point where liquid collected and formed a slug. The film traveled faster than the liquid front which continued to propagate down P2 as well. The second snapshot shows a slug forming in the first low point at 2.68 sec experimentally and 2.42 sec in the simulation. The slug then flowed up P3 where it decayed. The liquid front followed the decaying slug up P3 and completely filled the segment (third snapshot). The simulation was slower to reach this point in 4.32 sec as opposed to 3.80 sec experimentally. Just as in P2, the liquid flowed as a stratified film down P4 and slugs formed in the second low point. The first slug is shown in the fourth snapshot. It formed later in the simulation at 5.96 sec compared to 4.84 sec in the experiment. In total, five slugs formed at the second low point in the simulation while four formed in the experiment. Slugs going up the last pipe segment P5 are shown in the fifth snapshot. The last

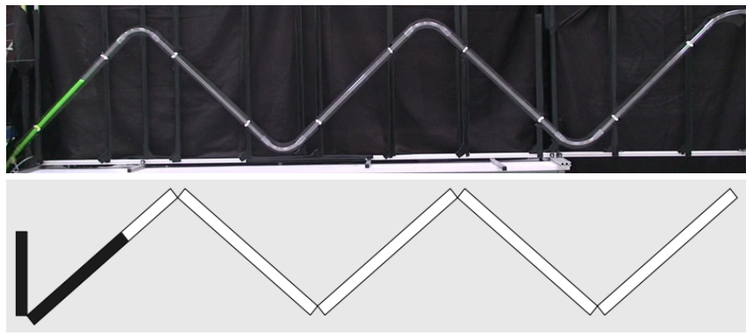

Figure 5: Experimental and simulated end states for water height 0.450 m above the inlet.

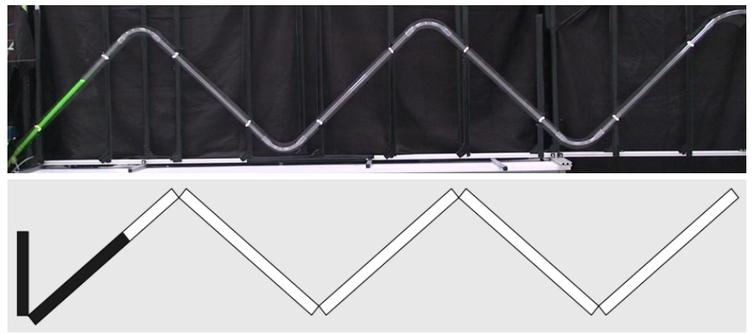

Figure 5: Experimental and simulated end states for water height 0.450 m above the inlet.

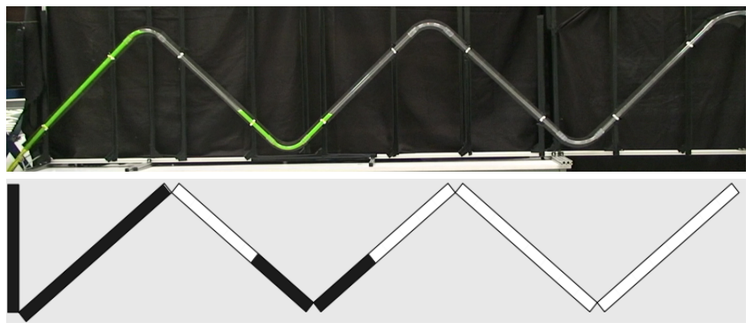

Figure 6: Experimental and simulated end states for water height 0.675 m above the inlet.

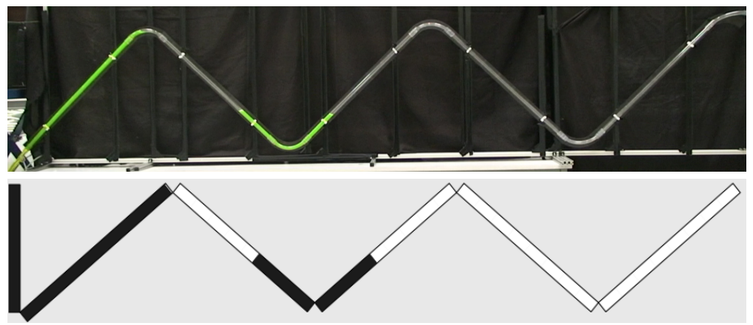

Figure 6: Experimental and simulated end states for water height 0.675 m above the inlet.

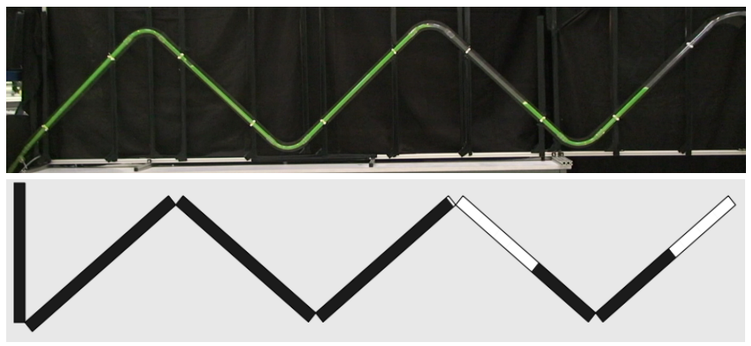

Figure 7: Experimental and simulated end states for water height 0.750 m above the inlet.

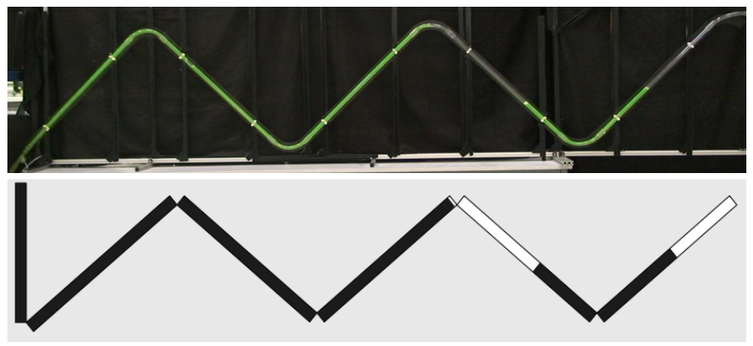

Figure 7: Experimental and simulated end states for water height 0.750 m above the inlet.

9

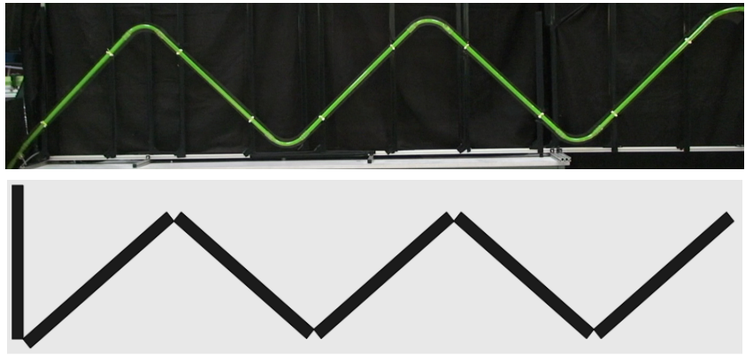

Figure 8: Experimental and simulated end states for water height 0.825 m above the inlet.

Liquid level above inlet (m)	Water height in segment (m)					Time to end state (sec)
	P1	P2	P3	P4	P5	
Experiment 0.450	0.448	0.000	0.000	0.000	0.000	7.20
Simulation 0.450	0.450	0.000	0.000	0.000	0.000	5.60
Experiment 0.675	0.680	0.267	0.237	0.000	0.000	6.30
Simulation 0.675	0.680	0.260	0.260	0.000	0.000	5.10
Experiment 0.750	full	full	0.681	0.286	0.330	7.50
Simulation 0.750	full	full	0.630	0.260	0.340	9.00
Experiment 0.825	full	full	full	full	full	7.30
Simulation 0.825	full	full	full	full	full	11.5

Table 2: Measurements of the liquid height in pipe segments at the final state and the time to reach the final state in experiments and simulations. Segments P1 to P5 correspond to the first through fifth pipe segments labeled in figure 1.

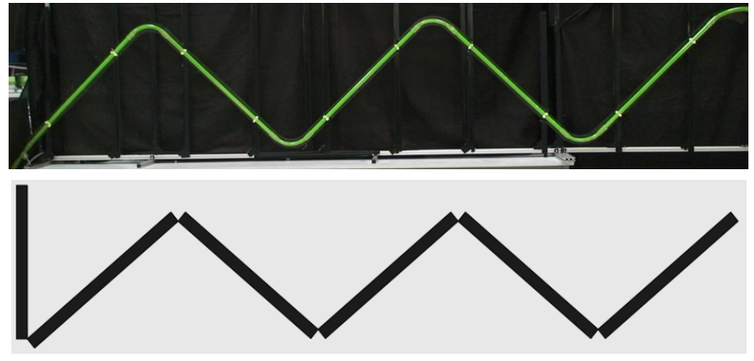

Figure 8: Experimental and simulated end states for water height 0.825 m above the inlet.

Liquid level above inlet (m)	Water height in segment (m)					Time to end state (sec)
	P1	P2	P3	P4	P5	
Experiment 0.450	0.448	0.000	0.000	0.000	0.000	7.20
Simulation 0.450	0.450	0.000	0.000	0.000	0.000	5.60
Experiment 0.675	0.680	0.267	0.237	0.000	0.000	6.30
Simulation 0.675	0.680	0.260	0.260	0.000	0.000	5.10
Experiment 0.750	full	full	0.681	0.286	0.330	7.50
Simulation 0.750	full	full	0.630	0.260	0.340	9.00
Experiment 0.825	full	full	full	full	full	7.30
Simulation 0.825	full	full	full	full	full	11.5

Table 2: Measurements of the liquid height in pipe segments at the final state and the time to reach the final state in experiments and simulations. Segments P1 to P5 correspond to the first through fifth pipe segments labeled in figure 1.

snapshot shows the end state where the pipeline is completely flushed with liquid.

Figure 10 shows snapshots at different times during filling when the liquid was 0.675 m above the inlet. In the first snapshot, the liquid has reached the top of P1 at the same time in the simulation and the experiment. The liquid film then flowed down into the first low point where a slug formed after 2.96 sec in the simulation and after 2.24 sec in the experiment. The liquid front has also entered into the downward segment P2. The low point then continued filling until an end state was reached, the last snapshots in figure 10. The liquid front reversed direction (bubble turning) and eventually came to rest at the top of the first peak.

More quantitatively, the plots in figure 11 show the position of the first liquid front plotted against time. The video analysis of the experimental data was not sensitive enough to pick out the front (or tail) of individual slugs. The position obtained was the position of the liquid front furthest from the inlet. For example, at the end state with a liquid level 0.675 m above the inlet, this would be the position of the top of the liquid column in P3. The video analysis also picked out the position of the front of the liquid film in downward inclined pipe segments (P2 and P4). The liquid front in both upward and downward pipes can be picked out from simulations run with the slug tracking scheme. Since the position of the liquid front was not comparable with the position of the liquid film as it ran downward, positions in downward inclined pipes were omitted in the plots. The front positions plotted correspond to the propagation of the first front in the upward inclined segments against time.

At all liquid levels above the inlet, the simulated results matched quite closely with the experimental front positions in filling P1. After that, the simulated liquid front reached the remaining pipe segments at a later time than in the experiments. At 0.450 m, the liquid level oscillated before settling both experimentally and in the simulation. At 0.675 m and 0.750 m, the simulated front reached almost the same final position as in experiments. At 0.825 m, the first simulated slug to exit the pipe reached the outlet much later than in the experiment but the end result was the same: the pipeline was flushed completely with liquid.

Additional information about slug formation and decay can be obtained from simulations. Slugs form when liquid collects in the low points and they may decay as they propagate along the upward inclined pipe segments. The plots in figure 12 show the positions of slug fronts and the bubble noses at the slug tail from simulations. When the bubble nose catches up to the slug front, the slug decays. In the 0.750 m simulation, two slugs formed at the first low point and eventually decayed. The first one decayed in the upward inclined segment P3, while the second one decayed in the beginning of the downward segment P4. In the 0.825 m simulation, one slug formed in the first low point and it decayed in P3. After forming, the slugs grew slightly before shrinking and decaying.

5 Conclusions

Experiments of water flushing an initially empty undulating pipeline have been run in a 0.016 m I.D pipe at atmospheric pressure. The results were compared with simulations from a slug tracking scheme investigating similarities between the final state and the transient liquid front position.

At first, simulations showed the pipes were completely flushed when liquid flow should have stopped. Improved predictions were obtained by including standard loss terms for valves and bends.

The flow transient includes liquid fronts propagating upwards, bubble turning in the downwards pipes, slug initiation in bends and a subsequent slug decay by bubble penetration. These phenomena were observed experimentally and also reproduced in the slug tracking simulations.

The end state results from the simulations were qualitatively similar to the experiments.

snapshot shows the end state where the pipeline is completely flushed with liquid.

Figure 10 shows snapshots at different times during filling when the liquid was 0.675 m above the inlet. In the first snapshot, the liquid has reached the top of P1 at the same time in the simulation and the experiment. The liquid film then flowed down into the first low point where a slug formed after 2.96 sec in the simulation and after 2.24 sec in the experiment. The liquid front has also entered into the downward segment P2. The low point then continued filling until an end state was reached, the last snapshots in figure 10. The liquid front reversed direction (bubble turning) and eventually came to rest at the top of the first peak.

More quantitatively, the plots in figure 11 show the position of the first liquid front plotted against time. The video analysis of the experimental data was not sensitive enough to pick out the front (or tail) of individual slugs. The position obtained was the position of the liquid front furthest from the inlet. For example, at the end state with a liquid level 0.675 m above the inlet, this would be the position of the top of the liquid column in P3. The video analysis also picked out the position of the front of the liquid film in downward inclined pipe segments (P2 and P4). The liquid front in both upward and downward pipes can be picked out from simulations run with the slug tracking scheme. Since the position of the liquid front was not comparable with the position of the liquid film as it ran downward, positions in downward inclined pipes were omitted in the plots. The front positions plotted correspond to the propagation of the first front in the upward inclined segments against time.

At all liquid levels above the inlet, the simulated results matched quite closely with the experimental front positions in filling P1. After that, the simulated liquid front reached the remaining pipe segments at a later time than in the experiments. At 0.450 m, the liquid level oscillated before settling both experimentally and in the simulation. At 0.675 m and 0.750 m, the simulated front reached almost the same final position as in experiments. At 0.825 m, the first simulated slug to exit the pipe reached the outlet much later than in the experiment but the end result was the same: the pipeline was flushed completely with liquid.

Additional information about slug formation and decay can be obtained from simulations. Slugs form when liquid collects in the low points and they may decay as they propagate along the upward inclined pipe segments. The plots in figure 12 show the positions of slug fronts and the bubble noses at the slug tail from simulations. When the bubble nose catches up to the slug front, the slug decays. In the 0.750 m simulation, two slugs formed at the first low point and eventually decayed. The first one decayed in the upward inclined segment P3, while the second one decayed in the beginning of the downward segment P4. In the 0.825 m simulation, one slug formed in the first low point and it decayed in P3. After forming, the slugs grew slightly before shrinking and decaying.

5 Conclusions

Experiments of water flushing an initially empty undulating pipeline have been run in a 0.016 m I.D pipe at atmospheric pressure. The results were compared with simulations from a slug tracking scheme investigating similarities between the final state and the transient liquid front position.

At first, simulations showed the pipes were completely flushed when liquid flow should have stopped. Improved predictions were obtained by including standard loss terms for valves and bends.

The flow transient includes liquid fronts propagating upwards, bubble turning in the downwards pipes, slug initiation in bends and a subsequent slug decay by bubble penetration. These phenomena were observed experimentally and also reproduced in the slug tracking simulations.

The end state results from the simulations were qualitatively similar to the experiments.

1. First pipe segment P1 filled.

1.80 s

1.05 s

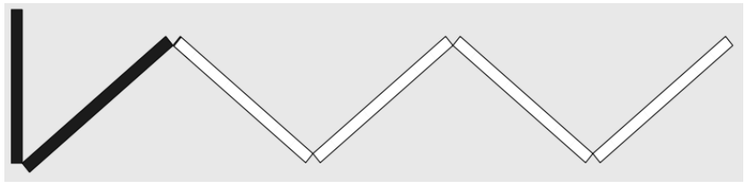

2. A slug forms at the first low point.

2.68 s

2.42 s

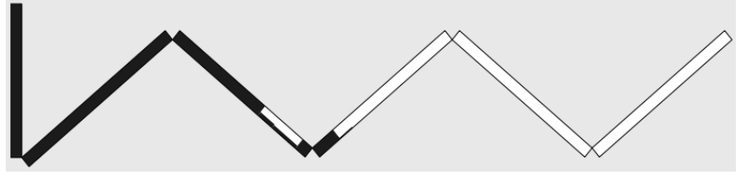

3. Third pipe segment P3 filled.

3.80 s

4.32 s

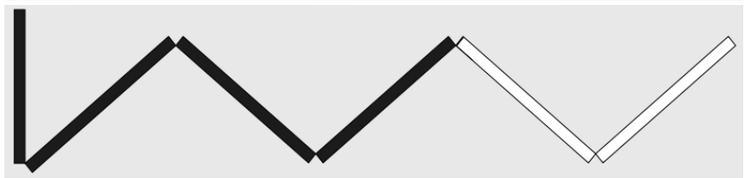

Figure 9: continued on next page...

1. First pipe segment P1 filled.

1.80 s

1.05 s

2. A slug forms at the first low point.

2.68 s

2.42 s

3. Third pipe segment P3 filled.

3.80 s

4.32 s

Figure 9: continued on next page...

...continued from previous page.

4. Slug forms at second low point.

4.84 s

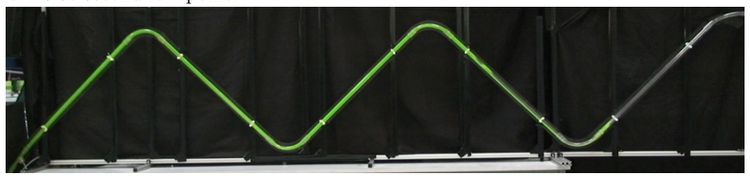

5.96 s

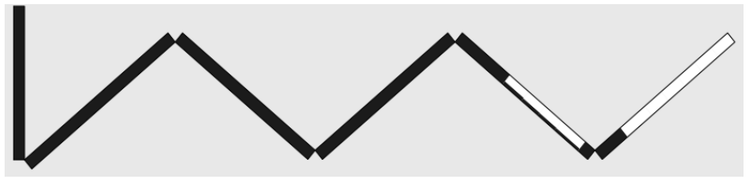

5. Fifth pipe segment P5 with slugs.

6.36 s

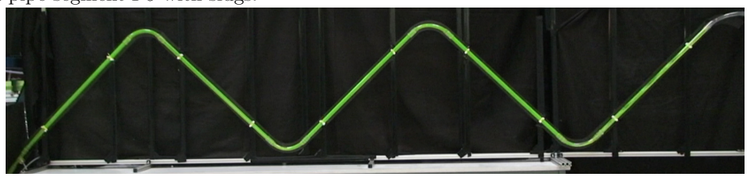

7.71 s

6. End state.

End

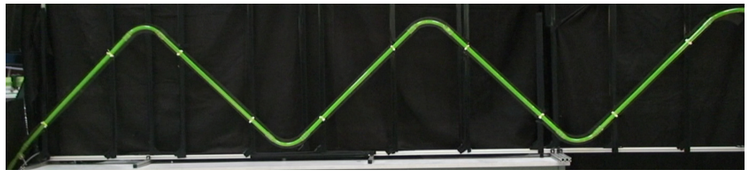

End

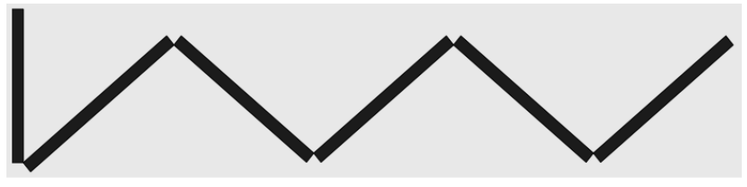

Figure 9: Snapshots from experiment and simulation with a liquid level of 0.825 m above the inlet. The time when the snapshot was taken is shown to the left of the images. The water phase is dyed green in experimental images and shown as black in the simulation snapshots.

...continued from previous page.

4. Slug forms at second low point.

4.84 s

5.96 s

5. Fifth pipe segment P5 with slugs.

6.36 s

7.71 s

6. End state.

End

End

Figure 9: Snapshots from experiment and simulation with a liquid level of 0.825 m above the inlet. The time when the snapshot was taken is shown to the left of the images. The water phase is dyed green in experimental images and shown as black in the simulation snapshots.

1. First pipe segment P1 filled.

1.20 s

1.23 s

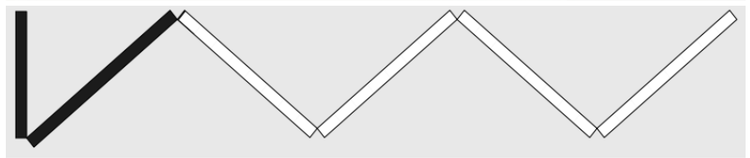

2. Slug forms in first low point.

2.24 s

2.96 s

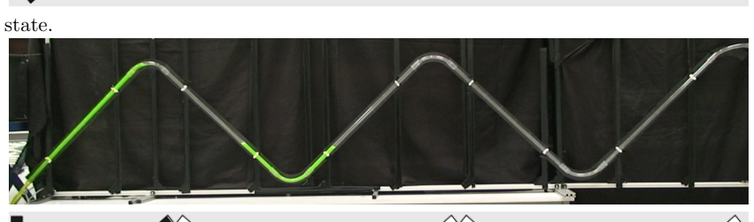

3. End state.

End

End

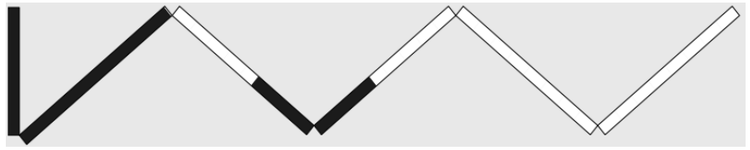

Figure 10: Snapshots from experiment and simulation with water 0.675 m above the inlet. The time when the snapshot was taken is shown to the left of the images. The water phase is dyed green in experimental images and shown as black in the simulation snapshots.

1. First pipe segment P1 filled.

1.20 s

1.23 s

2. Slug forms in first low point.

2.24 s

2.96 s

3. End state.

End

End

Figure 10: Snapshots from experiment and simulation with water 0.675 m above the inlet. The time when the snapshot was taken is shown to the left of the images. The water phase is dyed green in experimental images and shown as black in the simulation snapshots.

14

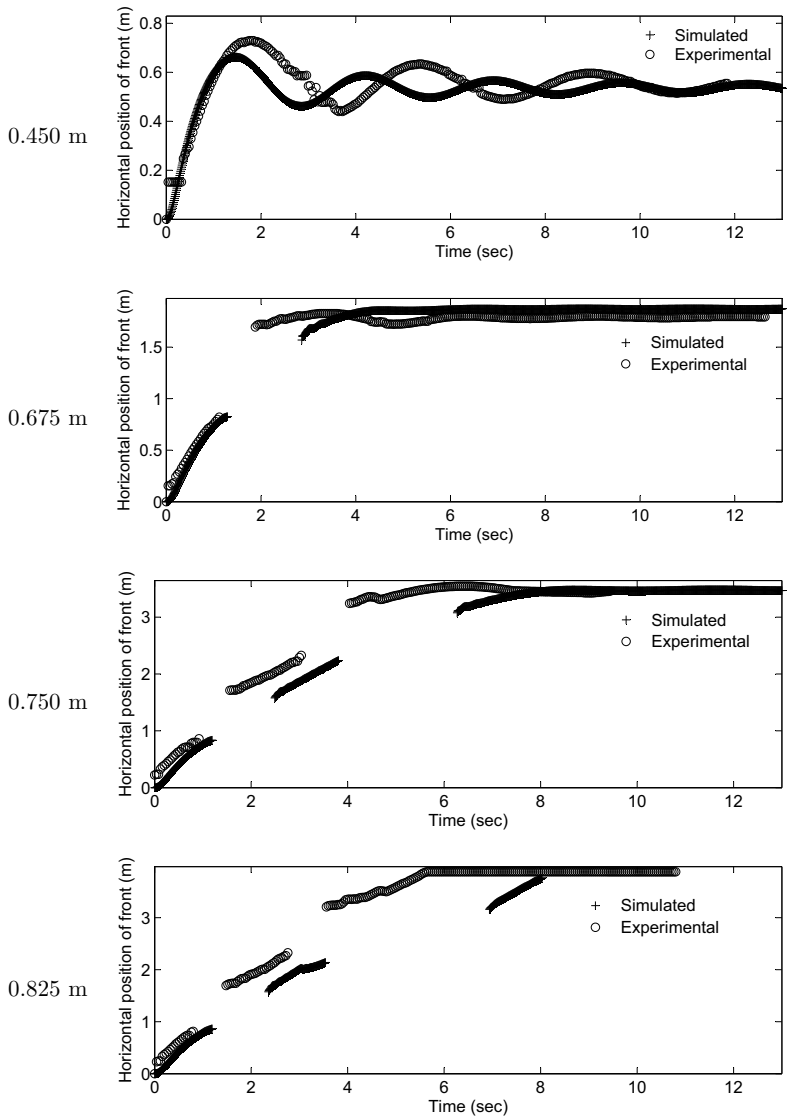

Figure 11: Plots of horizontal front position against time for experiments and simulations. The water level above the inlet is shown to the left of each plot.

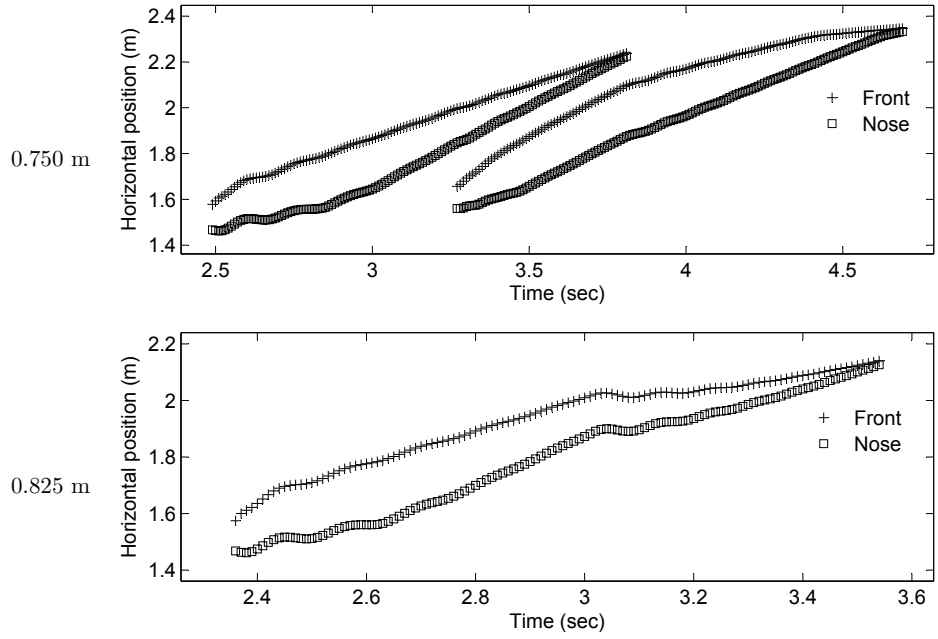

Figure 12: Plots of simulated slug front and bubble nose horizontal positions against time. The water level above the inlet is shown to the left of the plots.

The simulations, however, differed from the experiments by up to 4 sec in the time to reach the final state. The transient liquid front positions were very similar in simulations and experiments in the first pipe segment, however after that simulated front positions lagged behind the experimental results.

References

[1] K. H. Bendiksen. An experimental investigation of the motion of long bubbles in inclined tubes. *Int. J. Multiphase Flow*, 10:467–483, 1984.

[2] K. H. Bendiksen, D. Malnes, and O. J. Nydal. On the modelling of slug flow. *Chem. Eng. Comm.*, 141-142:71–102, 1996.

[3] A. De Leebeeck and O. J. Nydal. Large amplitude waves in a slug tracking scheme. In A. A. Mammoli and C. A. Brebbia, editors, *Computational Methods in Multiphase Flow V*, pages 99–110, New Forest, UK, 2009. WIT Press.

[4] S. Haaland. Simple and explicit formulas for the friction factor in turbulent pipe flow. *Journal of Fluids Engineering*, 105:89–90, 1983.

[5] M. Johansen. *An experimental study of the bubble propagation velocity in 3-phase slug flow.* PhD thesis, Norwegian University of Science and Technology, 2006.

[6] J. Kjølaas. *Plug propagation in multiphase pipelines.* PhD thesis, Norwegian University of Science and Technology, 2007.

[7] A. De Leebeeck and O. J. Nydal. Simulation of large amplitude waves in a slug tracking scheme compared to roll wave experiments at high pressure. *Int. J. Multiphase Flow*, 36:40–50, 2010.

[8] O. J. Nydal. Experiments in downwards flow on stability of slug fronts. In *Third International Conference on Multiphase Flow*, Lyon, France, 1998.

[9] O. J. Nydal, M. Audibert, and M. Johansen. Experiments and modelling of gas-liquid flow in an s-shape riser. In *Tenth international conference on Multiphase Technology*, Cannes, France, 2001.

[10] C. Reynolds and M. Yitayew. Low-head bubbler irrigation systems. part ii. air lock problems. *Agricultural water management*, 29:25–35, 1995.

[11] F. M. White. *Fluid Mechanics.* McGraw Hill, Boston, 5th international edition, 2005.

Appendix A

Conference paper: Experiments on Roll Waves in Air-Water Pipe Flow

This conference paper was presented at the 16th Australasian Fluid Mechanics Conference, Gold Coast, Australia, December 2-7, 2007.

Appendix A

Conference paper: Experiments on Roll Waves in Air-Water Pipe Flow

This conference paper was presented at the 16th Australasian Fluid Mechanics Conference, Gold Coast, Australia, December 2-7, 2007.

123

16th Australasian Fluid Mechanics Conference
Crown Plaza, Gold Coast, Australia
2-7 December 2007

Experiments on Roll Waves in Air-Water Pipe Flow

Angela De Leebeeck, Andreas Hoel Gaarder, Ole Jørgen Nydal[1)]
Department of Energy and Process Technology
Norwegian University of Science and Technology, Trondheim, Norway.
[1] Visiting the Department of Mechanical Engineering
University of Western Australia

Abstract

Experiments on air-water two phase flow in inclined pipes have been made, with emphasis on the roll wave regime. The motivation for the work is the improving of 1D flow models for multiphase pipeline transport of oil and gas mixtures. Pressure and liquid fractions are recorded in time, together with video recordings. The results show that large amplitude roll waves have associated pressure jumps across the fronts. Some implications for the flow modelling are discussed.

Introduction

Multiphase flow simulators are very important tools for the design and operation of sub-sea pipelines carrying mixtures of oil and gas from wells to a processing facility on a floater, or onshore. Design considerations include both steady operation (pressure drop, liquid content, temperatures) and dynamic flow conditions (operational transients, unstable flows). The basic flow models in these simulators are one dimensional, and as the closure relations cover averaged physical phenomena (averaged wall friction, interface drag, cross sectional phase distribution etc.) they are normally empirically determined. Experimental data at realistic flow conditions then become an important basis for the modelling work.

Flow with large amplitude roll waves is a regime which occurs in gas condensate pipelines, in particular for high pressure systems (high gas densities). Although this regime has some similarities with slug flow, it is often treated as averaged stratified flow in the flow models.

In slug flow, liquid slugs block the pipe cross section and the slug lengths normally exceed 10 number of diameters. The slugs carry the major part of the liquid transport and they propagate faster than the total mixture velocity. The slug fronts propagate over a liquid layer, which is absorbed and accelerated to the liquid velocity in the slug front. Liquid is then shed at the tail of the slugs (which has the form of a bubble nose), and decelerated as the trailing bubble propagates over it.

Some similarities can be noted for flows with large amplitude roll waves. The waves have sharp propagating fronts overrunning a liquid layer. The liquid layer behind a wave can decelerate from a larger velocity in the wave, see Figure 1 for schematic drawings.

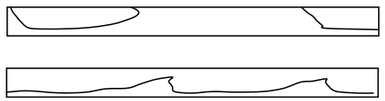

Figure 1. Sketch of a slug (top) and large amplitude waves (bottom)

Typical differences between the two flow regimes are the length scales (waves are in the order of a few diameters long) and the front velocities (waves propagate much slower than slugs). The wave regime is also more irregular, with larger spread in velocities and amplitudes. Waves can be seen to collapse and to merge with other waves, and the roll wave regime can indeed be speculated to be a transitional regime towards slug flow.

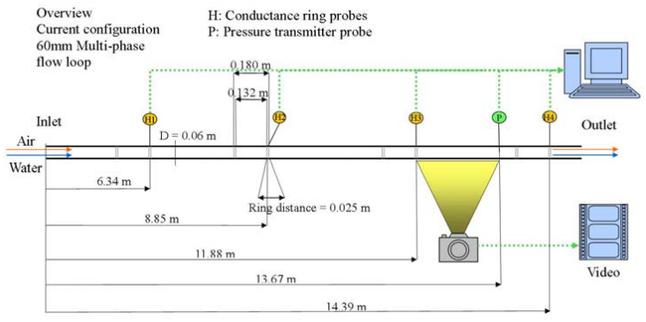

Figure 2. Location of liquid fraction probes, pressure sensor video and camera

16th Australasian Fluid Mechanics Conference
Crown Plaza, Gold Coast, Australia
2-7 December 2007

Experiments on Roll Waves in Air-Water Pipe Flow

Angela De Leebeeck, Andreas Hoel Gaarder, Ole Jørgen Nydal[1)]
Department of Energy and Process Technology
Norwegian University of Science and Technology, Trondheim, Norway.
[1] Visiting the Department of Mechanical Engineering
University of Western Australia

Abstract

Experiments on air-water two phase flow in inclined pipes have been made, with emphasis on the roll wave regime. The motivation for the work is the improving of 1D flow models for multiphase pipeline transport of oil and gas mixtures. Pressure and liquid fractions are recorded in time, together with video recordings. The results show that large amplitude roll waves have associated pressure jumps across the fronts. Some implications for the flow modelling are discussed.

Introduction

Multiphase flow simulators are very important tools for the design and operation of sub-sea pipelines carrying mixtures of oil and gas from wells to a processing facility on a floater, or onshore. Design considerations include both steady operation (pressure drop, liquid content, temperatures) and dynamic flow conditions (operational transients, unstable flows). The basic flow models in these simulators are one dimensional, and as the closure relations cover averaged physical phenomena (averaged wall friction, interface drag, cross sectional phase distribution etc.) they are normally empirically determined. Experimental data at realistic flow conditions then become an important basis for the modelling work.

Flow with large amplitude roll waves is a regime which occurs in gas condensate pipelines, in particular for high pressure systems (high gas densities). Although this regime has some similarities with slug flow, it is often treated as averaged stratified flow in the flow models.

In slug flow, liquid slugs block the pipe cross section and the slug lengths normally exceed 10 number of diameters. The slugs carry the major part of the liquid transport and they propagate faster than the total mixture velocity. The slug fronts propagate over a liquid layer, which is absorbed and accelerated to the liquid velocity in the slug front. Liquid is then shed at the tail of the slugs (which has the form of a bubble nose), and decelerated as the trailing bubble propagates over it.

Some similarities can be noted for flows with large amplitude roll waves. The waves have sharp propagating fronts overrunning a liquid layer. The liquid layer behind a wave can decelerate from a larger velocity in the wave, see Figure 1 for schematic drawings.

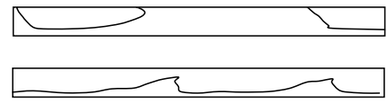

Figure 1. Sketch of a slug (top) and large amplitude waves (bottom)

Typical differences between the two flow regimes are the length scales (waves are in the order of a few diameters long) and the front velocities (waves propagate much slower than slugs). The wave regime is also more irregular, with larger spread in velocities and amplitudes. Waves can be seen to collapse and to merge with other waves, and the roll wave regime can indeed be speculated to be a transitional regime towards slug flow.

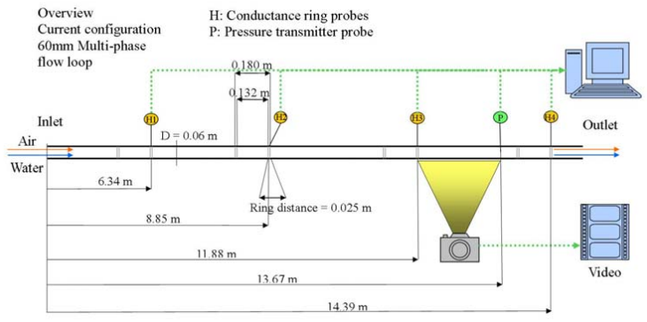

Figure 2. Location of liquid fraction probes, pressure sensor video and camera

Objectives

The objective of the work is to measure some characteristics of roll waves: pressures, amplitudes and propagation velocities. Some experimental studies have been made on roll waves before (10 cm internal diameter (I.D.) high gas densities, [1]). The added value of the present experiments will be the pressure response of individual waves, which is information lacking in most other previous experimental studies [1, 2, 3, 4, 5, 6]. An atmospheric flow loop with air and water is available for the experiments.

Experiments

Flow loop and instrumentation

The flow laboratory is located at the Norwegian University of Science and Technology. The experiments were made in a 16 m long acrylic pipe of 6 cm I.D. Pipe inclinations varied in the range of -1 to 3 degrees with the horizontal. The loop pressure was atmospheric.

The single phase flow rates are measured with electromagnetic meters (water) and vortex meters (air). The liquid fraction is recorded in time with impedance ring probes at 4 locations along the pipe, see Figure 2 and 3. Pressure is recorded with an absolute sensor located close to the last liquid fraction probe.

A video camera was used to monitor the flow at the position of the pressure sensor. The video has a time stamp, making it possible to identify the video picture of a wave with the time recordings of pressure and liquid fraction.

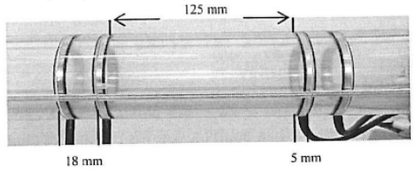

Figure 3. Image of internal flush mounted conductance ring probes for liquid fraction measurement. 6 cm I.D.

Experimental Procedure and Data Analysis

Qualitative observations were first made over quite a large range of air and water flow rates and pipe inclinations in search of the occurrence of roll waves at low frequencies. When several waves or slugs are present at the same time in the pipe, it becomes difficult to interpret the dynamics of the pressure recordings.
After the initial screening, measurements and video recordings were made at selected flow conditions.

The time trace analysis should provide velocities and amplitudes of liquid fractions and pressures variations relative to each wave phenomenon. Automatic data analysis for this purpose turned out to be difficult, because waves could decay or emerge in between the liquid fraction sensors, making the time traces non-coherent between the probes.

A simple first analysis was made by obtaining an averaged wave velocity from cross correlating the liquid fraction time traces from the four probes, giving three velocity measurements. The averaged amplitudes were taken as the 95% percentile value in the statistical distributions of all pressure and liquid fraction samples in a time series.

Results

The typical differences between a case with slug flow and a case with wavy flow are shown in Figures 4-6. The time traces have been shifted in time according to the cross correlation time, so that the waves should appear at the same location in the time plots. Usg and Usl are the superficial velocities of gas and liquid (volumetric flow rate pr. pipe area).

Overlapped liquid fraction time traces and the pressure time trace are matched to the corresponding video snapshot for an individual wave in Figure 6. The experiment has a cross correlated wave velocity of 1.86 m/s, a 95% percentile pressure value of 0.014 bar, and a 95% percentile liquid fraction of 0.28 from liquid fraction time trace 4. The individual wave moves with a velocity of 1.67 m/s, it has a peak pressure of 0.027 bar, and a peak liquid fraction of 0.32 in time trace 4.

The slug and the wave time traces have similarities with sharp fronts and a decaying tail. It can be difficult from liquid fraction time traces alone to discriminate between liquid waves and aerated slugs, so the synchronised video pictures were useful in the identification of the type of the phenomena which was recorded. The time traces in Figure 4 and 5 are predominantly waves and slugs. Other flow conditions could show a mixture of waves and slugs, making the averaged time trace analysis more uncertain.

Slugs travel faster than waves. Figure 7 shows the velocities from the cross correlations as function of total volumetric flow rates. Slug velocities increase with the flow rates, whereas the trends for the wave velocities are less clear.

Slugs exhibit a strong pressure jump across the liquid-gas front. The interesting results here is that waves also can show a pressure jump, although of a smaller magnitude than for slugs, Figure 8.

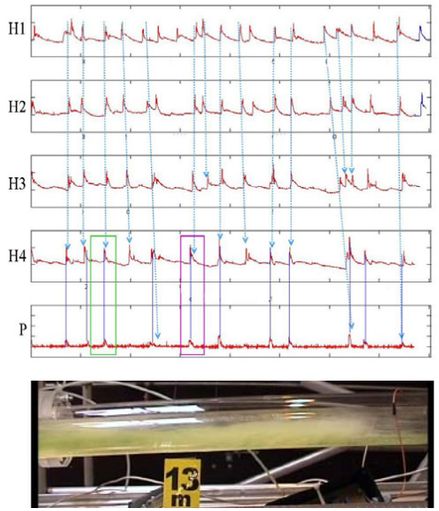

Figure 4. Time traces of liquid fraction probes (no. 1 at the top) and of pressure in bar (at the bottom). 1 degree upwards pipe inclination, Usg = 4.34 m/s and Usl = 0.13 m/s. The video snap shot is for the wave enclosed in the first rectangle (green).

Objectives

The objective of the work is to measure some characteristics of roll waves: pressures, amplitudes and propagation velocities. Some experimental studies have been made on roll waves before (10 cm internal diameter (I.D.) high gas densities, [1]). The added value of the present experiments will be the pressure response of individual waves, which is information lacking in most other previous experimental studies [1, 2, 3, 4, 5, 6]. An atmospheric flow loop with air and water is available for the experiments.

Experiments

Flow loop and instrumentation

The flow laboratory is located at the Norwegian University of Science and Technology. The experiments were made in a 16 m long acrylic pipe of 6 cm I.D. Pipe inclinations varied in the range of -1 to 3 degrees with the horizontal. The loop pressure was atmospheric.

The single phase flow rates are measured with electromagnetic meters (water) and vortex meters (air). The liquid fraction is recorded in time with impedance ring probes at 4 locations along the pipe, see Figure 2 and 3. Pressure is recorded with an absolute sensor located close to the last liquid fraction probe.

A video camera was used to monitor the flow at the position of the pressure sensor. The video has a time stamp, making it possible to identify the video picture of a wave with the time recordings of pressure and liquid fraction.

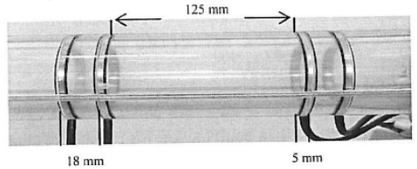

Figure 3. Image of internal flush mounted conductance ring probes for liquid fraction measurement. 6 cm I.D.

Experimental Procedure and Data Analysis

Qualitative observations were first made over quite a large range of air and water flow rates and pipe inclinations in search of the occurrence of roll waves at low frequencies. When several waves or slugs are present at the same time in the pipe, it becomes difficult to interpret the dynamics of the pressure recordings.
After the initial screening, measurements and video recordings were made at selected flow conditions.

The time trace analysis should provide velocities and amplitudes of liquid fractions and pressures variations relative to each wave phenomenon. Automatic data analysis for this purpose turned out to be difficult, because waves could decay or emerge in between the liquid fraction sensors, making the time traces non-coherent between the probes.

A simple first analysis was made by obtaining an averaged wave velocity from cross correlating the liquid fraction time traces from the four probes, giving three velocity measurements. The averaged amplitudes were taken as the 95% percentile value in the statistical distributions of all pressure and liquid fraction samples in a time series.

Results

The typical differences between a case with slug flow and a case with wavy flow are shown in Figures 4-6. The time traces have been shifted in time according to the cross correlation time, so that the waves should appear at the same location in the time plots. Usg and Usl are the superficial velocities of gas and liquid (volumetric flow rate pr. pipe area).

Overlapped liquid fraction time traces and the pressure time trace are matched to the corresponding video snapshot for an individual wave in Figure 6. The experiment has a cross correlated wave velocity of 1.86 m/s, a 95% percentile pressure value of 0.014 bar, and a 95% percentile liquid fraction of 0.28 from liquid fraction time trace 4. The individual wave moves with a velocity of 1.67 m/s, it has a peak pressure of 0.027 bar, and a peak liquid fraction of 0.32 in time trace 4.

The slug and the wave time traces have similarities with sharp fronts and a decaying tail. It can be difficult from liquid fraction time traces alone to discriminate between liquid waves and aerated slugs, so the synchronised video pictures were useful in the identification of the type of the phenomena which was recorded. The time traces in Figure 4 and 5 are predominantly waves and slugs. Other flow conditions could show a mixture of waves and slugs, making the averaged time trace analysis more uncertain.

Slugs travel faster than waves. Figure 7 shows the velocities from the cross correlations as function of total volumetric flow rates. Slug velocities increase with the flow rates, whereas the trends for the wave velocities are less clear.

Slugs exhibit a strong pressure jump across the liquid-gas front. The interesting results here is that waves also can show a pressure jump, although of a smaller magnitude than for slugs, Figure 8.

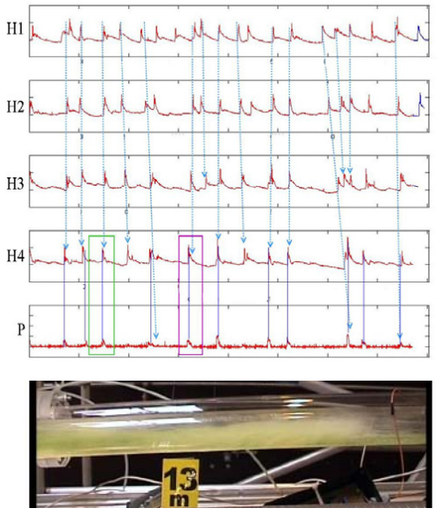

Figure 4. Time traces of liquid fraction probes (no. 1 at the top) and of pressure in bar (at the bottom). 1 degree upwards pipe inclination, Usg = 4.34 m/s and Usl = 0.13 m/s. The video snap shot is for the wave enclosed in the first rectangle (green).

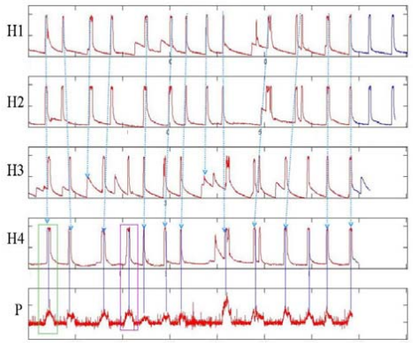

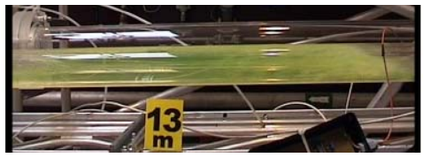

Figure 5. Time traces of liquid fraction probes (no. 1 at the top) and of pressure in bar (at the bottom). 0 degrees pipe inclination, Usg = 1.53 m/s and Usl = 0.34 m/s. The video snap shot is for the wave enclosed in the first rectangle (green).

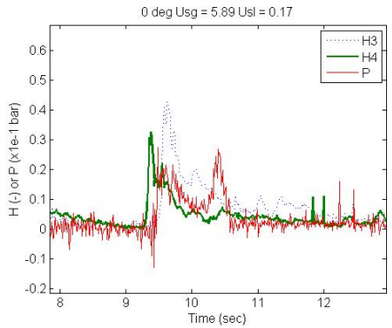

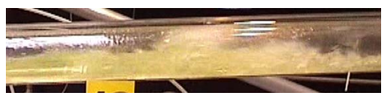

Figure 6: Overlapped signals for liquid fraction time trace 3 and 4 and the pressure time trace and the matching video snapshot for the 0 degrees, Usg = 5.89 m/s and Usl = 0.17 m/s. The pressure signal is multiplied by a factor of 10 so that it can be seen on the same plot as the liquid fraction.

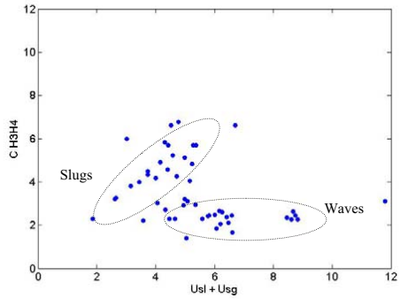

Figure 7: Velocities from cross correlation of time traces no. 3 and 4.

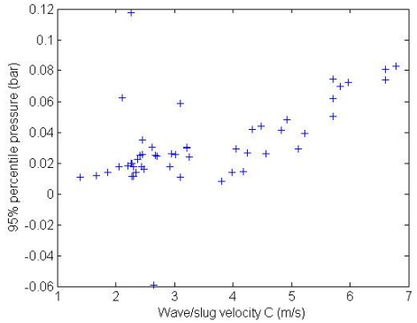

Figure 8: 95% percentile pressure in bar vs. the cross correlated disturbance velocity between liquid fraction time trace 3 and 4 in m/s for all experiments. Experiments with both waves and slugs are included in the plot.

Flow Models

On the length scale of a pipe diameter, slug flow and wavy flow appears as dynamic flows, with time fluctuations in the flow parameters. General 1D models can be solved numerically on a small grid, in order to capture the dynamics of individual slugs. This has been demonstrated using a two fluid model, with a set of conservation equations for both phases [7,8]. Such models are, however, very sensitive to the numerical scheme, and the computational times are prohibitive for simulation of long two phase flow pipelines.

Alternative schemes bases on slug tracking instead of capturing have been tested [9]. These schemes employ a grid moving with the fronts, allowing for computations with orders of magnitudes less grid points than with an Eulerian front capturing scheme. The grid velocities in such tracking schemes are the characteristic bubble propagation velocity in slug flow and the front velocities, as derived from mass balances across the fronts.

For simulation of long pipelines with lengths in the order of 10 or 100 kilometers, the small scale dynamics of slug flow is often of less importance, and slug flow is then treated as a quasi stationary flow, with averaged pressure drop and liquid fraction over several slug-bubble units. The numerical grid in such simulations would typically be much larger than slug-bubble

H1
H2
H3
H4
P
13
m
Figure 5. Time traces of liquid fraction probes (no. 1 at the top) and of pressure in bar (at the bottom). 0 degrees pipe inclination, Usg = 1.53 m/s and Usl = 0.34 m/s. The video snap shot is for the wave enclosed in the first rectangle (green).
0 deg Usg = 5.89 Usl = 0.17
H3
H4
P
H (-) or P (x1e-1 bar)
Time (sec)
Figure 6: Overlapped signals for liquid fraction time trace 3 and 4 and the pressure time trace and the matching video snapshot for the 0 degrees, Usg = 5.89 m/s and Usl = 0.17 m/s. The pressure signal is multiplied by a factor of 10 so that it can be seen on the same plot as the liquid fraction.
C H3H4
Slugs
Waves
Usl + Usg
Figure 7: Velocities from cross correlation of time traces no. 3 and 4.
95% percentile pressure (bar)
Wave/slug velocity C (m/s)
Figure 8: 95% percentile pressure in bar vs. the cross correlated disturbance velocity between liquid fraction time trace 3 and 4 in m/s for all experiments. Experiments with both waves and slugs are included in the plot.
Flow Models
On the length scale of a pipe diameter, slug flow and wavy flow appears as dynamic flows, with time fluctuations in the flow parameters. General 1D models can be solved numerically on a small grid, in order to capture the dynamics of individual slugs. This has been demonstrated using a two fluid model, with a set of conservation equations for both phases [7,8]. Such models are, however, very sensitive to the numerical scheme, and the computational times are prohibitive for simulation of long two phase flow pipelines.
Alternative schemes bases on slug tracking instead of capturing have been tested [9]. These schemes employ a grid moving with the fronts, allowing for computations with orders of magnitudes less grid points than with an Eulerian front capturing scheme. The grid velocities in such tracking schemes are the characteristic bubble propagation velocity in slug flow and the front velocities, as derived from mass balances across the fronts.
For simulation of long pipelines with lengths in the order of 10 or 100 kilometers, the small scale dynamics of slug flow is often of less importance, and slug flow is then treated as a quasi stationary flow, with averaged pressure drop and liquid fraction over several slug-bubble units. The numerical grid in such simulations would typically be much larger than slug-bubble
293

units, and the dynamics of such simulations would typically be on pipeline scales (transport times and riser lengths) and not on diameter scales. Quasi steady state slug flow models "unit cell models" can be formulated as a combination of models for bubbly flow in the slug region and separated flow in the bubble region, with the two regions coupled with mass balances for gas and liquid [10]. Such "unit cell models" can be solved as a point model, and integrated into dynamic simulators for resolving the large scale dynamics.

Wavy flows

Wavy flow is often modelled as averaged separated flow, assuming flat interface geometry, and with empirically tuned wall and interface friction relations. This is probably a reasonable approach when the waves are small. For the roll wave regime, with breaking waves and significant liquid transport in the waves, the question is whether improvements can be made along the modelling lines similar as for slug flow.

As for slug flow, it has been demonstrated that numerical schemes can be designed to capture formation and propagation [8] of large amplitude waves. Point models have also been derived for the roll wave regime, based on the combination of discontinuous numerical solutions of the set of momentum and mass conservation equations for gas and liquid [1].

The present experiments have shown that a pressure jump over the waves constitutes a large part of the pressure drop in large amplitude wavy flows. This could suggest a modelling approach along similar lines as for slug flow, including both "unit cell" point models as well as dynamic tracking models. An integral wave model is then needed, providing in particular relations for the wave velocity, wave amplitude and pressure drop across the wave. The present experimental data needs further analysis to extract single wave data as a basis for the further modelling considerations.

Conclusions

Experiments have been made with air-water, near horizontal pipe flows in order to measure details in the pressure response related to large amplitude waves.

Time trace recordings of four liquid fraction probes and one pressure sensor, together with synchronised video recordings, show that large amplitude roll waves are associated with a pressure jump.

This suggests that further modelling efforts of roll waves could be made along similar lines as for slug flow, both regarding steady state and dynamic models.

Acknowledgments

The work has been sponsored by Total EP Stavanger, Norway. The work is part of a joint PhD program with industry on "Multiphase Transport" at the Norwegian University of Science and Technology, Trondheim, Norway.
O.J. Nydal acknowledges the support of the University of Western Australia for hosting him as a visitor.

References

[1] Johnson, G. W., *A Study of Stratified Gas-Liquid Pipe Flow*, PhD thesis, University of Oslo, 2005.

[2] Lin & Hanratty, Detection of slug flow from pressure Measurements, *Int. J. of Multiphase Flow*, **13**, 1987, 13-21.

[3] Miya et al. A model for roll waves in gas-liquid flow, *Chemical Engineering Science*, **26**, 1971, 1915-1931.

[4] Soleimani & Hanratty, Critical liquid flows for the transition from the pseudo-slug and stratified patterns to slug flow, *Int. J. Multiphase Flow*, **29**, 2003, 51-67.

[5] Woods et al., Mechanism of slug formation in downwardly inclined pipes, *Int. J. of Multiphase Flow*, **26**, 2000, 977-998.

[6] Woods et al., Frequency and development of slugs in a horizontal pipe at large liquid flows, *Int. J. of Multiphase Flow*, **32**, 2006, 902-925.

[7] Issa, R & Kempf, M.H.W. Simulation of slug flow in horizontal and nearly horizontal pipes with the two fluid model. *Int. J. of Multiphase Flow*, **29**, 2003, 69-95.

[8] Fabien, R. A Lagrangian slug capturing scheme for gas-liquid flows in pipes *PhD thesis*, Norwegian University of Science and Technology, 2007.

[9] Nydal, O.J., Audibert M., Johansen, M. Experiments and modelingof gas-liquid flow in an S-shaped riser. *10th Int. Conference on Multiphase Technology, BHRG Cannes* 2001

[10] Bendiksen, K., Malnes, D. Nydal, O.J. On the modeling of slug flow. Chem. Eng. Com. 1414, 1996, 71-102.

.

Appendix B

Tables of Experimental and Simulated Data

B.1 Roll waves at atmospheric pressure

Table B.1: Experimentally measured characteristic quantities in large roll waves and slugs at atmospheric pressure for given angle of pipe inclination and superficial phase velocities. H1 through H4 are the characteristic liquid fraction measured at the first through fourth conductance probes. U_{12}, U_{23} and U_{34} are the characteristic velocities of waves or slugs from cross correlations of H1-H2, H2-H3 and H3-H4 respectively.

Angle (deg)	U_{sg} (m/s)	U_{sl} (m/s)	H1	H2	H3	H4	P (bar)	U_{12} (m/s)	U_{23} (m/s)	U_{34} (m/s)
-1.0	3.63	0.52	0.48	0.47	0.43	0.44	0.05	4.92	4.66	4.92
-1.0	5.86	0.30	0.27	0.27	0.28	0.27	0.03	1.79	2.06	2.67
-1.0	8.37	0.45	0.18	0.20	0.23	0.25	0.12	1.83	2.08	2.26
-1.0	8.37	0.25	0.20	0.19	0.19	0.17	0.02	0.83	2.08	2.26
-1.0	8.37	0.30	0.08	0.07	0.05	0.05	0.06	2.24	2.39	2.64
-1.0	11.51	0.29	0.14	0.15	0.18	0.17	0.06	3.14	3.12	3.10
0.0	1.53	0.34	0.94	0.93	0.92	0.89	0.01	2.35	2.13	2.28
0.0	2.33	0.32	0.76	0.69	0.47	0.49	0.02	3.39	3.12	3.26
0.0	3.38	0.35	0.37	0.40	0.39	0.37	0.04	2.56	4.04	4.33
0.0	3.79	0.22	0.26	0.34	0.31	0.34	0.01	2.24	2.46	4.18
0.0	3.84	0.22	0.27	0.25	0.28	0.30	0.03	2.18	1.71	3.02
0.0	4.08	0.26	0.32	0.32	0.33	0.36	0.02	3.26	2.26	2.70
0.0	4.65	0.33	0.32	0.32	0.33	0.33	0.03	5.34	2.61	5.12
Continued on next page...										

...continued from previous page.

Angle (deg)	U_{sg} (m/s)	U_{sl} (m/s)	H1	H2	H3	H4	P (bar)	U_{12} (m/s)	U_{23} (m/s)	U_{34} (m/s)
0.0	4.74	0.20	0.26	0.30	0.27	0.30	0.02	1.99	2.30	2.92
0.0	4.87	0.17	0.27	0.27	0.26	0.28	0.01	1.93	1.74	1.39
0.0	5.32	0.26	0.30	0.29	0.30	0.30	0.02	2.15	2.44	2.28
0.0	5.56	0.22	0.21	0.25	0.28	0.28	0.02	1.62	1.84	2.41
0.0	5.89	0.17	0.24	0.25	0.28	0.28	0.01	1.38	1.63	1.86
0.0	6.01	0.20	0.27	0.26	0.28	0.29	0.02	1.81	1.99	2.06
0.0	6.34	0.25	0.27	0.27	0.26	0.29	0.03	1.92	2.48	2.46
0.0	6.43	0.17	0.25	0.27	0.25	0.25	0.01	1.21	1.13	1.66
0.0	8.53	0.22	0.18	0.19	0.20	0.20	0.04	2.15	1.89	2.46
1.0	2.35	0.27	0.69	0.69	0.52	0.49	0.03	3.26	3.03	3.22
1.0	3.31	0.14	0.31	0.33	0.31	0.35	0.01	4.18	3.84	3.98
1.0	3.47	0.27	0.40	0.42	0.43	0.39	0.04	4.25	4.39	4.48
1.0	3.89	0.42	0.41	0.37	0.41	0.42	0.07	5.46	5.51	5.84
1.0	4.09	0.34	0.34	0.36	0.37	0.36	0.06	2.46	5.22	5.70
1.0	4.22	0.19	0.29	0.34	0.33	0.35	0.03	2.92	4.73	4.56
1.0	4.32	0.27	0.33	0.39	0.36	0.39	0.04	5.23	4.66	5.23
1.0	4.34	0.13	0.26	0.31	0.32	0.28	0.02	2.44	2.57	2.30
1.0	5.15	0.20	0.27	0.29	0.31	0.26	0.03	2.28	2.44	2.95
1.0	5.87	0.13	0.25	0.28	0.26	0.26	0.02	2.59	2.12	2.49
1.0	6.20	0.27	0.25	0.28	0.31	0.31	0.06	2.41	1.97	2.11
1.0	6.21	0.20	0.26	0.28	0.25	0.27	0.02	2.32	2.50	2.37
1.0	6.45	0.26	0.27	0.30	0.30	0.31	0.07	2.56	2.71	6.61
2.0	2.62	0.39	0.36	0.38	0.36	0.38	0.07	5.84	5.51	5.98
2.0	3.45	0.12	0.24	0.26	0.25	0.23	0.02	2.79	1.94	2.20
2.0	4.24	0.29	0.29	0.31	0.32	0.33	0.08	2.56	6.18	6.61
2.0	4.40	0.37	0.29	0.31	0.32	0.32	0.08	6.28	6.73	6.78
2.0	4.82	0.17	0.29	0.31	0.31	0.34	0.03	2.70	2.57	3.22
2.0	5.70	0.11	0.20	0.20	0.23	0.21	0.02	2.20	2.12	2.44
2.0	6.09	0.18	0.28	0.28	0.29	0.28	0.03	2.99	2.63	2.61
2.0	8.35	0.11	0.12	0.12	0.16	0.13	0.01	2.37	1.28	2.35
2.8	3.09	0.06	0.24	0.27	0.31	0.30	0.01	3.98	3.70	3.80
2.8	4.61	0.05	0.19	0.23	0.23	0.25	0.01	1.79	3.09	2.30
2.8	4.61	0.11	0.27	0.23	0.27	0.27	0.03	4.65	3.99	4.25
2.8	5.02	0.35	0.33	0.36	0.35	0.36	0.07	5.98	5.72	5.70
2.8	5.04	0.13	0.25	0.23	0.27	0.27	0.03	3.22	3.88	4.05
2.8	5.04	0.23	0.29	0.32	0.31	0.31	0.05	5.46	0.59	5.70
2.8	5.05	0.04	0.19	0.20	0.18	0.20	0.01	3.14	2.46	3.10
2.8	5.05	0.18	0.25	0.29	0.28	0.28	0.04	2.95	2.71	4.83

Table B.2: Experimental and simulated results (wave velocities and pressure gradients) for large roll waves in a 0.06 m I.D. pipe at atmospheric pressure, various angles of pipe inclination and superficial phase velocities.

Angle (deg)	U_{sg} (m/s)	U_{sl} (m/s)	Experimental U_{wave} (m/s)	Simulated U_{wave} (m/s)	Experimental P gradient (Pa/m)	Simulated P gradient (Pa/m)
-1	5.86	0.30	2.67	2.11	216	41.2
-1	8.37	0.25	2.64	2.53	297	62.3
-1	8.37	0.30	2.26	2.38	403	75.5
0	4.74	0.20	2.92	1.37	80.6	41.1
0	4.87	0.17	1.39	1.29	40.3	22.7
0	5.32	0.26	2.28	1.95	121	105
0	5.89	0.17	1.86	1.35	76.9	31.2
0	6.01	0.20	2.06	1.61	128	58
0	6.34	0.25	2.46	2.14	168	121
0	6.43	0.17	1.66	1.55	80.6	36.5
1	4.34	0.13	2.30	1.73	80.6	124
1	5.15	0.20	2.95	2.37	135	233
1	5.87	0.13	2.49	2.23	117	165
1	6.21	0.20	2.36	2.38	172	260
2	5.7	0.11	2.43	1.26	154	275
2	6.09	0.18	2.61	2.77	187	286
2	8.35	0.11	2.34	1.88	205	263

B.2 Roll waves at 8 bar

Table B.3: Experimental (Exp) and simulated (Sim) roll wave characteristic velocities and average pressure drops from a 0.1 m I.D. pipe at 8 bar. The length is the experimentally determined average length between consecutive wave peaks. Experimental data is from [17].

Angle (deg)	U_{sg} (m/s)	U_{sl} (m/s)	Length (m)	Exp U_{wave} (m/s)	Sim U_{wave} (m/s)	Exp P gradient (Pa/m)	Sim P gradient (Pa/m)
0.00	1.00	0.20	1.22	1.08	0.98	24.74	35.00
0.00	1.50	0.20	0.49	1.20	1.13	39.56	25.00
0.00	2.00	0.20	0.47	1.34	1.33	54.85	41.00
0.00	2.50	0.20	7.78	1.52	1.58	75.88	52.00
0.00	3.00	0.20	5.62	1.65	1.80	96.62	73.00
0.00	3.50	0.20	2.65	1.81	1.89	121.70	119.00
0.00	4.00	0.20	2.87	1.96	2.04	150.24	155.00
0.00	4.50	0.20	2.42	2.13	2.16	181.62	189.00
0.00	1.00	0.40	5.34	1.56	1.53	44.94	49.00
0.00	1.50	0.40	4.34	1.70	1.64	68.18	83.00
0.00	2.00	0.40	4.73	1.85	1.44	93.06	140.00
0.00	2.50	0.40	6.95	2.04	1.68	120.03	160.00
0.00	3.00	0.40	3.04	2.30	2.21	155.00	181.00
0.00	3.50	0.40	3.58	2.45	2.43	191.06	223.00
0.00	4.00	0.40	3.44	2.69	2.61	231.18	251.00
0.00	4.50	0.40	4.11	2.81	2.80	268.95	294.00
0.10	1.00	0.20	3.74	1.09	1.10	32.92	30.00
0.10	2.20	0.20	4.73	1.39	1.51	67.22	49.00
0.10	3.00	0.20	4.20	1.64	1.80	98.39	79.00
0.10	3.50	0.20	3.68	1.79	1.97	125.01	103.00
0.10	4.00	0.20	3.96	1.93	2.13	148.48	125.00
0.10	4.50	0.20	1.95	2.09	2.15	183.32	195.00
0.10	2.60	0.23	8.07	1.58	1.69	88.19	63.00
0.10	1.40	0.25	1.32	1.29	1.15	51.37	63.00
0.10	1.80	0.25	0.76	1.41	1.36	62.01	44.00
0.10	1.00	0.35	5.00	1.47	1.30	51.75	58.00
0.10	1.40	0.40	3.48	1.70	1.78	72.73	86.00
0.10	1.80	0.40	4.60	1.80	1.74	92.70	115.00
0.10	2.20	0.40	6.83	2.00	1.45	114.40	141.00
0.10	2.60	0.40	4.41	2.15	1.96	135.16	157.00
0.10	3.00	0.40	3.51	2.40	2.22	161.26	181.00
0.10	3.50	0.40	3.56	2.43	2.39	196.69	196.00

Continued on next page...

...continued from previous page.

Angle (deg)	U_{sg} (m/s)	U_{sl} (m/s)	Length (m)	Exp U_{wave} (m/s)	Sim U_{wave} (m/s)	Exp P gradient (Pa/m)	Sim P gradient (Pa/m)
0.10	4.00	0.40	3.04	2.67	2.57	231.04	238.00
0.10	4.50	0.40	3.74	2.92	2.78	282.82	282.00
0.25	1.60	0.20	6.13	1.20	1.16	54.79	35.00
0.25	2.00	0.20	13.30	1.30	1.06	66.38	65.00
0.25	2.40	0.20	7.29	1.42	1.55	80.74	57.00
0.25	2.60	0.20	7.66	1.50	1.62	88.63	64.00
0.25	3.00	0.20	2.38	1.62	1.68	106.87	105.00
0.25	3.50	0.20	3.00	1.76	1.84	130.19	140.00
0.25	4.00	0.20	3.32	1.95	1.99	158.87	168.00
0.25	4.50	0.20	2.69	2.10	2.19	189.69	187.00
0.25	1.80	0.30	5.10	1.49	1.24	78.91	112.00
0.25	2.20	0.40	6.74	1.98	1.30	121.34	155.00
0.25	2.60	0.40	7.56	2.21	1.50	143.16	181.00
0.25	3.00	0.40	6.13	2.39	1.73	173.36	229.00
0.25	3.50	0.40	5.02	2.45	2.42	202.22	227.00
0.25	4.00	0.40	3.88	2.65	2.64	243.11	261.00
0.25	4.50	0.40	2.62	2.81	2.78	283.82	291.00
1.00	2.00	0.10	4.63	0.91	0.92	80.79	79.00
1.00	2.50	0.10	10.80	1.05	1.30	85.24	89.00
1.00	3.00	0.10	6.23	1.22	1.30	100.00	91.00
1.00	3.50	0.13	3.72	1.45	1.40	123.00	108.00
1.00	4.00	0.10	7.84	1.53	1.52	133.58	123.00
1.00	4.50	0.10	1.72	1.68	1.66	157.60	164.00
1.00	2.00	0.20	7.15	1.40	1.01	108.98	121.00
1.00	2.50	0.20	7.04	1.38	1.19	116.00	127.00
1.00	3.00	0.20	3.08	1.50	1.64	137.16	160.00
1.00	3.50	0.20	2.11	1.65	1.77	151.52	136.00
1.00	4.00	0.20	4.66	1.82	1.99	174.70	187.00
1.00	4.50	0.20	2.11	2.06	2.09	210.46	227.00
1.00	3.50	0.28	5.15	2.01	2.00	191.97	159.00
1.00	2.50	0.30	4.93	1.93	1.10	153.37	204.00
1.00	3.00	0.30	3.20	1.87	1.81	171.87	246.00
1.00	4.00	0.30	3.29	2.25	2.18	226.83	278.00
1.00	4.50	0.30	4.18	2.45	2.50	265.20	275.00

Appendix C

Snapshots of Filling an Undulating Pipeline

C.1 Liquid height 0.450 m

The following snapshots were taken from video and simulation of an initially empty undulating pipeline being filled from a tank where the liquid height in the tank was 0.450 m above the inlet. As the first pipe segment fills, the liquid level in the segment oscillates before coming to rest. First the liquid level in the segment reaches a maximum before retreating down the segment to a minimum. Finally it comes to rest in the end state position.

1. The maximum liquid level in first pipe segment is reached at 2.20 sec into the experiment and 1.51 sec into the simulation.

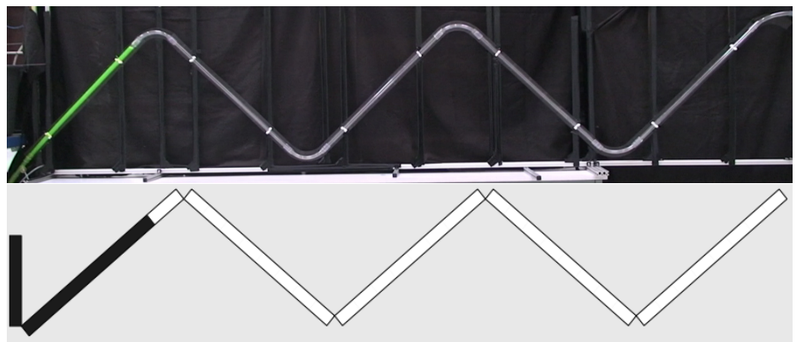

2. The liquid then retreats in the segment reaching a minimum height at 3.56 sec into the experiment and 3.01 sec into the simulation.

Appendix C

Snapshots of Filling an Undulating Pipeline

C.1 Liquid height 0.450 m

The following snapshots were taken from video and simulation of an initially empty undulating pipeline being filled from a tank where the liquid height in the tank was 0.450 m above the inlet. As the first pipe segment fills, the liquid level in the segment oscillates before coming to rest. First the liquid level in the segment reaches a maximum before retreating down the segment to a minimum. Finally it comes to rest in the end state position.

1. The maximum liquid level in first pipe segment is reached at 2.20 sec into the experiment and 1.51 sec into the simulation.

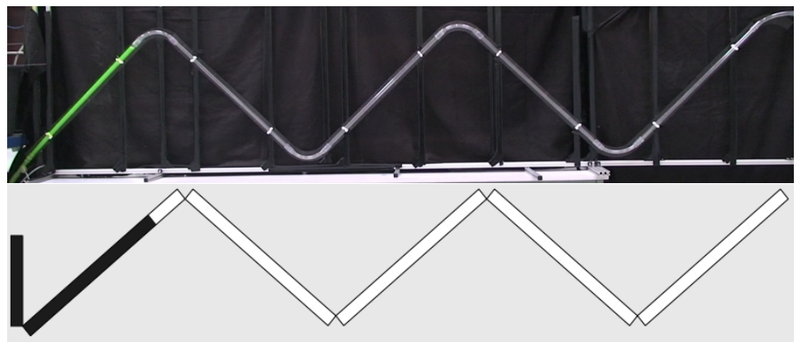

2. The liquid then retreats in the segment reaching a minimum height at 3.56 sec into the experiment and 3.01 sec into the simulation.

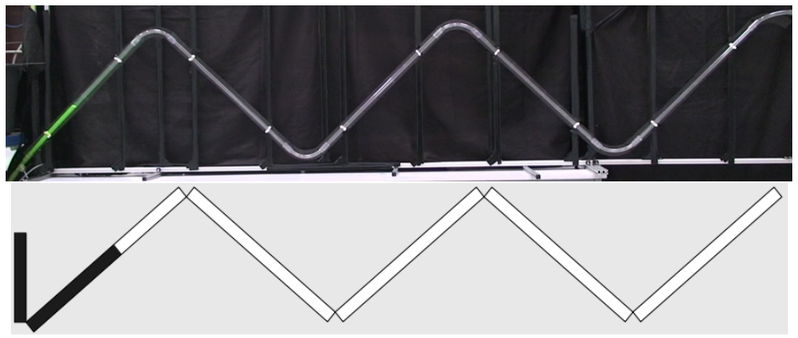

3. Finally, the end state is reached where the liquid comes to rest.

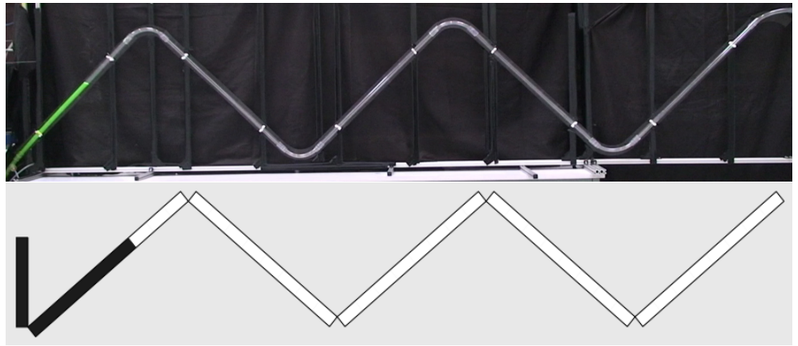

C.2 Liquid height 0.675 m

These snapshots were taken from video and simulation of an initially empty undulating pipeline being filled from a tank where the liquid height was 0.675 m above the inlet. The first pipe segment is completely filled with liquid and a slug forms in the first low point, trapping an air bubble in the second pipe segment.

1. The first pipe segment is filled after 1.20 sec experimentally and 1.23 sec in the simulation.

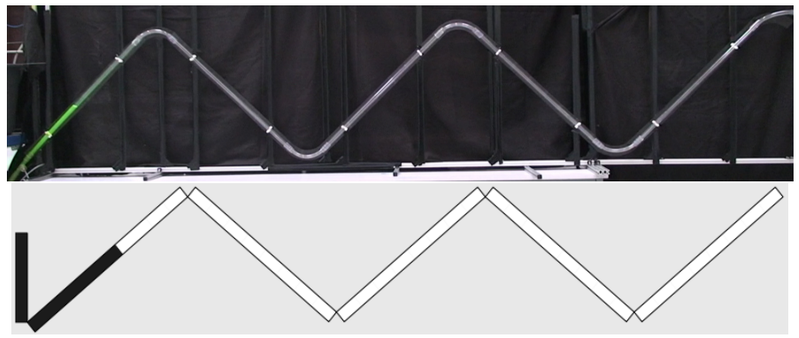

3. Finally, the end state is reached where the liquid comes to rest.

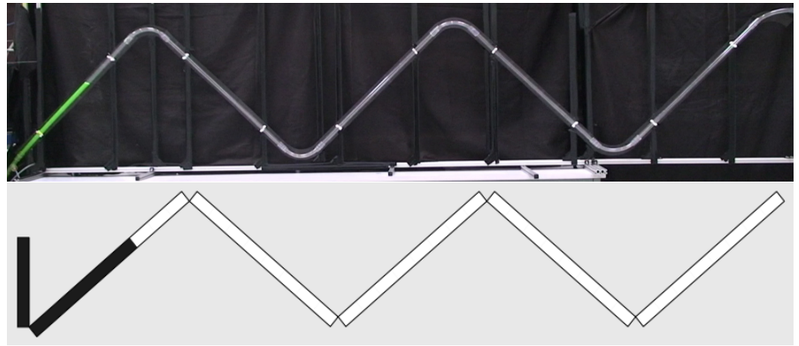

C.2 Liquid height 0.675 m

These snapshots were taken from video and simulation of an initially empty undulating pipeline being filled from a tank where the liquid height was 0.675 m above the inlet. The first pipe segment is completely filled with liquid and a slug forms in the first low point, trapping an air bubble in the second pipe segment.

1. The first pipe segment is filled after 1.20 sec experimentally and 1.23 sec in the simulation.

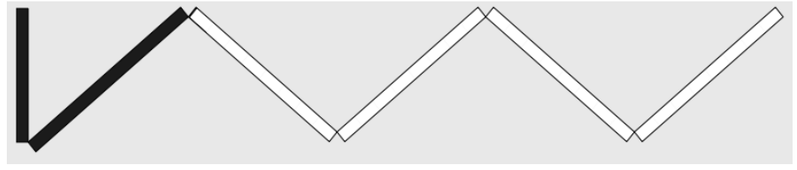

2. A slug forms in first low point after 2.24 sec experimentally and 2.96 sec in the simulation.

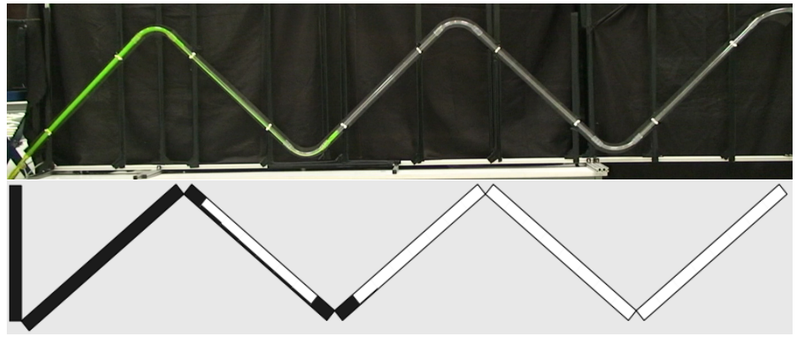

3. The final state is reached.

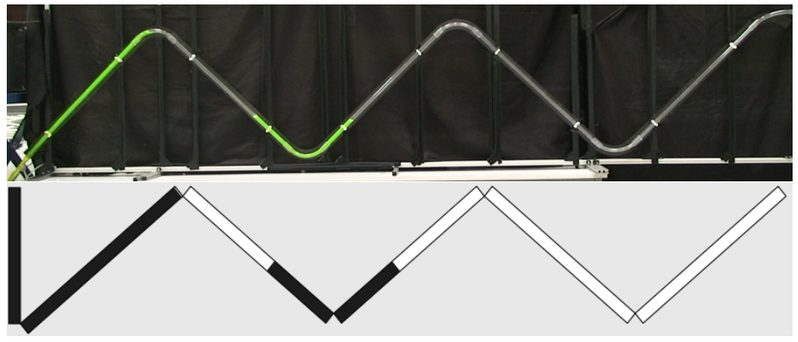

C.3 Liquid height 0.750 m

The following snapshots were taken as liquid fills the undulating pipeline when the liquid level in the tank was 0.750 m above the inlet. Both experimental and simulated results are shown. Liquid enters and fills the first three pipe segments and collects in the second low point trapping an air bubble in the fourth pipe segment.

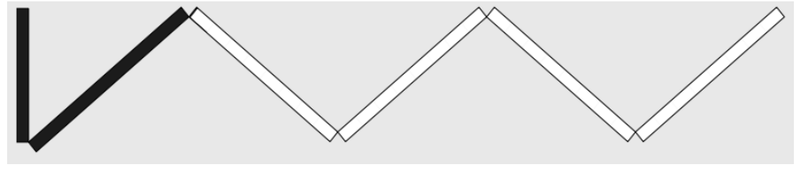

2. A slug forms in first low point after 2.24 sec experimentally and 2.96 sec in the simulation.

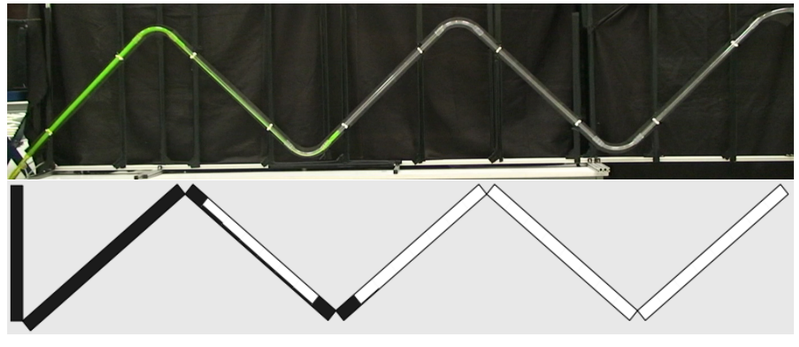

3. The final state is reached.

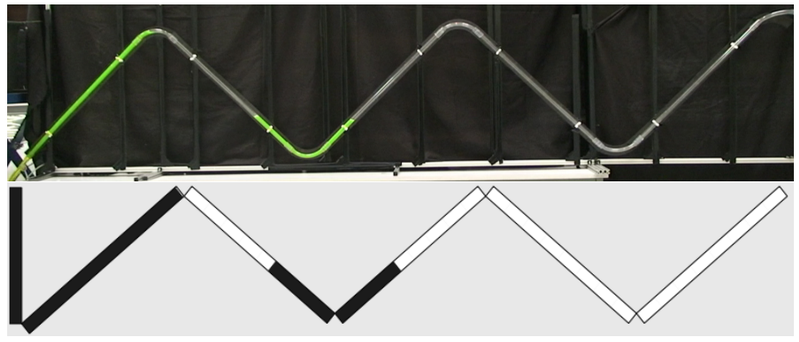

C.3 Liquid height 0.750 m

The following snapshots were taken as liquid fills the undulating pipeline when the liquid level in the tank was 0.750 m above the inlet. Both experimental and simulated results are shown. Liquid enters and fills the first three pipe segments and collects in the second low point trapping an air bubble in the fourth pipe segment.

1. The first pipe segment is filled after 1.32 sec experimentally and 1.11 sec in the simulation.

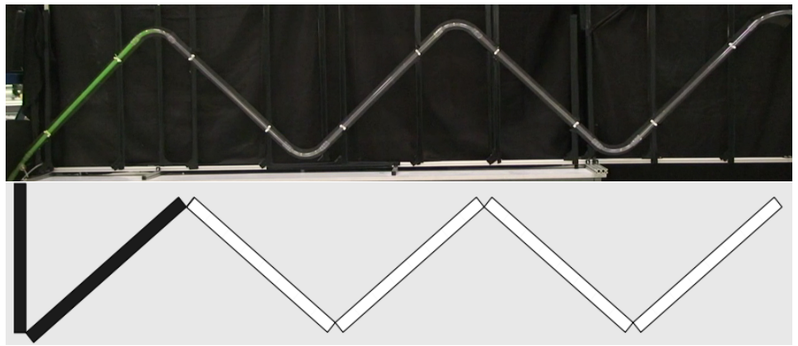

2. A slug forms in first low point after 2.20 sec in the experiment and 2.66 sec in the simulation.

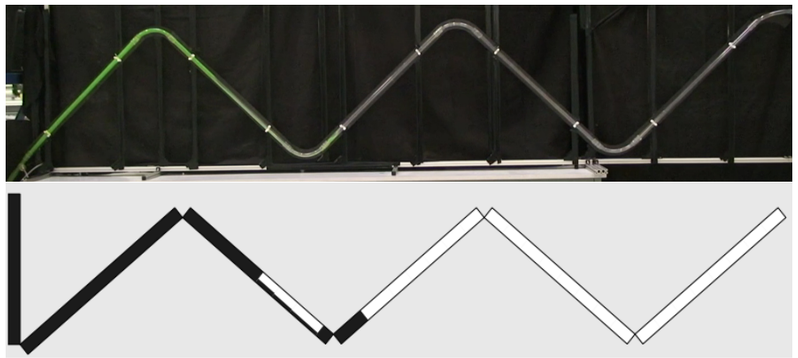

3. The third pipe segment is filled after 3.60 sec experimentally and 4.41 sec in the simulation.

1. The first pipe segment is filled after 1.32 sec experimentally and 1.11 sec in the simulation.

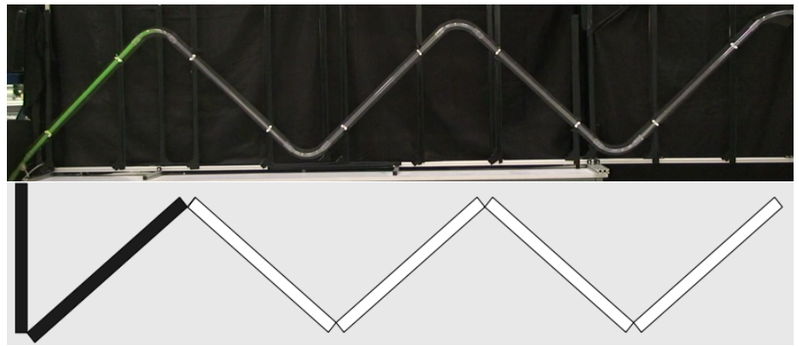

2. A slug forms in first low point after 2.20 sec in the experiment and 2.66 sec in the simulation.

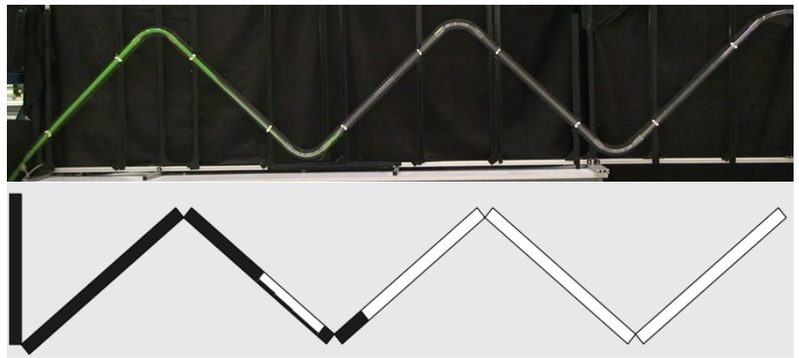

3. The third pipe segment is filled after 3.60 sec experimentally and 4.41 sec in the simulation.

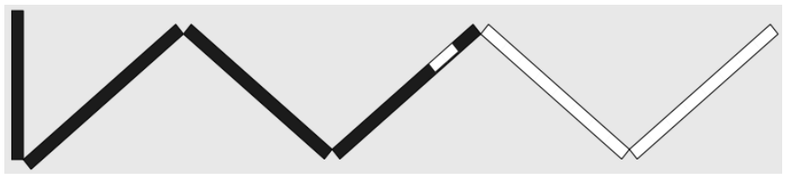

4. A slug forms in second low point after 4.60 sec experimentally and 6.49 sec in the simulation.

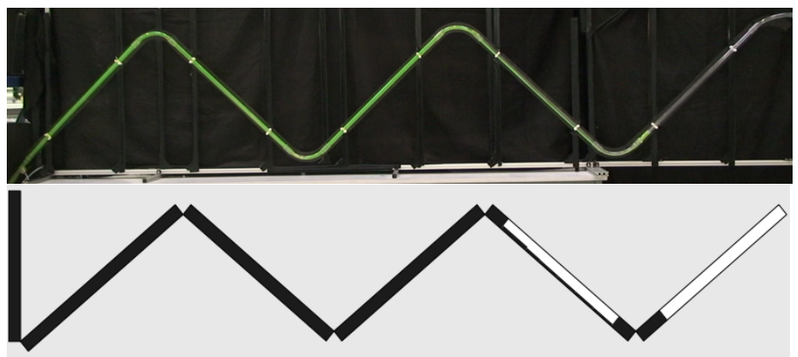

5. The final state is reached.

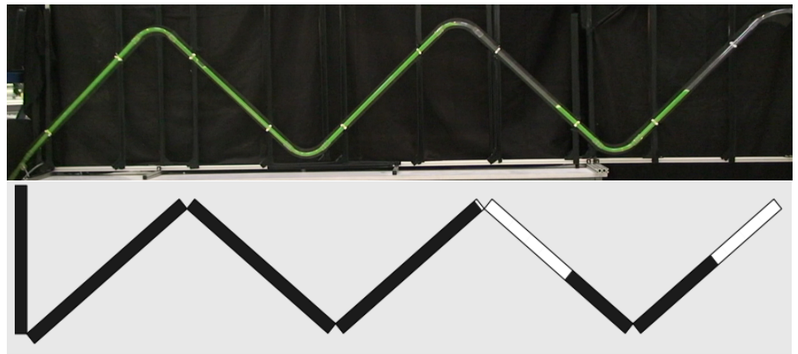

C.4 Liquid height 0.825 m

These snapshots were taken as liquid filled and flushed an initially empty undulating pipeline where the liquid height was 0.825 m in a tank above the inlet. Snapshots come from videos of the experiment and visualizations of simulated results.

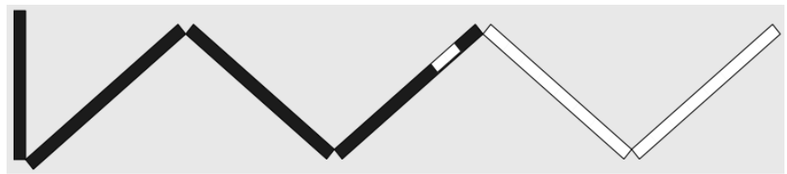

4. A slug forms in second low point after 4.60 sec experimentally and 6.49 sec in the simulation.

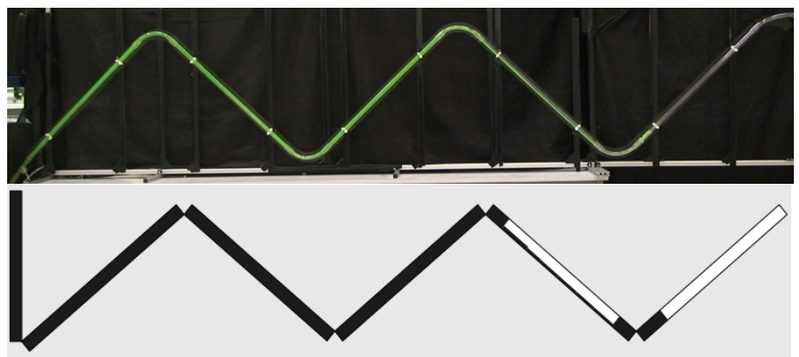

5. The final state is reached.

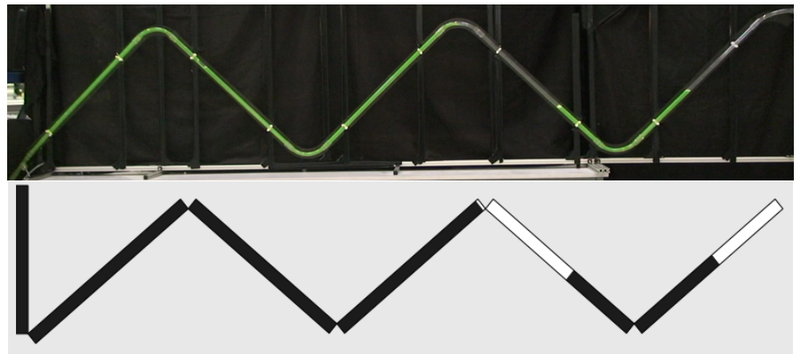

C.4 Liquid height 0.825 m

These snapshots were taken as liquid filled and flushed an initially empty undulating pipeline where the liquid height was 0.825 m in a tank above the inlet. Snapshots come from videos of the experiment and visualizations of simulated results.

139

1. The first pipe segment is filled after 1.80 sec experimentally and 1.05 sec in the simulation.

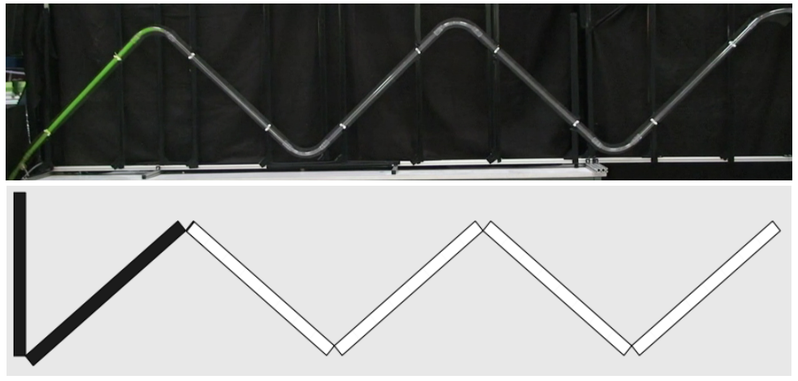

2. A slug forms at the first low point in 2.68 sec experimentally and 2.42 sec in the simulation.

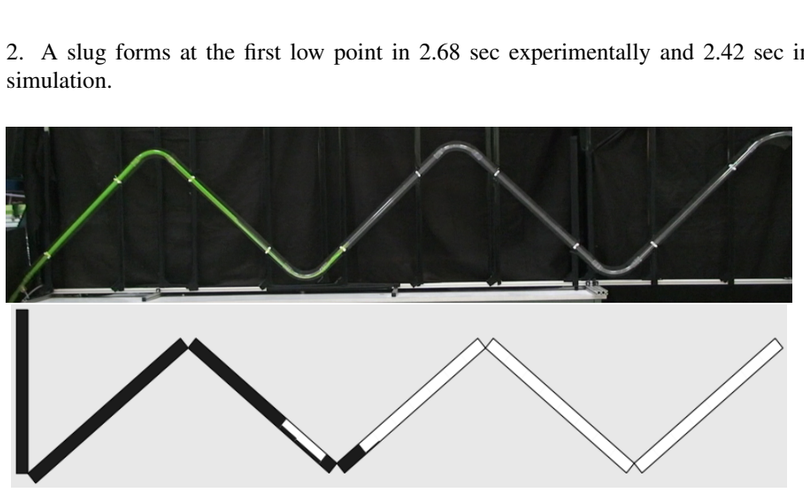

3. The third pipe segment is filled after 3.80 sec experimentally and 4.32 sec in the simulation.

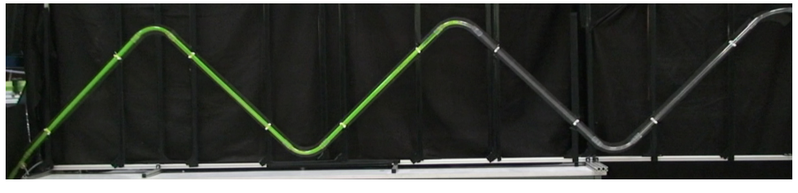

1. The first pipe segment is filled after 1.80 sec experimentally and 1.05 sec in the simulation.

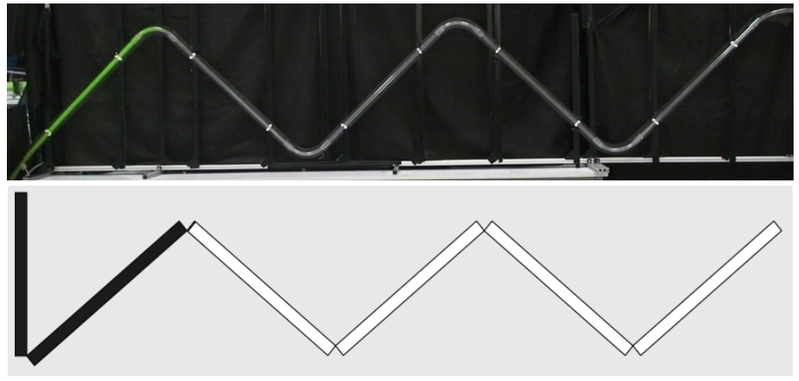

2. A slug forms at the first low point in 2.68 sec experimentally and 2.42 sec in the simulation.

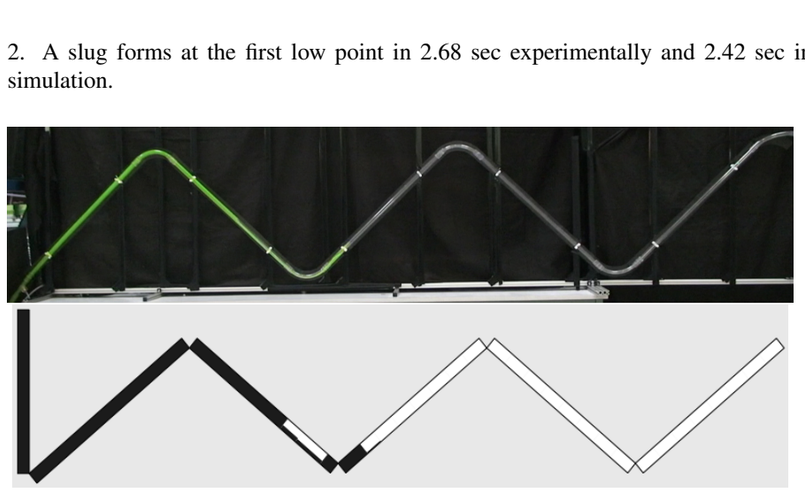

3. The third pipe segment is filled after 3.80 sec experimentally and 4.32 sec in the simulation.

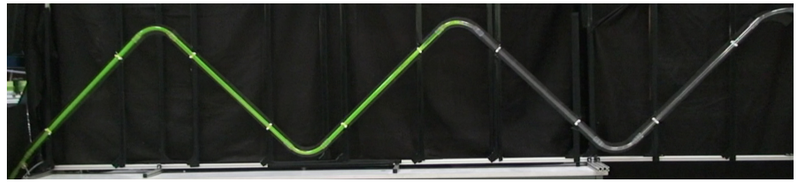

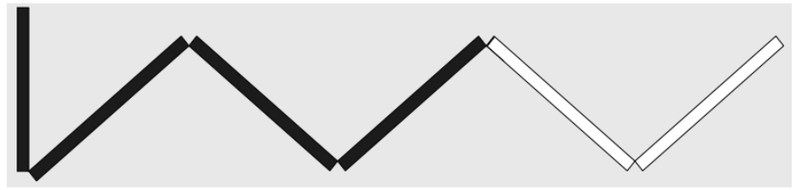

4. A slug forms at the second low point after 4.84 sec experimentally and 5.96 sec in the simulation.

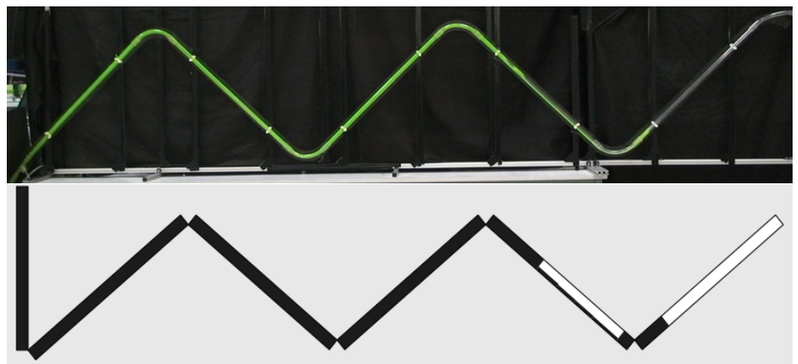

5. The fifth pipe segment contains slugs and bubbles at 6.36 sec in the experiment and 7.71 sec in the simulation.

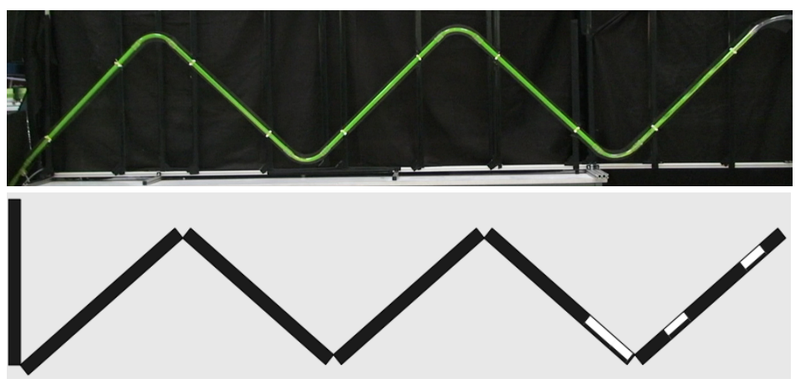

6. Finally, the end state is reached.

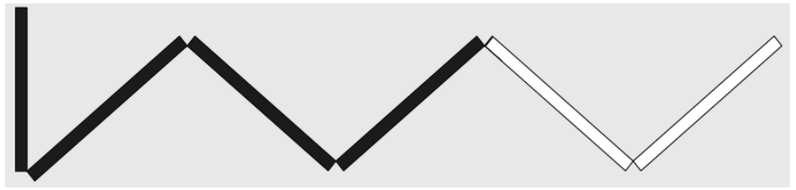

4. A slug forms at the second low point after 4.84 sec experimentally and 5.96 sec in the simulation.

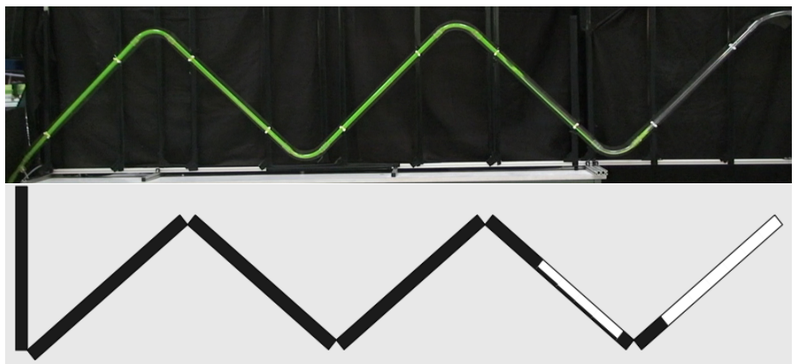

5. The fifth pipe segment contains slugs and bubbles at 6.36 sec in the experiment and 7.71 sec in the simulation.

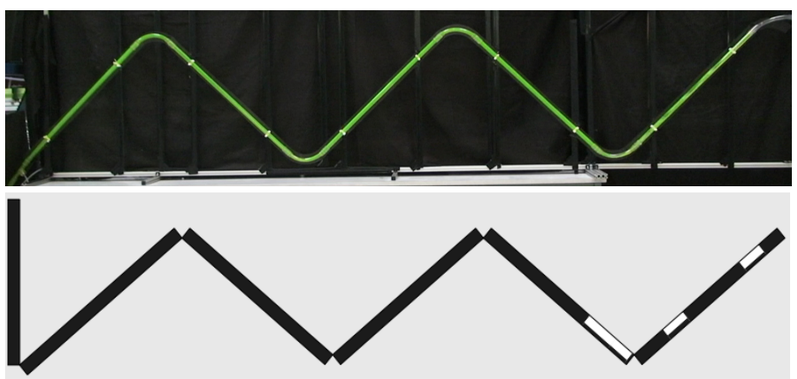

6. Finally, the end state is reached.

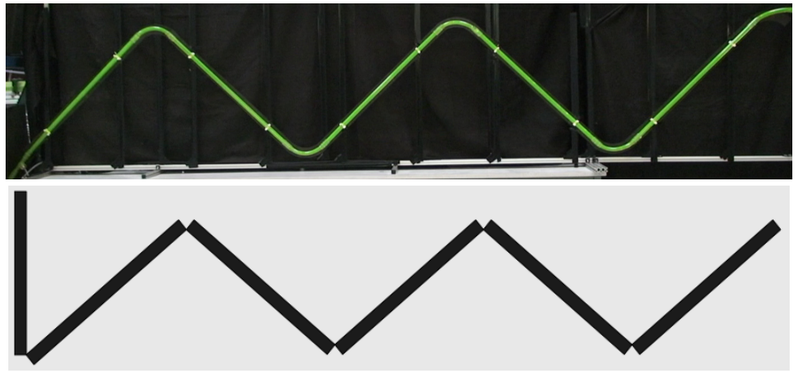

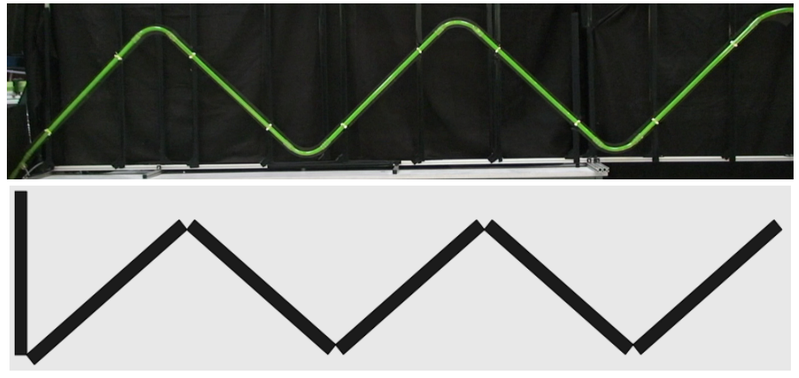

142